AFRL-ML-TY-TR-2005-4584

OPTICAL REMOTE SENSING TO DETERMINE STRENGTH OF NONPOINT SOURCES:
Duke Forest Validation Study (ESTCP # CP-0214)

Ravi Varma, Ram Hashmonay, Robery Kagann and Adam Bolch
ARCADIS Geraghty & Miller, Inc.
4915 Prospectus Drive, Suite F
Durham, NC 27713

Final Report, November 2005

Air Force Research Laboratory
Materials and Manufacturing Directorate
Airbase Technologies Division
139 Barnes Drive, Suite 2
Tyndall AFB, FL 32403-5323

NOTICE

Using Government drawings, specifications, or other data included in this document for any purpose other than Government procurement does not in any way obligate the U.S. Government. The fact that the Government formulated or supplied the drawings, specifications, or other data does not license the holder or any other person or corporation; or convey any rights or permission to manufacture, use, or sell any patented invention that may relate to them.

This technical report was reviewed and cleared for public release by the Air Force Research Laboratory Tyndall Site (AFRL/MLQ) Public Affairs Office (PAO) and is releasable to the National Technical Information Service (NTIS). Reference PAO Case Number: AFRL/MLQ-05-086, 28 Nov 2005.

This report is releasable to the National Technical Information Service (NTIS) where it will be available to the general public, including foreign nationals.

5285 Port Royal Road
Springfield VA 22161
Telephone (703) 487-4650, (703) 487-4639 (TDD for the hearing impaired)
e-mail: orders@ntis.fedworld.gov
http://www.ntis.gov/index.html

This technical report is approved for publication.

//signed//
PATRICK SULLIVAN
Work Unit Manager

//signed//
SANDRA R. MEEKER
Chief, Weapons System Logistics Branch

//signed//
JIMMY L. POLLARD, Colonel, USAF
Chief, Airbase Technologies Division

This report is published in the interest of scientific and technical information exchange and its publication does not constitute the Government's approval or disapproval of its ideas or findings.

REPORT DOCUMENTATION PAGE

Form Approved
OMB No. 0704-0188

PLEASE DO NOT RETURN YOUR FORM TO THE ABOVE ADDRESS.

1. REPORT DATE *(DD-MM-YYYY)*	2. REPORT TYPE	3. DATES COVERED *(From - To)*
08-11-2005	Final Technical Report	26 Aug 2002 - 31 Dec 2004

4. TITLE AND SUBTITLE

Optical Remote Sensing to Determine Strength of Nonpoint Sources; Duke Forest Control Experiments (ESTCP # CP-0214)

5a. CONTRACT NUMBER

F08637-02-C-7024

5b. GRANT NUMBER

5c. PROGRAM ELEMENT NUMBER

63104D

6. AUTHOR(S)

Ravi Varma, Ram Hashmonay, Robery Kagaan, Adam Bolch

5d. PROJECT NUMBER

DODT

5e. TASK NUMBER

0029

5f. WORK UNIT NUMBER

DODT0029

7. PERFORMING ORGANIZATION NAME(S) AND ADDRESS(ES)

ARCADIS Geraghty & Miller, Inc.
4915 Prospectus Drive, Suite F
Durham NC 27713

8. PERFORMING ORGANIZATION REPORT NUMBER

RN007640

9. SPONSORING/MONITORING AGENCY NAME(S) AND ADDRESS(ES)

Air Force Research Laboratory
Materials and Manufacturing Directorate
139 Barnes Drive, Suite 2
Tyndall AFB, FL 32403-5323

10. SPONSOR/MONITOR'S ACRONYM(S)

11. SPONSOR/MONITOR'S REPORT NUMBER(S)

AFRL-ML-TY-TR-2005-4584

12. DISTRIBUTION/AVAILABILITY STATEMENT

Distribution Statement A: Approved for public release; distribution unlimited.
Available from www.estcp.org as a download of the project final report.

13. SUPPLEMENTARY NOTES

Technical monitor: Dr Patrick Sullivan, AFRL/MLQL, (850) 283-0430 (DSN 523-0430)

14. ABSTRACT

Currently there is no suitable standardized method for measuring area source emissions. Under EPA and DOE support, a new method of directly measuring area sources has been developed. This method, Radial Plume Mapping (RPM), uses a scanning optical sensor, and asymmetrically placed array of reflectors, wind measurements, and optimization algorithms to calculate area source emissions from non-point sources using open-path Fourier Transform Infra-Red spectrometer (OP-FTIR). Trace gases, nitrous oxide, ethylene and acetylene, propylene and propane, are released in a controlled manner and their locations of release are recorded. By radial scanning on a horizontal plane close to the ground and the location of the point releases are reconstructed. Area sources were simulated with soaker hoses laid out in "H"-shape configurations and by scanning beams in a vertical plane downwind from the sources, the fluxes were computed and compared to the known actual release rates. The results show that the source locations were reconstructed successfully to within 10% of the diagonal length of the investigated area using the horizontal RPM and the calculated mass flux agreed with the known release rates to within a few percent, under stable experimental conditions.

15. SUBJECT TERMS

Optical Remote Sensing, OP-FTIR, Radial Plume Mapping, Visible Opacity, CEM

16. SECURITY CLASSIFICATION OF:			17. LIMITATION OF ABSTRACT	18. NUMBER OF PAGES	19a. NAME OF RESPONSIBLE PERSON
a. REPORT	b. ABSTRACT	c. THIS PAGE			Patrick Sullivan
U	U	U	SAR	103	19b. TELEPHONE NUMBER *(Include area code)* 850-283-0430

Reset

Standard Form 298 (Rev. 8/98)
Prescribed by ANSI Std. Z39.18

Table of Contents

List of Figures

List of Tables

List of Acronyms

APPCD	Air Pollution Prevention and Control Division
ARCADIS	ARCADIS G&M, Inc.
CAM	Compliance assurance monitoring
CCF	Concordance Correlation Factor
DoD	Department of Defense
DOE	Department of Energy
ECAM	Environmental Cost Analysis Methodology
EPA	United States Environmental Protection Agency
ES&T	Environmental Science and Technology
HSP	Health and Safety Protocol
IR	Infrared
JA&WMA	Journal of the Air and Waste Management Association
MACT	Maximum Achievable Control Technology
MART	Multiplicative algebraic reconstruction technique
NESHAP	National Emission Standards for Hazardous Air Pollutants
NNLS	Non-negative least square
NOx	Nitrogen oxides
OAQPS	Office of Air Quality Planning and Standards
OP	Open-path
OP-FTIR	Open-path Fourier-Transform Infrared
ORS	Optical Remote Sensing
PIC	Path integrated concentration
PI-ORS	Path-integrated optical remote sensing
PM	Particulate matter
PM2.5	Particulate matter smaller than 2.5 microns in diameter
QA/QC	Quality Assurance/Quality Control
RPM	Radial Plume Mapping
SBFM	Smooth basis functions minimization
SIP	State Implementation Plan
SRI	Southern Research Institute
SSE	Sum of Squared Errors
VOC	Volatile organic compound

Abstract

Currently there is no suitable standardized method for measuring non-point source emissions. Under EPA and DOE support, a new method of directly measuring non-point sources has been developed. This method, Radial Plume Mapping (RPM), uses a scanning optical sensor, an asymmetrically placed array of reflectors, wind measurements, and optimization algorithms to calculate non-point source emissions. This report describes this innovative method, and presents results from a controlled demonstration study that applied this approach to directly measure emissions from non-point sources using open-path Fourier Transform Infra-Red spectrometer (OP-FTIR) or other open-path devices. Trace gases, nitrous oxide, ethylene and acetylene, propylene and propane, are released in a controlled manner and their locations of release are recorded. By radial scanning on a horizontal plane close to the ground and the location of the point releases are reconstructed. Area sources were simulated with soaker hoses laid out in “H”-shape configurations and by scanning beams in a vertical plane downwind from the sources, the fluxes were computed and compared to the known actual release rates. The results show that the source locations were reconstructed successfully to within 10% of the diagonal length of the investigated area using the horizontal RPM and the calculated mass flux agreed with the known release rates to within a few percent, under stable experimental conditions.

1. Introduction

1.1 Background

No standard protocol exists for making non-point source measurements of an air emission flux. An accurate and cost-effective method is needed to quantify non-point emission sources. Department of Defense (DoD) military activities are a category that will experience increasing attention as regulation of major industrial sources reaches a point of diminishing returns. Current estimation techniques based on emission factors are imprecise and typically overestimate drastically. Multiple point measurements are locally accurate but may not be representative of the entire plume, and they are expensive in the quantities required to characterize larger area sources. The Radial Plume Mapping approach, utilizing path-integrated optical remote sensing (PI-ORS), e.g., open-path Fourier-Transform Infrared (OP-FTIR) spectroscopy, uses multiple beam paths and optimizing algorithms to give a time-averaged, mass-equivalent concentration field across a plume of contaminants. In conjunction with wind data, the integrated mass through a downwind vertical plane is used to directly determine the emission rate from the non-point source based on the acquired concentration data.

First, reflectors are deployed in an asymmetric, radial pattern that includes the emission area source, from which the approximate boundaries of the plume's origin can be determined. When the plume is located, the array of reflectors is redeployed in a vertical plane immediately downwind so that the beams are perpendicular and centered to the centerline of the plume. The PI-ORS system scans from reflector to reflector in a constant pattern, separately accumulating values for each reflector to generate a long-term average in each spatial element. The novelty is in placing a two-dimensional array of reflectors so the absorption information can be directly translated, by an optimization algorithm, into time-averaged area concentrations without using dispersion model estimates.

1.2 Objectives of the Demonstration

The objectives of this demonstration were to: (1) demonstrate the ability of the method to locate the plume-emitting source by horizontally scanning an OP-FTIR system to a horizontal array of retro-reflecting mirrors close to the ground; and (2) to demonstrate the ability of the method to quantify the mass flux from a non-point source by vertically scanning the PI-ORS system to a vertical array of retro-reflecting mirrors mounted on a tower downwind of the source during various atmospheric conditions.

This validation report discusses the results of this initial controlled validation field study, conducted at the Duke Forest facility of Duke University, School of Environment, located in Chapel Hill, North Carolina from the late Fall of 2002 to the Spring of 2003. This validation study is part of a larger demonstration project to demonstrate the PI-ORS measurement method for non-point sources in a real-world, industrial setting at full-scale. During the follow-on studies, actual emission rates from at least three non-point DoD sources will be measured. Typical subjects for measurement will most likely include a wastewater treatment plant, a tank farm, a small industrial area, or a landfill. Typical compounds to be measured from these sources

include methane, ammonia, volatile organic compounds (VOCs), and hazardous air pollutants (HAPs). The purpose of this initial validation study is to vary the parameters of this methodology, to help determine the appropriate parameters to be used at each of the non-point DoD sources.

Advantages of this PI-ORS technology – in comparison to the alternative conventional technology of using an array of SUMMA canisters and inverse dispersion modeling to obtain the mass flux – include increased data quality and quantity, as well as lower cost. The PI-ORS demonstrated approach provides higher quality data by avoiding the inaccuracies introduced by assumptions required for the dispersion modeling. This technique allows samples to be taken at intervals of minutes instead of hours, which in turn gives information on temporal variations of emissions that simply are not available with a canister method.

Significant cost savings can be achieved by the use of this technology. In addition, the proposed approach that utilizes PI-ORS is far superior to the current approach in that the PI-ORS fully and directly characterizes the non-point source flux emissions in near-real time.

1.3 Regulatory Drivers

With enactment of the Clean Air Act Amendments eleven years ago, Congress directed the United States Environmental Protection Agency (EPA) to improve air emissions monitoring from all sources, including those located at federal facilities. Acting on that directive, EPA now requires emission quantifications and improved monitoring from units subject to the air operating permits brought about by Title V. For the first time, many units previously grandfathered from regulations and the corresponding emission monitoring requirements are now required to be identified and to have ongoing emissions monitoring and testing. Moreover, persons responsible for operation of the units (i.e., base and post commanders) must certify compliance with emissions limits and other permit terms and conditions based upon data collected by the emission monitors. Submission of false certifications is a criminal offense.

It is increasingly common for Title V permitting authorities to require both identification and quantification of unit emissions to be submitted as part of permit applications before work under an operating permit can commence. This direction is clear and will only increase in intensity and urgency on the part of regulating authorities.

Another monitoring component brought about by Title V is the compliance assurance monitoring (CAM) rule which focuses on large units with active control devices used to reduce particulate matter and volatile organic compound emissions. Under the CAM rule, owners and operators (i.e., military bases and posts) obtain direct emissions data or parametric data to ensure that the active control device operation remains consistent with the operation recorded during a previous emissions test that demonstrated compliance with the emissions limits. Operators and owners should be planning and obtaining data now in preparation for development of CAM plans.

Units not subject to Title V need to have data that continue to show emissions are below applicability thresholds. From a practical perspective, these units need monitoring data equivalent to what would be found in Title V permits in order to make such demonstrations. The Maximum Achievable Control Technology (MACT) standards, or new National Emission

Standards for Hazardous Air Pollutants (NESHAP), are designed to use direct emissions measurements, where feasible. Responsible officials will need to rely on monitoring data to certify emissions of units subject to the standards, as well as to show that other units emissions do not exceed the standards applicability threshold levels.

Accurate monitoring data will prove necessary should individual sites choose to participate in emissions trading programs under development at the EPA. Further regulatory pressures will occur in areas having particulate matter (PM) and ozone non-attainment issues. State Implementation Plans (SIP) and new source reviews will increasingly look for PM2.5, volatile organic compound (VOC), and nitrogen oxides (NOx) reductions from smaller sources, area sources, and mobile sources. PM2.5, VOC, and NOx emissions from these types of emitters will soon need to be quantified by military installations in order to use them for offsets and SIP reductions. Those programs allow for increased unit operation flexibility in exchange for increased monitoring data used to quantify site emissions. Such programs can include fugitive, as well as point source, emissions.

The EPA shift towards a national cap-and-trade strategy, as described in the previous paragraph, was discussed in detail at EPA's July 31-August 1, 2001 workshop by John D. Bachmann, who is the Senior Science Advisor for the Office of Air Quality Planning and Standards. He confirmed this new order and strongly suggested all facilities quantify all of their emissions, both criteria and toxic pollutants, in order to prepare themselves for the forthcoming emission caps and trading allowances.

While most emission units will not be subject to the CAM rule until their Title V permit is renewed (generally five years after the permit is first issued), DoD should be concerned now. Implementation delays were put into the CAM rule so that prudent source owners and operators could experiment with differing approaches and select the most relevant parameters and algorithms in advance of the mandated deadline. Moreover, new emission units that are added to a source, after submission of Title V permit applications or after receipt of a Title V permit, must meet the CAM rule requirements upon startup.

1.4 Stakeholder/End-User Issues

The primary decision-making factors for any of the potential end-users – whether DoD or the manufacturing environment – will be the decreased time and cost associated with the use of the PI-ORS approach to obtain a high quality determination of emission flux from an area source. It is anticipated that at the conclusion of this demonstration project, with the support of EPA's Emission Measurement Center in the Office of Air Quality Planning and Standards (OAQPS), an approved EPA methodology will be developed. This will allow the use of this technology by personnel at the field technician level. Because this technology is a stand-alone optical measurement method, there are no barriers to implementation related to integration into the manufacturing environment, or for its use at any of the potential DoD sites.

2. Technology Description

2.1 Technology Development and Application

The emission measurement technology to be demonstrated in this program uses multiple-beam PI-ORS and mathematical optimization techniques to provide spatial information on the target plumes. These plume maps in conjunction with wind data allow the determination of emission fluxes. This technology was developed by the University of Washington and ARCADIS G&M, Inc. (ARCADIS), under support of the Department of Energy (DOE) and the EPA Air Pollution Prevention and Control Division (APPCD) within the National Risk Management Research Laboratory. This method is documented in several peer-reviewed publications (such as Environmental Science and Technology (ES&T), Journal of the Air and Waste Management Association (JA&WMA), and Atmospheric Environment) and in U.S. Patent Number 6,542,242. References are provided in Section 7.

OP-FTIR technology, which will be deployed in this study as the example PI-ORS, has been developed and evaluated for the last decade by EPA, and a compendium method for measurement of pollutant concentrations in ambient air was published in 1999 (TO-16). Some advantages of using OP-FTIR include the ability to detect a large number of compounds simultaneously at low detection levels compared to other ORS methods. The technology is also fairly easy to operate, and several products are commercially available. Disadvantages of using OP-FTIR include the fact that a few VOCs have higher detection limits and that the path length is limited to about 500 m.

Figure 2-1 illustrates a typical horizontal array of nine retro-reflectors and the concentration-dimension map the technique generated in a controlled field experiment funded by EPA's APPCD. The source (denoted by the star) was relocated several times. Each time the reconstructed plume successfully identified the origin of the plume (denoted by the small square), and showed the shape of the plume to align with the measured wind direction. The Concordance Correlation Factor (CCF) was used to represent the goodness-of-fit in the path-integrated domain, and compared the path integrated concentration (PIC) values at the end of reconstruction procedure against the measured PIC values.

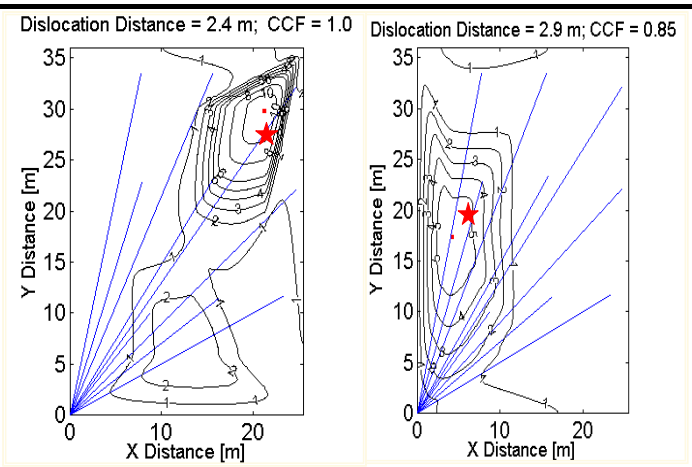

Figure 2-1. Examples of experimental ethylene source localization using OP-FTIR scanning in the radial configuration.

When the plume is located, the array of reflectors is redeployed in a downwind vertical plane centered around the plume, and the PI-ORS is then placed so as to project across it in the plane. A two-dimensional, five-reflector array covering a vertical plane downwind from a non-point emission source is illustrated in Figure 2-2. The OP-FTIR scans from reflector to reflector in a constant pattern, separately accumulating values for each reflector to generate a long-term average in each beam path. The novelty is in placing a two-dimensional array of reflectors so the PIC information can be directly translated, by an optimization algorithm, into time-averaged area concentrations, without using dispersion model estimates. Source strength is effectively the product of the sum of the area concentration elements multiplied times the average component of the wind speed normal to the measurement plane during the determinations.

This technology can be applied in any of the same situations where SUMMA canisters and dispersion modeling (or similar methodology) are currently being used for the determination of emission flux from an non-point source.

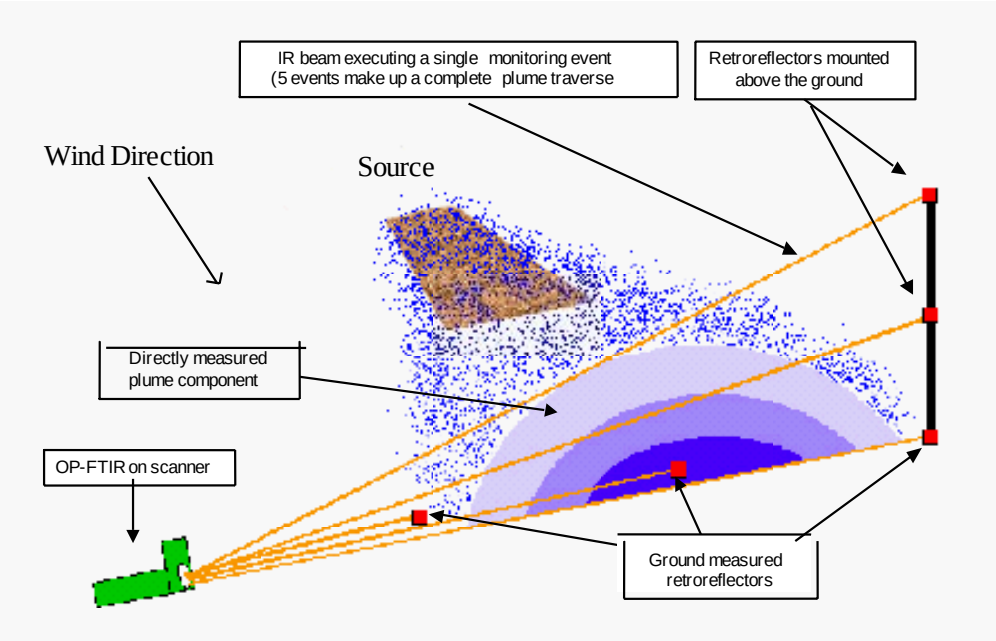

Figure 2-2. Example of a plume's characterization and emission calculation under a crosswind using the PI-ORS method.

2.2 Previous Testing of the Technology

Two controlled validation studies of this PI-ORS technology were performed under EPA funding (References are provided in Section 7). The first study, performed at the EPA's Jenkins Road facility in Research Triangle Park (RTP), was to evaluate the surface hot spot localization approach (see Figure 2-1). The surface radial scanning approach successfully identified the location of the controlled release to within 10 percent of the scan distance.

The second study, performed at a regional airport at Oxford, NC, used the downwind vertical scanning plane perpendicular to the wind direction (as illustrated in Figure 2-2) to measure emission fluxes. The emission flux was successfully determined within 10 to 30 percent, depending on atmospheric stability, as shown in Figure 2-3.

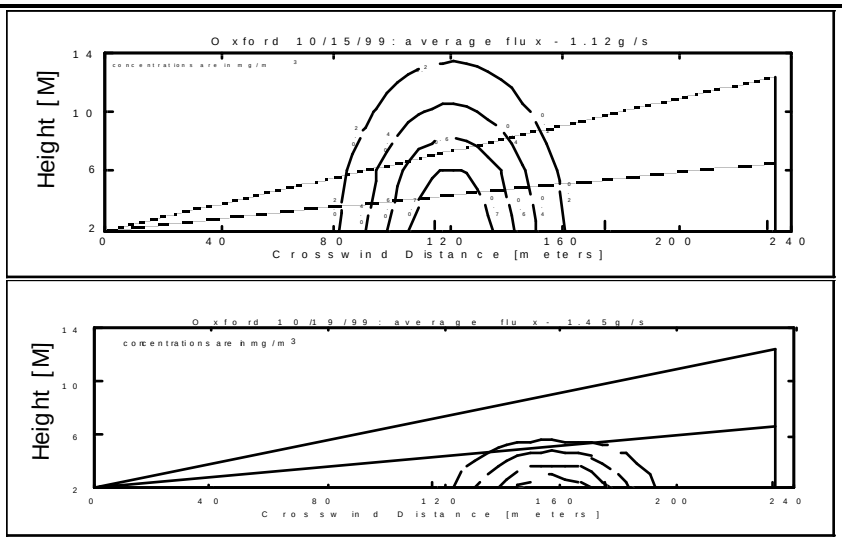

Figure 2-3. Examples of emission calculations for a controlled release under stable and unstable atmospheric conditions, respectively

2.3 Factors Affecting Cost and Performance

This interim report is for the first in a series of demonstrations of the PI-ORS methodology, and is therefore not appropriate for the application of the Environmental Cost Analysis Methodology (ECAM). However, a theoretical cost comparison between the current conventional approach of an air monitoring plan utilizing SUMMA canisters and dispersion modeling (for which no EPA method/protocol exists or is planned) and the PI-ORS approach proposed in this project is still possible and highlights the significant cost savings potential of this technology. Table 2-1 details the estimated cost savings of the new methodology for the major tasks associated with this type of sampling effort.

It should be emphasized that these two approaches will not provide the same information. The proposed approach that utilizes PI-ORS is far superior to the current approach in that the PI-ORS fully and directly characterizes the non-point source flux emissions in near-real time. These "value added" attributes of the PI-ORS methodology are not reflected in the numbers shown in Table 2-1.

Table 2-1: Theoretical Cost Comparison Between Conventional and PI-ORS Approaches.

Task	Conventional	PI-ORS+Conventional
Preparation	22,000	7,000
Field Set-up	6,000	3,000
Field Testing	50,000	30,000
Report	25,000	10,000
Travel	7,000	5,000
Subcontractor Expenses	60,000	15,000
Other Expenses	20,000	30,000
Total:	**190,000**	**100,000**

2.4 Advantages and Limitations of the Technology

The primary advantages to the PI-ORS technology include low cost and the ability to determine non-point source flux emissions, accurately and in near real-time. The alternative conventional technology is to use an array of SUMMA canisters and inverse dispersion model. The radial PI-ORS approach avoids inaccuracies introduced by assumptions required for the dispersion modeling. Also, data can be acquired at intervals of minutes instead of hours, giving information on temporal variations of emissions that simply is not available with a canister method.

Limitations of the technology include higher detection limits than canister samples and a limited number of compounds that can be measured. These limitations are not serious, as most of the compounds of interest can be measured by PI-ORS and should not prevent the use of this methodology for any of the anticipated sampling sites. For any analytes of interest that cannot be measured by PI-ORS, a limited number of canister samples can be run in conjunction with the PI-ORS to encompass a wider range of analytes. The overall time and cost savings associated with such an integrated effort will still be significant when compared to the conventional approach alone.

3. Demonstration Design

3.1 Performance Objectives

Detailed cost accounting (ECAM) will be used to accurately quantify the end-user costs of implementing the technology at the completion of the demonstration project. Complete technical success will be tracer gas mass balances of 100 ± 10 percent, and within 10 percent of the area diagonal distance for the displacement of the artificial hot spot. Even a slightly poorer agreement (± 25 percent, depending on measurement conditions) will still validate the concept and deliver a revolutionary improvement in the state of the art. Direct involvement of the regulatory community (in particular, EPA providing an approved method) virtually ensures its consideration as an improvement over emission factor methods for source strength determinations. This measurement data can also be used as input for the source terms in dispersion modeling.

3.2 Selecting Test Sites/Facilities

For this validation portion of the effort, measurements were made of controlled releases of tracer gasses. An open field was all that was required for the validation tests. The Duke Forest facility of Duke University School of Environment, located in Chapel Hill, North Carolina was selected due to its location convenient to both the EPA and ARCADIS. Significant benefits to this location over the others examined are that it contains on-site power, a sampling trailer, and storage facilities, is relatively flat and open, and is relatively secure. Based on the past eight years of meteorological data from the National Weather Service located at the Raleigh-Durham airport, winds during the planned period are relatively sustained and are primarily from the southwest or northeast.

The 150-meter square field is well suited for addressing the demonstration/validation objectives of the project. It is a secure site where instruments and equipment may be left in their working configurations overnight and on weekends if desired by the participants, and where there is sufficient space for setting up all equipment needed. These conveniences are particularly important for the extensive equipment requirements of ARCADIS, which include multiple retro-reflectors that must be carefully aligned to fit each experiment.

The 120-meter square field selected has a uniform cover of fairly tall tufted grass, providing some roughness, and gentle terrain features. Trees directly adjacent to the field are sufficiently short that they should not interfere appreciably with wind patterns within the site. Downwind distances of 200 meters are available for most likely combinations of source location and wind direction. Figure 3-1 shows the location of the Duke Forest site.

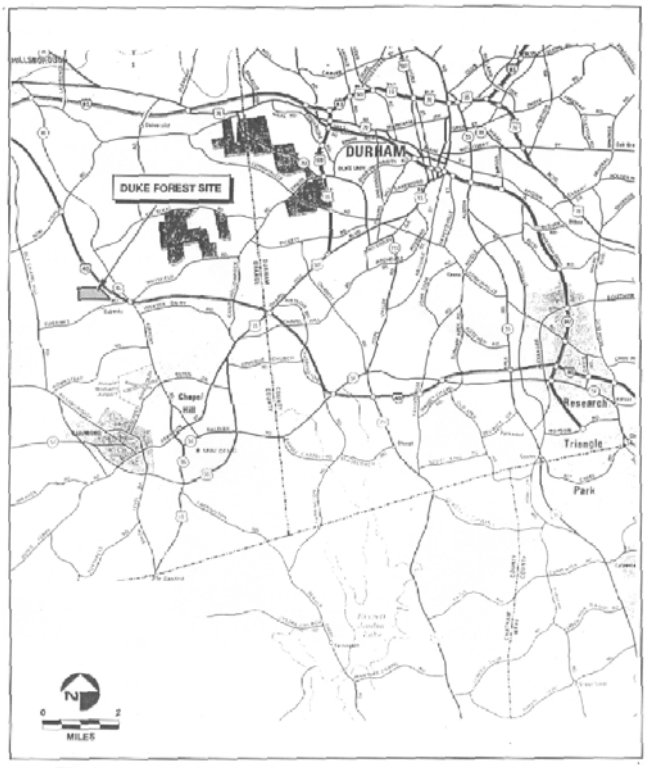

Figure 3-1. Location of the Duke Forest site.

3.3 Test Site/Facility History/Characteristics

The Duke Forest site is owned by Duke University, and is managed by the Duke University School of the Environment. The office phone number for the school is (919) 613-8013. The selected site has been used in the past to conduct wind flow and other research projects, and was the site used by the Southern Research Institute (SRI) to conduct OP-FTIR validation studies in 1992 and 1993.

The entrance to the Blackwood Division of Duke Forest is located on Eubanks Road in Orange County, North Carolina. Eubanks Road is located a few hundred meters south of Interstate 40, between the towns of Hillsborough and Chapel Hill, North Carolina. To reach the site when traveling south on Highway 86, turn left on Eubanks Road and proceed 2 to 4 miles to Duke Forest entrance gate No. 34. The gate is located on the right and requires a key to unlock. After entering the gate, proceed in a northeasterly direction down the dirt road for about 200 meters, at which point a large open field will be visible. This is the southwest corner of a non-forested area. A square area at the southwest corner of the Blackwood division of Duke Forest, 150 meters in length and width, was selected for controlled release of gases and their subsequent detection and quantification by the PI-ORS combined with RPM techniques.

3.4 Present Operations

The validation tests were conducted at sufficient distances from other research projects at Duke Forest, such that the site was representative of a natural environment.

3.5 Pre-Demonstration Testing and Analysis

The purpose of this initial study was to validate the PI-ORS measurements with RPM methodology by the controlled release of tracer gasses. There is no pre-demonstration testing against which this validation test is being compared. It should be noted that this demonstration is evaluating the methodology, and not the instrumentation.

3.6 Testing and Evaluation Plan

3.6.1 Demonstration Set-Up and Start-Up

The demonstration set-up took two people one, eight-hour day. The first half of the day was spent loading and transporting the trailer to the site, then towing the tower (mounted on a trailer) to the site. The afternoon was spent surveying the site and determining the source locations and the placement of the intermediate mirrors on the tower line. Because this was a secure site, the equipment could be left in place. The weather conditions determined when sampling would occur.

Gas was used to power two generators – one for the trailer and the OP-FTIR, and a second for the meteorological instrument at the tower. The tower was battery operated, and internal batteries supplied the power for the scales used to weigh the gas cylinders. There were no major maintenance issues associated with this validation study.

The experimental configuration is as shown in Figure 3-2. The first step in performing the experiment was to divide the horizontal area where emissions of gas species are present into nine cells of equal size. One retroreflector was placed in each cell and was located so that the beam would pass through the center of the cell. After the nine retroreflectors were in place in their respective cells, a theodolite was used to measure the radial coordinates (radial distance, azimuth angle) for each retroreflectors, relative to the PI-ORS sensor. These coordinates are used to determine a kernel matrix containing information about beam length in each pixel, which is input to the horizontal RPM algorithm for locating the hot spot sources. There are nine beams in total, one to each retroreflector. The OP-FTIR source and detector are placed on a scanner at the origin (0,0).

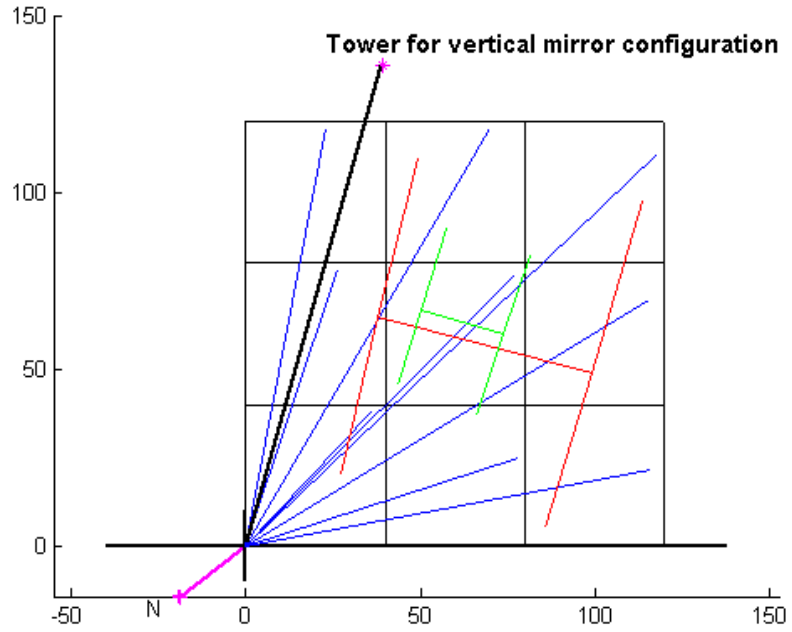

Figure 3-2. Experimental setup for horizontal scanning, with the tower configuration for vertical scanning.

When favorable wind conditions occur, a 40-foot high tower is set up at the location marked in Figure 2-2 and the flux through the vertical plane is computed with gases released in the small and large area source configurations. A two-dimensional, up to five-reflector array covering a plane 140 meters wide by 13 meters high (as illustrated in Figure 3-3) is set up for vertical scanning purposes with 3 mirrors on the tower.

All work on this project was carried out in compliance with the ARCADIS Corporate Health and Safety Manual. Specific safety information for the project is contained in this Health and Safety Protocol (HSP). The HSP includes a list of activities that may involve potential physical and chemical hazards while conducting research activities. The physical hazards involve the moving of heavy objects, setting up of scaffolding, handling of pressurized gas cylinders and liquid nitrogen. These are typical situation that our field personnel encounter. Sufficient number of personnel or labor saving devices will be employed when dealing with transporting heavy object. Appropriate protection equipment such as splash goggles and low temperature gloves will be provided for handing liquid nitrogen. The gases that may be utilized for this project may include nitrous oxide, acetylene, propane, propylene and ethylene. MSDS for these gases will be provided for the personnel. In the field, personnel may be exposed to a low level of common landfill gases. Depending on the level of exposures, appropriate protection equipment will be utilized. All field personnel were required to read the HSP prior to starting of the field activities.

3.6.2 Period of Operation

Measurements were taken between 8:00 am and 6:00 pm weekdays, weather permitting, from November 13, 2002 to May 6, 2003.

3.6.3 Amount/Treatment Rate of Material to be Treated

Not applicable.

3.6.4 Residuals Handling

This measurement method does not use any hazardous materials. No residuals are generated.

3.6.5 Operating Parameters for the Technology

This technology was operated in batch mode, with the operating parameters (e.g., number of mirrors, sampling duration/residence time) being varied under controlled conditions.

3.6.6 Experimental Design

The OP FTIR scans from reflector to reflector in a constant pattern, separately accumulating values for each reflector to generate a long-term average in each beam path.

3.6.6.1 Horizontal RPM

Figure 3-2 illustrates the nine-beam setup for the radial hot spot determination. The instrument is placed at the origin (0,0) and beams are preferably scanned with increasing angle from x-axis. The OP FTIR scans from reflector to reflector in a constant pattern, separately accumulating values for each reflector to generate a long-term average in each beam path.

When using OP-FTIR, the residence time on each beam is important for plumes that have low concentrations (close to detection levels). The longer the instrument collects data on each beam, the lower the detection level. In this demonstration, three residence times will be demonstrated: 10, 30, and 60 seconds. Randomly chosen point source locations were tested, with at least one source location in every pixel. For each source location, there were 3 runs (each run with a different residence time as mentioned above) of 12 complete cycles (a cycle is completed when data is collected for the 9 beams). A simulated area source (H pattern) released concurrently a different gas to demonstrate that the method can determine the existence of a hot spot or whether the source is homogeneous.

3.6.6.2 Vertical RPM

Once the horizontal scanning is done, the plume sources are determined. To quantify the emission from the area, the flux of gases exiting the area in the downwind direction is measured by vertical scanning. Using the RPM method, once the source is located after horizontal scanning, the array of reflectors is redeployed in a vertical plane centered downwind from the source. A two-dimensional, five-reflector array covering a plane 230-meters wide by 13-meters high is illustrated in Figure 3-3.

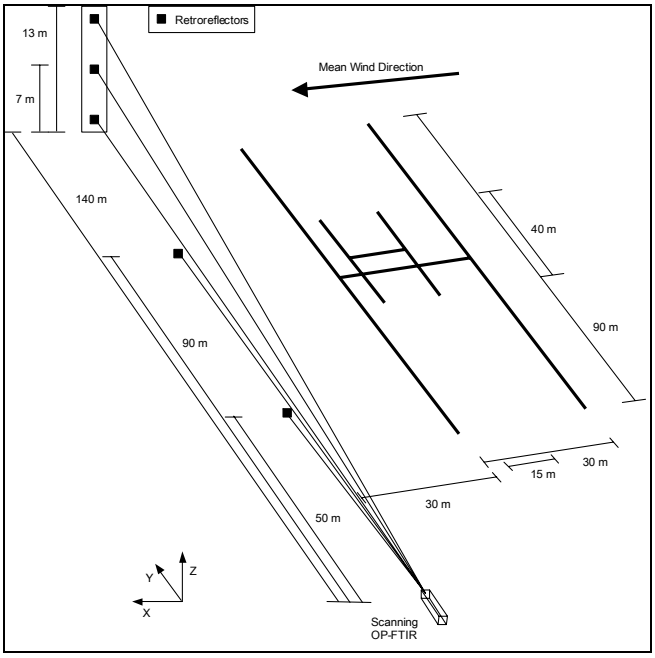

Figure 3-3: Configuration for crosswind plume measurement

Three basic downwind vertical beam configurations were to be validated and demonstrated. The 5-beam configuration was similar to the one in Figure 3-3. Configurations of 3-beams and 2-beams were also demonstrated to show the feasibility of this arrangement for the flux measurement, especially when resources are limited. The use of fewer beams will shorten the cycle time and may have better temporal residence on the significant beams, which are #3, and # 5 in Figure 3-3 (the bottom and top beams on the tower). To validate the range of source dimensions applicable for this method, the two simulated H-pattern sources differed in size, and the tracer gasses were released at a known flow rate.

Again, various time procedures were demonstrated, and each experiment took at least one hour. The entire sampling event – which had to take into consideration atmospheric conditions (wind direction and speed) and equipment issues – was completed from 13 November 2002 to 6 May 2003.

3.6.7 Demobilization

All equipment used for this validation study was portable. There are no significant demobilization issues associated with the use of this technology.

3.7 Selection of Analytical/Testing Methods and Testing Laboratory

The proposed PI-ORS technology does not require analytical testing methodology or the use of an analytical laboratory.

4. Data Analysis, Interpretation and Evaluation

Methods adopted for data analysis are explained in the following section with details.

4.1 OP-FTIR Data Processing

The interferogram is the initial form of a spectrum collected by OP-FTIR. The interferogram is the initial form of a spectrum collected by FTIR. Prior to use, the data must be converted to absorbance units and then to concentrations. The conversion from an interferogram to absorbance spectrum is performed using GRAMS-32 (by Galactic). GRAMS-32 is also the software that controls the Midac OP-FTIR instrument and creates the original interferogram file, which is archived.

The conversion from interferogram to absorbance spectrum is a multi-step process. First, the interferogram is converted to a single-beam spectrum by way of Fast Fourier Transform. Secondly, the absorbance spectrum is created by ratioing the sample single-beam spectrum to a reference single-beam spectrum. The absorbance spectra may be considered the final result of GRAMS-32.

The conversion of absorbance data to concentration-pathlength was performed using AIL-RAM 2000 software (AIL). Reference spectra will be both standard spectra generated by Infrared Analytics, Inc., and theoretical spectra generated by the HiTran program. Concentration-path length data will be converted to concentration through division by the optical pathlength. With the instrument operating in a monostatic mode, the optical pathlength is exactly twice the physical distance from the instrument head to the retroreflector.

4.2 Horizontal RPM

As described earlier, the area scanned by the FTIR is divided into pixels of equal size in such a way that each pixel has one beam ending in it. The kernel matrix, as explained in the following section, provides information about the amount of light absorbed from each beam in every pixel, if path integrated absorption measurements are provided. Once this information is obtained, a Non Negative Least Squares method (NNLS) gives the best fit for the concentration of the trace gas in each pixel. Interpolations are performed to smooth the concentration contours over the scanned area and the Concordance Correlation Factor (CCF) will be calculated for accuracy of the source location retrieved. A higher value of the coefficient of concordance means a stronger association. The reconstruction algorithm for obtaining concentration contour maps consists of two stages. First, an iterative inversion algorithm is used to retrieve average concentration in each of the nine pixels. Then, an interpolation procedure is applied to these 9 concentration values to calculate concentration in higher spatial resolution.

For the first stage of reconstructing the 9 average pixel concentrations, we apply an iterative algebraic deconvolution algorithm. The PIC, as a function of the field of concentration, is given by equation (1) as such:

$$PIC_k = \sum_m K_{km} c_m \qquad (1)$$

Where:

K = Kernel matrix that incorporates the specific beam geometry with the pixel dimensions

k = Number index for the beam paths

m = Number index for the pixels

c = Average concentration in the m^{th} pixel

Each value in the Kernel matrix *K* is the length of the k^{th} beam in the m^{th} pixel; therefore, the matrix is specific to the beam geometry. To solve for the average concentrations (one for each pixel) the NNLS was applied. The NNLS is similar to a classical least square optimization algorithm, but is constrained to provide the best fit of non-negative values. The NNLS algorithm was tested and compared to the relaxation multiplicative algebraic reconstruction technique (MART) program previously developed and used. Both algorithms gave very similar results when reached to the same maximal level of fit between the predicted PIC and the observed PIC, but the NNLS was much faster. Therefore, the NNLS algorithm will be applied in this study. This iterative procedure proceeds until the difference of the criteria parameter between sequential steps drops below a very small threshold value (tolerance). Multiplying the resulted vertical vector of averaged concentration by the matrix *K*, yields the end vector of predicted PIC data.

The CCF was used to represent the level of fit for the reconstruction in the path-integrated domain (predicted versus observed PIC). The second stage of the plume reconstruction is interpolation among the nine points, providing a peak concentration not limited only to the center of the pixels. The triangle-based cubic interpolation procedure will be used. To extrapolate data values beyond the peripheral pixel centers and within the rectangle measurement domain, we will assign the corner pixel concentration to the corner of the domain.

4.3 Vertical RPM

In earlier VRPM studies (Hashmonay and Yost, 1999a; Hashmonay et al., 2001), a bivariate Gaussian function was directly fitted to PI-ORS data to reconstruct the plume map in a vertical plane. In this smooth basis function minimization (SBFM) approach, a smooth basis function is assumed to describe the distribution of concentrations, and the search is for the unknown parameters of the basis function. Since interests were in the plane-integrated concentration and not the exact map of concentrations in the plane, only one smoothed basis function (one bivariate Gaussian) was fitted to reconstruct the smoothed map.

This process was computationally intensive and occasionally had difficulty converging to a reasonable solution with a high concordance correlation factor (CCF). Moving forward towards automated streamlined post analysis software and real-time measurement of flux has led to the

examination of more computationally favorable approaches. A two-phase computational approach was examined where a one-dimensional SBFM approach (Hashmonay and Yost, 1999b) to the ground level segmented beam paths was first applies, and then the reconstructed parameters as fixed values were substituted in the bivariate Gaussian function. This approach affords more degrees of freedom in the two-dimensional SBFM solution which was searching for only two parameters with five beams. The results of this approach were identical to the two-dimensional approach whenever it succeeded to converge to the same level of fit (comparable CCF).(Hashmonay et al., 2001) Therefore, modifying the two-dimensional SBFM approach to the two-phase SBFM approach (first univariate and bivariate Gaussian) did not change the resulting flux values but significantly improved the completeness of the analysis, as the search algorithm converged much faster and occasionally to a higher level of fit.

Since the second phase searches only for two parameters (vertical gradient and the magnitude of plume), it was realized that only the concentration data collected along the ground level long beam and the two elevated beams were essential for solving the equation and calculating the flux. The remaining ground level beam paths are essential to qualitatively assess the plume's peak location and dispersion but redundant for the plane integrated concentration used for the flux calculation. One can assume a wide range of plume's peaks and dispersion parameters and still get the same flux values. More detailed justifications for these assumptions are in the mathematical derivations that follow.

Once the parameters of the function are solved, the concentration values for every 2x2 m square elementary unit in a vertical plain are calculated. These values are then integrated incorporating wind speed data at each height level to compute the flux. At this stage, the concentration values are converted from parts per million by volume to grams per cubic meter, considering the molecular weight of the target gas, and ambient pressure and temperature. This enables the flux in grams per second using wind speed data in meters per second to be calculated directly.

Two Dimensional SBFM

Originally, it was assumed that the search algorithm for the unknown parameters must be simultaneous. A typical 5-beam VRPM configuration was found sufficient for the reconstruction procedure of one bivariate Gaussian. This beam geometry includes 5 beam paths in the crosswind vertical plane of which 3 beams of different pathlengths are at ground level and two beams are elevated by a vertical structure.

In each iterative step of the SBFM search procedure, the measured PIC values are compared with assumed PIC values, calculated from the new set of parameters. In order to compute the assumed PIC values, the basis function is integrated along the beam path's direction and path-length.

In the VRPM beam geometry, it was convenient to express the bivariate Gaussian function G in polar coordinates r and θ:

$$G(A,\rho_{12},m_y,m_z,\sigma_y,\sigma_z)=\frac{A}{2\pi\sigma_y\sigma_z\sqrt{1-\rho_{12}^2}}\exp\left\{-\frac{1}{2\left(1-\rho_{12}^2\right)}\left[\frac{(r\cdot\cos\theta-m_y)^2}{\sigma_y^2}-\frac{2\rho_{12}\left(r\cdot\cos\theta-m_y\right)\left(r\cdot\sin\theta-m_z\right)}{\sigma_y\sigma_z}+\frac{\left(r\cdot\sin\theta-m_z\right)^2}{\sigma_z^2}\right]\right\}$$

(4.3.1)

The bivariate Gaussian equation has six unknown independent parameters:

- A - normalizing coefficient which adjusts for the peak value of the bivariate surface;
- ρ_{12} - correlation coefficient which defines the direction of the distribution-independent variations in relation to the Cartesian directions y and z (ρ_{12}=0 means that the distribution variations overlap the Cartesian coordinates);
- m_y and m_z - peak locations in Cartesian coordinates;
- σ_y and σ_z - standard deviations in Cartesian coordinates.

Six independent beam paths would be sufficient to determine one bivariate Gaussian that has six independent unknown parameters. However, some reasonable assumptions have to be made to reduce the number of unknown parameters to four; e.g., setting the correlation parameter ρ_{12} equal to zero. This assumes that the reconstructed bivariate Gaussian is limited only to changes in the vertical and crosswind directions. When ground level emissions were known to exist the peak location in the vertical direction is also fixed to the ground level. This assumption can always be confirmed by examining the input PIC data. If the PIC of the ground level long beam is the highest of the three vertical beams, this assumption is valid. However, in this methodology, there is no requirement to apply *a priori* information on the source location and configuration. Under the above reasonable assumptions Eq. 1 is reduced to:

$$G(A,m_y,\sigma_y,\sigma_z)=\frac{A}{2\pi\sigma_y\sigma_z}\exp\left\{-\frac{1}{2}\left[\frac{(r\cdot\cos\theta-m_y)^2}{\sigma_y^2}+\frac{\left(r\cdot\sin\theta\right)^2}{\sigma_z^2}\right]\right\} \qquad (4.3.2)$$

To fit the unknown parameters of the smooth basis function to the PIC data, an error function for minimization has to be defined. The Sum of Squared Errors (SSE) function was defined in this study as:

$$SSE\left(A,m_y,\sigma_y,\sigma_z\right)=\sum_i\left(PIC_i-\int_0^{r_i}G(r_i,\theta_i,A,m_y,\sigma_y,\sigma_z)dr\right)^2 \qquad (4.3.3)$$

Where *PIC* represents the measured PIC values and the index *i* represents the different beams. The SSE function is minimized using the Simplex method (Press et al., 1992), to solve for the unknown parameters.

A typical result of this reconstruction procedure that uses data from a 5-beam VRPM configuration is shown in Figure 2. As previously mentioned, this process occasionally ended before completion of the search (low CCF) and was quite sensitive to the choice of the initial parameters (first guess). It was critical to find a more robust approach that would exhaust all opportunities to find the best fitted solution. This was when the two-phase SBFM approach was conceived.

As described in our earlier studies (Hashmonay et al., 1999; Hashmonay et al., 2001), the Concordance Correlation Factor (CCF) was used to represent the level of fit for the reconstruction in the path-integrated domain (predicted vs. observed PIC). The CCF is similar to the Pearson correlation coefficient, but is adjusted to account for shifts in location and scale. Like the Pearson correlation coefficient, CCF values are bounded between –1 and 1, yet the CCF can never exceed the absolute value of the Pearson correlation factor. For example, the CCF will be equal to the Pearson correlation when the linear regression line intercepts the ordinate at 0, its slope equals 1, and its absolute value will be lower than the Pearson correlation when the above conditions are not met.

CCF is defined as the product of two components:

$$CCF = rA \tag{4.3.4}$$

Where *r* is the Pearson correlation coefficient, and *A* is a correction factor for the shift in population and location. This shift is a function of the relationship between the averages and standard deviations of the measured and predicted PIC vectors:

$$A = \left[\frac{1}{2} \left(\frac{\sigma_{PIC_P}}{\sigma_{PIC_M}} + \frac{\sigma_{PIC_M}}{\sigma_{PIC_P}} + \left(\frac{\overline{PIC_P} - \overline{PIC_M}}{\sqrt{\sigma_{PIC_P} \sigma_{PIC_M}}} \right)^2 \right) \right]^{-1} \tag{4.3.5}$$

Where σ_{PIC_P} and σ_{PIC_M} are the standard deviations of the predicted and measured PIC vectors, respectively. $\overline{PIC_P}$ and $\overline{PIC_M}$ are the means of the predicted and measured PIC vectors, respectively. The Pearson correlation coefficient is a good indicator of the quality of fit to the Gaussian mathematical model. In our procedure typically *r* close to 1 will be followed by *A* very close to 1r. This means that the averages and standard deviations in the two concentration vectors are very similar and the mass is conserved (good flux value). However, when a poor CCF is reported (CCF<0.80) at the end of the fitting procedure it does not directly mean that the mass is not conserved. It could be a case where only a poor fit to the Gaussian function occurred if the correction factor *A* was still very close to 1 (A>0.90). However, when both *r* and *A* are low one can assume that the flux estimate is inaccurate.

Two-Phase SBFM

The two-phase SBFM approach replaced the direct bivariate SBFM approach in all cases where there were more than 3 beams along the ground level. In the two-phase SBFM approach, a one-dimensional SBFM reconstruction procedure is first applied in order to reconstruct the smoothed ground level and crosswind concentration profile. Then, the reconstructed parameters can be substitute into the bivariate Gaussian function before applying the two-dimensional SBFM procedure. The resulting plume map is identical to the simultaneous two dimensional plume map, and actually the plume map illustrated in Figure 2 is a result of the two phase process. This is the preferred approach which has been applied to the VRPM software in the last 3 years.

A one dimensional SBFM reconstruction is applied to the ground level segmented beam paths (Figure 1) of the same beam geometry to find the cross wind concentration profile (Hashmonay and Yost 1999b). As before, a Gaussian function is fitted to measured PIC ground level values, but now as a univariate function. The error function for the minimization procedure is again the Sum of Squared Errors (SSE) function and it is defined in the one dimensional SBFM approach as follows:

$$SSE(B_j, m_{y_j}, \sigma_{y_j}) = \sum_i \left(PIC_i - \sum_j \frac{B_j}{\sqrt{2\pi}\sigma_{y_j}} \int_0^{r_i} \exp\left[-\frac{1}{2}\left(\frac{m_{y_j} - r}{\sigma_{y_j}} \right)^2 \right] dr \right)^2 \qquad (4.3.6)$$

Where B is equal to the area under the one dimensional Gaussian distribution (integrated concentration), r_i is the pathlength of the i^{th} beam, m_y is the mean (peak location) and σ_y is the standard deviation of the j^{th} Gaussian function. PIC_i is the measured path integrated concentration value of the i^{th} path. Again, the same simplex algorithm is used to retrieve the unknown parameters. It was shown (Hashmonay and Yost, 1999b) that when there are more than 3 beams at the ground level, two Gaussian functions can be fitted to retrieve skewed and sometimes bi-modal concentration profiles (see Figure 3). This is the reason for the index j in Eq. 6.

Substituting the standard deviation and peak location retrieved in the one-dimensional SBFM procedure in Eq. 3 for applying the two-dimensional phase of the two-phase process yields:

$$G(A, \sigma_z) = \frac{A}{2\pi\sigma_{y-1D}\sigma_z} \exp\left\{ -\frac{1}{2}\left[\frac{(r \cdot \cos\theta - m_{y-1D})^2}{\sigma_{y-1D}^2} + \frac{(r \cdot \sin\theta)^2}{\sigma_z^2} \right] \right\} \qquad (4.3.7)$$

Where $\sigma_{y\text{-}1D}$ and $m_{y\text{-}1D}$ are the standard deviation and peak location respectively along the crosswind direction that are found in the one dimensional SBFM procedure. Since only two parameters are left to be found in the second phase, it is sufficient to apply only three beams in the second phase of the search. This led to the recognition that only the one long beam along the ground level and the two elevated beams that sample the vertical gradient are essential

information for the flux values through the vertical plane. On occasions when the qualitative crosswind location and width of the plume are not necessary it is strongly recommended to apply the three-beam VRPM configuration and not to waste time and resources collecting concentration data for the intermediate ground-level beam-paths.

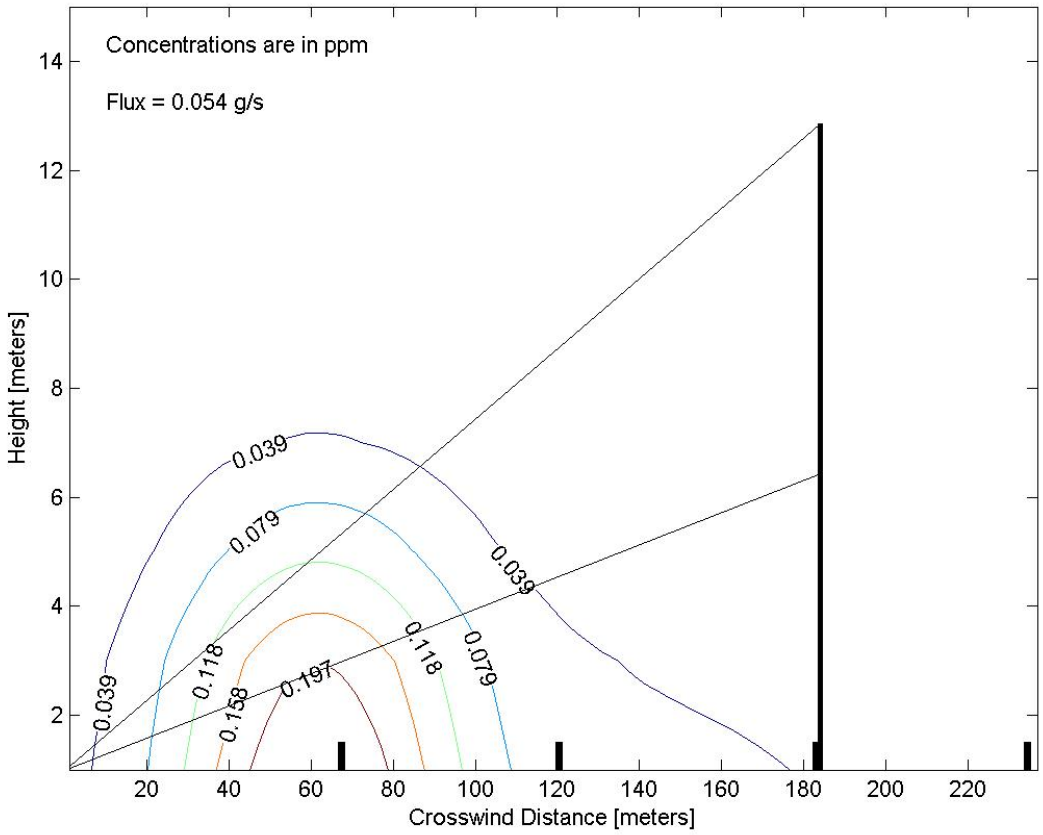

Figure 4.3.2 – An example of a two bivariate Gaussian fit for four beams along the ground level (HF emissions from phosphate industry.

Three Beam VRPM Configuration

When the VRPM configuration consists only of 3 beam paths, one at the ground and the other two elevated, the one-dimensional phase can be skipped, assuming that the plume is very wide. In this scenario, peak location can be arbitrarily assigned to be in the middle of the configuration. Therefore the 3-beam VRPM configuration is most suitable for area sources (where no localized hot spot is expected) or for sources with a series of point and fugitive sources that are known to be distributed across the upwind area. In this case the bivariate Gaussian has the same two unknown parameter as in the second phase (Eq. 5) but information about the plume width or location is not known. The standard deviation in the crosswind direction is typically assumed to

be about 10 times that of the ground level beam path. If r_1 represents the length of the vertical plane the bivariate Gaussian would be as follows:

$$G(A,\sigma_z) = \frac{A}{2\pi(10r_1)\sigma_z}\exp\left\{-\frac{1}{2}\left[\frac{(r\cdot\cos\theta - \tfrac{1}{2}r_1)^2}{(10r_1)^2} + \frac{(r\cdot\sin\theta)^2}{\sigma_z^2}\right]\right\} \qquad (4.3.8)$$

This process is for determining the vertical gradient in concentration. This allows an accurate integration of concentrations across the vertical plane as the long beam ground level PIC provides a direct integration of concentration at the lowest level.

A visual example of a typical plume map reconstruction for the 3-beam configuration is given in Figure 4.

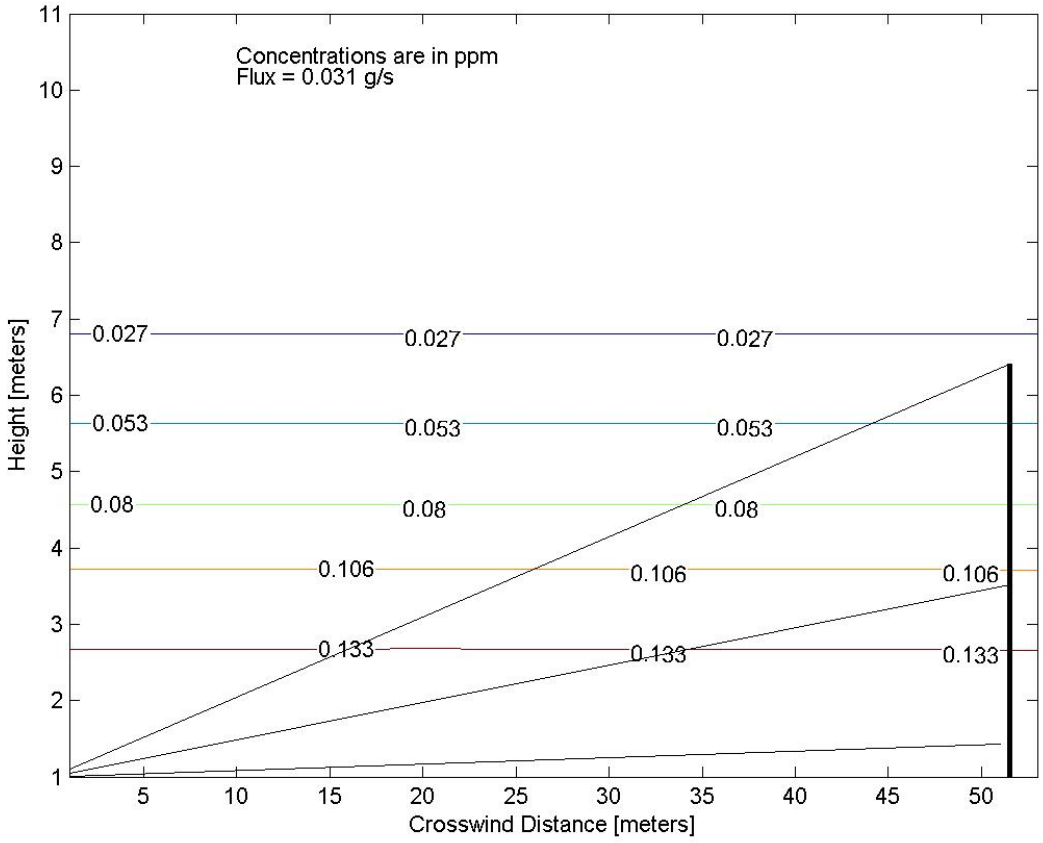

Figure 4.3.3 – An example of 3-beam reconstruction from Costco gas station.

Averaging scheme

In order to develop a reliable time-averaged plume profile, replicate measurements at each beam path are necessary. Therefore, the sampling time at each retroreflector should be as short as

practical limits allow. Then the PIC data are averaged for each beam path prior to application of the reconstruction method.

Using moving averages of several grouped cycles of path-integrated concentrations prior to the reconstruction yields better prediction of the flux. Since fluxes are expected to be most representative of the emission rate of the source when wind direction is close to perpendicular, it is essential to slide these grouped cycles. For example, if the PICs from cycle 1 through cycle 3 are averaged and then the PICs from cycle 4 through 6 are averaged, a group of cycles in between (2-4 or 3-5) that might have better wind conditions for the emission rate estimate could be missed. This has historically been the source for the underestimation of the emission rates measured during unstable wind conditions before this data averaging scheme was implemented. (Hashmonay et al., 2001) In order to assess the quality-of-fit for each reconstruction, the CCF is computed. The CCF is found to be significantly better using moving averages for a group of three cycles or more. Furthermore, variability in flux determinations is significantly reduced for moving averages for a group of three cycles or more. (see Figure 5).

5. Cost Assessment

At the completion of this demonstration project, the ECAM will be used to develop and validate, to the extent possible, the expected operational costs of the IP-ORS technology. However, Section 2.3 presents a theoretical cost comparison between the current conventional approach of an air monitoring plan utilizing SUMMA canisters and dispersion modeling and the proposed PI-ORS methodology.

6. Implementation Issues

At the completion of this demonstration project, the regulatory and end-user issues for this proposed technology will be presented.

7. Results and Discussion

7.1 Vertical RPM for Flux Measurements

The plane-integrated concentration from a reconstructed mass equivalent concentration map, along with the averaged wind data, provides an estimate of the total flux from the upwind emission source. Source strength is effectively the product of the sum of the area concentration elements multiplied by the average component of the wind speed normal to the measurement plane during the determinations. In addition to the five-beam configuration, this study used a three-beam configuration geometry (the three mirrors on the tower were used, the bottom mirror being close to the ground) and a two-beam configuration geometry (the top and bottom mirrors on the tower were used) for measuring flux from the simulated area source. The results of plume reconstruction and flux measurements from an area were compared from the three configurations described above.

In order to demonstrate the ability of this method to measure fluxes from an area source, ethylene was released in the small area setup as shown in Figure 3-3. The results shown here are from a five-beam configuration in which the three mirrors on the ground locate the plume maximum in the vertical scanning plane. Figure 7-1 shows the mass equivalent reconstructed plume for ethylene release on 25 November 2002.

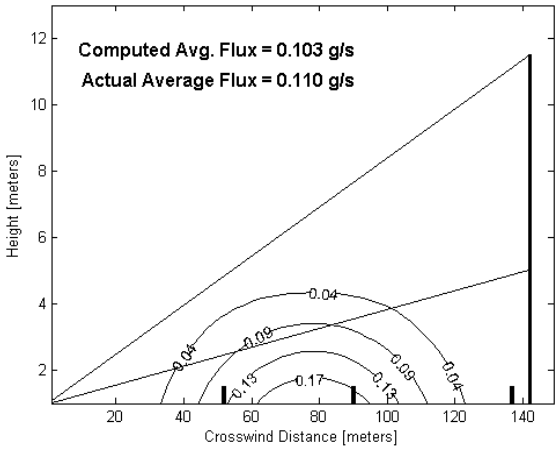

Figure 7-1: Ethylene plume reconstruction in the vertical for flux measurements

Dependence of the flux calculations and moving average grouping is shown in Figure 7-2. In order to assess the quality-of-fit of the plume reconstruction procedure for each moving average grouping, CCFs are computed for each reconstruction. Typically CCF is found to be greater than 0.9 for moving averages of a group of three or larger.

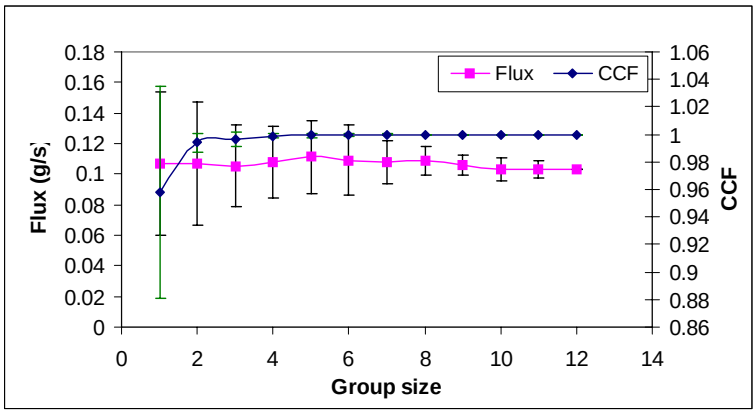

Figure 7-2: Dependence of flux estimation on group size for moving average

A time plot of the flux estimation for ethylene trace release with a moving average of a group of three cycles is shown in Figure 7-3. The solid horizontal line corresponds to the actual mass released for the entire duration of 69 minutes. The total emission estimation depends on the wind condition perpendicular to the plane of vertical scanning. Average wind direction perpendicular to the vertical plane of scanning is also shown in the figure. The strong anti-correlation between the wind direction from perpendicular and the total emission estimation can be observed in the figure when wind direction is larger than 30^0. Examining the differences of fluxes over time revealed a wind direction range of 40º where fluxes did not correlate with wind direction. The range of wind angles from normal to the VRPM plane was between -10^0 and $+30^0$. This indicates that when winds where within this range of angles there was a good plume capture and flux differences could be attributed to changes in release rate and atmospheric fluctuations. In this case most of the plumes were likely to be captured with the setup.

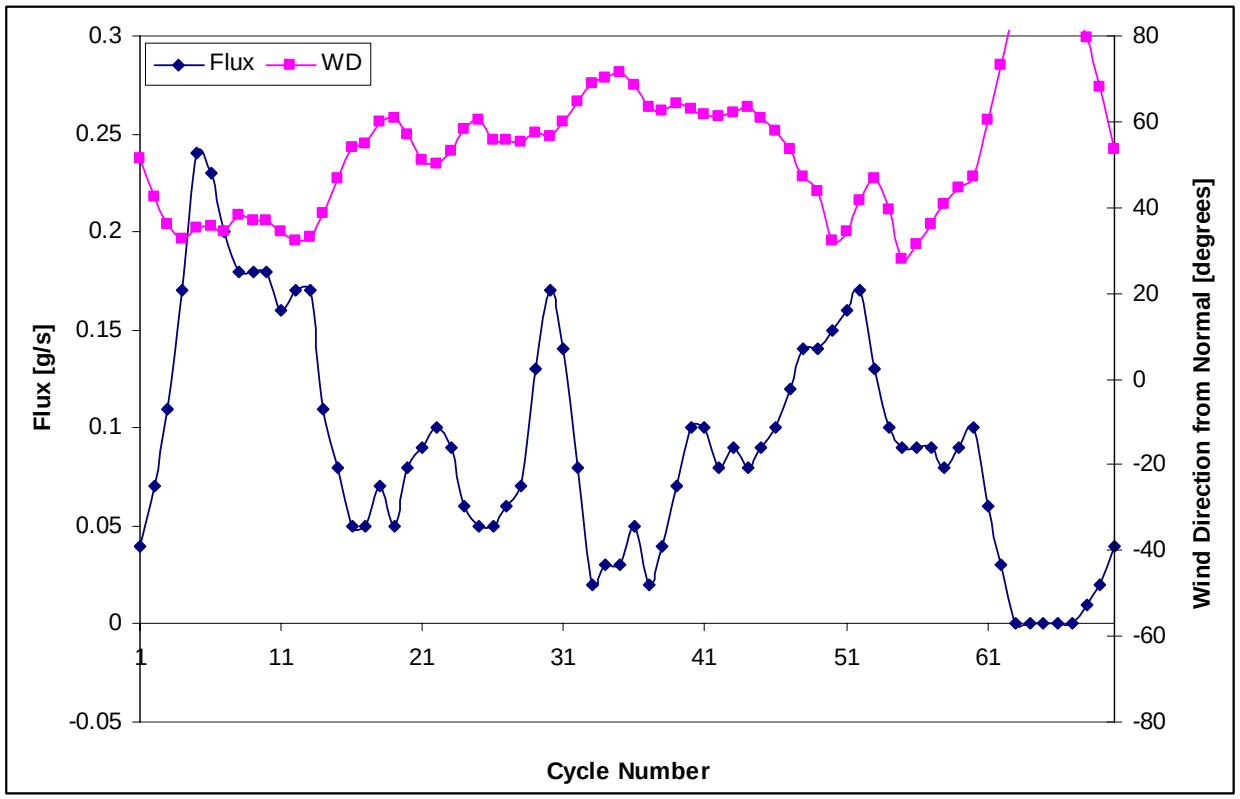

Figure 7-3: Time series of emission calculation for Ethylene release as an area source

In the following we present the data with a grouping size of 3 for the moving averages, although in some cases it may be better to average more number of lines. All the figures presented will be the run average.

The first 5-beam experiment to be analyzed was performed on 2 October 2002, and involved the controlled release of ethylene gas monitored for 12 cycles at 60-second intervals. As can be seen in the data tables and figures in Section 1 of Appendix A, the overall run averages gives a CCF of 1.00, a flux of 0.98 g/s, wind speed of 1.81 m/s, and wind direction of 2° from perpendicular. This slightly underestimates the average actual flux of 1.01 g/s.

The next 5-beam experiment to be analyzed was performed on 25 November 2002, and involved the controlled release of ethylene gas monitored for 12 cycles at 60-second intervals. As can be seen in the data tables and figures in Section 1 of Appendix A, the overall run averages give a flux of 0.11 g/s. The table shows averages calculated with a grouping of 3. The actual average flux of 0.11 g/s was perfectly calculated for this run.

The next set of vertical scan results another 5-beam experiment with the release of ethylene gas. In this setup, which was conducted on 25 November 2002, involved monitoring for 24 cycles at 30-second intervals. Averaging with a grouping of three gives an average flux of 0.22. the actual average flux of 0.20 g/s, was overestimated by 10%.

The third run for 5-beam vertical scans was taken on 23 December 2003, when the release of ethylene gas was monitored for 72 cycles at 10-second intervals. As can be seen in the table and Figure the underestimation of the results is due to wind directions far from perpendicular. If we calculate the fluxes only for wind directions smaller than 40^0 (no winds below 30^0 in this run) the emission rate estimate is 0.16 g/s which is under estimating the actual (0.21 g/s) by 25%. This run is brought in this report to demonstrate that even though wind direction were out of the acceptable range for this experimental configuration (-10^0 - $+30^0$) reasonable emission rate estimate can be retrieved within 25% of the actual release rate.

Table 7-1 summarizes the results of all applicable runs (acceptable wind direction range and all instruments functioning) for 5-beam and 3-beam VRPM configurations. The fluxes given in Table 7-1 include a separate column for the time periods when the acceptance criteria for wind direction was met and for the whole run. The fact that the % difference for the whole run fluxes is a always equal or greater then the % difference for the selected fluxes (emission rate) in the acceptable wind direction range is evidence that the plume capture is partially outside the acceptable wind direction range. This acceptable wind direction range is very specific for the coupled configuration and source sizes. However, examining the correlations, as above, would indicate the acceptable range for good plume capture. Furthermore, this range would not necessarily be symmetric around the direction normal to plane as was shown in previous simulation studies (Hashmonay and Yost, 1999a). All emission rate estimates in the 3-beam runs of the Duke Forest study were within ±10% of the actual average release rate.

The 2-beam configurations provided severe underestimation (more than -50%) of the actual flux for all time resolution. This is because of below detection level readings for the upper-beam (for all applicable runs). Assuming 0 concentration value for very low rate releases negatively biases the flux calculations. In order to demonstrate the feasibility of the 2-beam VRPM configuration the controlled release should be repeated in much higher release rate or with more sensitive ORS instrument.

Table 7-1: Summary of the controlled releases performance.

	# of beams	Time Resolution	Gas	Emission Rate Estimate [% difference] -10^0 – $+30^0$	Measured Flux [% difference] All run	Wind direction Range
NH 10/02	5	60	Ethylene	-4	-4	-15^0 and $+7^0$
DF 11/25/02	5	60	Ethylene	+3	+3	-7^0 and $+8^0$
DF 11/25/02	5	30	Ethylene	+10	+10	-6^0 and $+25^0$
DF 12/13/02	5	30	Ethylene	-54	-24	$+28^0$ and $+88^0$
DF 01/09/03	3	10	Ethylene	-6.5	-19	-3^0 and $+51^0$
DF 01/29/03	3	30	Ethylene	-1.8	-8.9	-18^0 and $+15^0$
DF 01/29/03	3	60	Ethylene	+6.9	-15	-17^0 and -3^0
DF 05/06/03	3	10	Propane	+5.2	+1.2	$+9^0$ and $+34^0$
DF 05/06/03	3	10	Ethylene	+8.6	-13	$+9^0$ and $+34^0$

7.2 Radial Horizontal (Surface) Scanning for Source Locations

Several trace gases were released at random locations chosen arbitrarily and measurements made with 10 sec, 30 sec and 60 sec scan/mirror. We discuss in this section the results obtained from the controlled release at random locations. The OP-ORS method with RPM algorithm was able to locate accurately the source of release in most cases, although exceptions are there due to various instabilities. The conditions for which one ought to be careful while using RPM techniques are discussed later in Section 7.3. Figure 7-4 shows an example of source location using the ORS method. Acetylene was released close to the center of pixel 8 and was reconstructed. This experiment was performed on November 14, 2003 with 30 second scanning on each mirror and 18 scanning loops in total. This figure shows the computation from the average of all the loops. The computed location of the source (red star) was located close to the actual acetylene source location (red circle) on all loops. The dislocation distance (distance between actual release location and the predicted one) is shown with double headed arrow. The error in plume location in this case is 17 m.

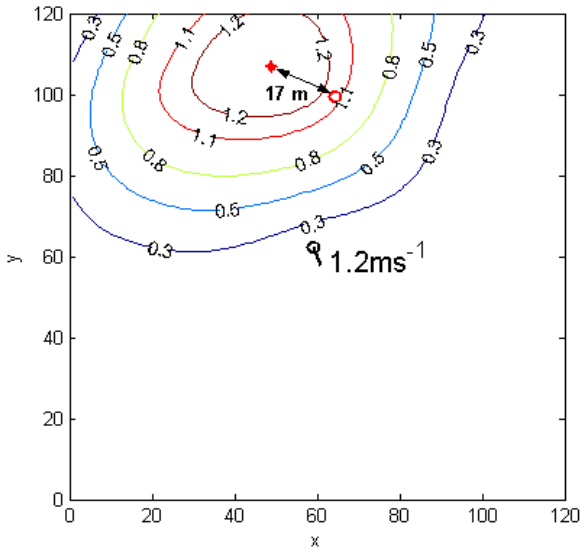

Figure 7-4: Plume source location using ORS method by horizontal scanning

We found the moving averages of the path-integrated concentrations prior to the reconstruction yields better prediction of the source location. Dependence of the moving average and the distance between actual and predicted source location is shown in Figure 7-5. In order to assess the accuracy of reconstruction for each moving average group, concordance correlation coefficients (CCF) are computed for each reconstruction. CCF is found to be better for moving averages of a group of four or larger.

The CCF is similar to the Pearson correlation coefficient, but is adjusted to account for shifts in location and scale. CCF values are bounded between 0 and 1, yet the CCF can never exceed the

absolute value of the Pearson correlation factor. For example, the CCF will be equal to the Pearson correlation when the linear regression line intercepts the ordinate at 0 and the slope equals 1. The absolute value will be lower than the Pearson correlation when the above conditions are not met.

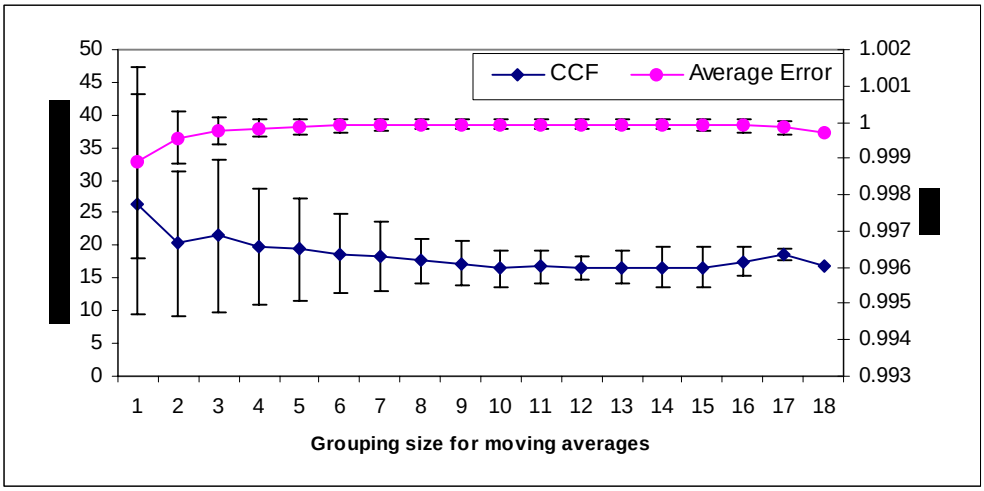

Figure 7-5: Dependence of source location accuracy on group size for moving average

Source location reconstruction of the area sources were performed, with nitrous oxide as trace gas, in a similar manner and obtained similar results.

In the following we present the data with a grouping size of 4 for moving averages, although in some cases it may be better to average more number of lines. All the figures presented will be the run average. It should be noted that the pixel placement of the controlled-release gases and chronological ordering of scans were randomly chosen. The results will be here discussed, however, according to ascending pixel numbers, for the purpose of a more logical summary progression.

The first set of data to be discussed from Pixel 9, measured on 5 February 2003, involved the monitoring at 10-second intervals of an acetylene gas release. As can be seen in Section 1 of Appendix B, the analyzed results give an average CCF of 1.00 with a standard deviation of 0.00, and an average distance from actual release to the predicted one of 17.08 m with a standard deviation of 0.00. A quick examination of the data table and figures reveals evidence of the accuracy of the findings, as these results closely approach the ideal.

The next set of results from Pixel 9 was measured on 14 November 2002, and depicts the release of ethylene monitored at 30-second intervals. The table in Section 1 of Appendix B details the findings, which yield an average CCF of 1.00 with a standard deviation of 0.00 and an average predicted distance from actual source of 21.05 m with a standard deviation of 3.36. These numbers are deceptive; however, as can be seen in the data table, which lists a sharp drop in distance readings in the last group to 8.90 m. Excluding the anomalous group #15 data, the average distance for the run is calculated at 21.92 m with a standard deviation of 0.035.

Finally, acetylene released in Pixel 9 was measured on 5 February 2003 at 60-second intervals, and the results are shown in Section 1 of Appendix B. The table gives an average CCF of 1.00 with a standard deviation of 0.00 and an average distance from actual to predicted release of 17.46 m with a standard deviation of 0.41. Here again the unambiguous nature of the data is reflected in the data tables and figures.

The first set of data to be discussed from Pixel 8, measured on 13 November 2002, involved the monitoring at 10-second intervals of an acetylene gas release. As can be seen in Section 2 of Appendix B, the analyzed results give an average CCF of 1.00 with a standard deviation of 0.00, and an average distance from actual release to the predicted one of 8.38 m with a standard deviation of 6.28. These numbers are deceptive, however, as can be seen in the data table. For the vast majority of the groups, the distance is recorded as steady at 6.88 with no variation; however, the readings for groups 3 through 6 depict a sudden fluctuation giving a spike at 35.68 m for group #4. With this data (groups 3 through 6) removed from the results, the average distance is 6.88 m with a standard deviation of 0.00 for the remaining 17 groups. This spike would seem to be an anomaly. Although no wind data is available for correlation, it is suspected that a sudden gust of wind may have caused the source to be picked up by a neighboring beam, and thus registered erroneously in Pixel 9 for a brief moment.

The next set of results from Pixel 8 was also measured on 13 November 2002, and depicts the release of acetylene monitored at 30-second intervals. The table in Section 2 of Appendix B details the findings, which yield an average CCF of 1.00 with a standard deviation of 0.00 and an average predicted distance from actual source of 6.88 m with a standard deviation of 0.00. These findings are nearly perfect, as shown in the figures and data table. Furthermore, there is a clear correlation between these results and the majority of the readings from the 10-second monitoring discussed in the previous paragraph. This would seem to confirm the aforementioned theory concerning the anomalous data spike in the 10-second monitoring data.

Finally, ethylene released in Pixel 8 was measured on 5 February 2003 at 60-second intervals, and the results are shown in Section 2 of Appendix B. The table gives an average CCF of 1.00 with a standard deviation of 0.000 and an average distance from actual to predicted release of 15.73 m with a standard deviation of 0.00. Here again the simplicity of the data is reflected in the data tables and figures.

The first set of data to be discussed from Pixel 7, measured on 5 February 2003, involved the monitoring at 10-second intervals of a propylene gas release. As can be seen in Section 3 of Appendix B, the analyzed results give an average CCF of 1.00 with a standard deviation of 0.00, and an average distance from actual release to the predicted one of 10.06 m with a standard deviation of 0.00. A quick examination of the data table and figures reveals evidence of the accuracy of the findings, as these results closely approach the ideal.

The next set of results from Pixel 7 was measured on 13 November 2002, and depicts the release of propane monitored at 30-second intervals. The table in Section 3 Appendix B details the findings, which yield an average CCF of 1.00 with a standard deviation of 0.00 and an average predicted distance from actual source of 4.12 m with a standard deviation of 0.00. Again, the findings are nearly perfect, as shown in the figures and data table.

Finally, ethylene released in Pixel 7 was measured on 5 February 2003 at 60-second intervals, and the results are shown in Section 3 of Appendix B. The table gives an average CCF of 1.00 with a standard deviation of 0.000 and an average distance from actual to predicted release of 10.06 m with a standard deviation of 0.00. Here the unanticipated similarity to the results of the aforementioned 10-second monitoring should be noted, along with the lucidity of the data tables and figures.

The only set of results to be presented from Pixel 6 was measured on 14 November 2002, and depicts the release of propylene monitored at 30-second intervals. The table in Section 4 of Appendix B details the findings, which yield an average CCF of 0.99 with a standard deviation of 0.004 and an average predicted distance from actual source of 8.60 m with a standard deviation of 0.24. Here the clarity of the data table and figures should be noted, as the results provide very little variation.

The first set of data to be discussed from Pixel 5, measured on 5 November 2002, involved the monitoring at 10-second intervals of an ethylene gas release. As can be seen in Section 5 of Appendix B, the analyzed results give an average CCF of 0.98 with a standard deviation of 0.004, and an average distance from actual release to the predicted one of 5.43 m with a standard deviation of 0.000. A quick examination of the data table and figures reveals evidence of the accuracy of the findings.

The next set of results from Pixel 5 was also measured on 5 November 2002, and depicts the release of ethylene monitored at 30-second intervals. The table in Section 5 of Appendix B details the findings, which yield an average CCF of 0.97 with a standard deviation of 0.006 and an average predicted distance from actual source of 5.43 m with a standard deviation of 0.000. Here the similarity to the results of the aforementioned 10-second monitoring should be noted along with the clarity of the data table and figures.

Finally, ethylene released in Pixel 5 was measured on 12 December 2002 at 60-second intervals, and the results are shown in Section 5 of Appendix B. The table gives an average CCF of 0.62 with a standard deviation of 0.094 and an average distance from actual to predicted release of 32.78 m with a standard deviation of 27.87. These numbers are deceptive, however, as can be seen in the data table. Groups 1 through 4 show consistent distance readings of 3.40 with a CCF of 0.55 at a standard deviation of 0.005, while a sharp change for groups 5 through 9 gives consistent distance measurements of 56.28 and a CCF of 0.68 with a standard deviation of 0.092. This surprising change coincides with a sudden wind shift from 150° to 210°.

The first set of data to be discussed from Pixel 4, measured on 20 November 2002, involved the monitoring at 10-second intervals of a propane gas release. As can be seen in Section 6 of Appendix B, when the results are analyzed, the average CCF is 0.89 with a standard deviation of 0.103, and the average distance from actual release to the predicted one is 21.7 m with a standard deviation of 15.8. The table reveals that the CCF moved over a wide range, registering from 0.62 to 1.00 and that the range of the distance readings is even more extensive, with a low of 3.05 and a high of 39.25. There seems to be a correlation in the results that when the CCF is high, as in groups 2 through 6 and groups 14 through 18 (group 19 seems to be an anomaly), the distance results are also high. For these groups only, the average CCF is 0.97 with a standard deviation of 0.022, and the average distance is 37.04 m with a standard deviation of 1.6.

The next set of results from Pixel 4 was measured on 18 November 2002, and depicts the release of propane monitored at 30-second intervals. The table in Section 6 of Appendix B details the findings, which yield an average CCF of 0.81 with a standard deviation of 0.119 and an average predicted distance from actual source of 21.4 m with a standard deviation of 6.4. The CCF is at its highest in the last three groups, which calculate an average of 0.99 with a standard deviation of 0.006 and an average distance of 28.13 with a standard deviation of 0.069. For the most part, however, the results are rather variable, and the CCF is somewhat low.

Finally, propane released in Pixel 4 was also measured on 18 November 2002 at 60-second intervals, and the results are shown in Section 6 of Appendix B. The table gives an average CCF of 0.83 with a standard deviation of 0.080 and an average distance from actual to predicted release of 17.73 m with a standard deviation of 1.059. Although the distance readings are generally consistent here, the CCF values are again a bit low.

The first set of data for Pixel 3, measured on 19 November 2002, involved the monitoring at 10-second intervals of a propylene gas release. As can be seen in Section 7 of Appendix B, the average CCF is 0.99 with a standard deviation of 0.034, and the average distance from actual release to the predicted one is 17.50 m with a standard deviation of 4.3. An obvious deviation appears in the last two groups, however, in which the CCF is 0.89 and the distance is 30.04. Excluding these two groups, the results for groups 1 through 19 give a CCF of 1.00 with a standard deviation of 0.002, and an average distance of 16.10 m with a standard deviation of 0.45.

Another set of readings for Pixel 3 at 10-second intervals involved the release of propylene gas on 20 November 2002. These results were more uniform throughout than the case under similar conditions mentioned above. The CCF and distance from actual to predicted sources were very steady for all 21 groups, yielding average values of 1.00 with a standard deviation of 0.002 and 5.1 m with a standard deviation of 0.2, respectively.

The next set of results from Pixel 3 was measured on 20 November 2002, and depicts the release of propylene monitored at 30-second intervals. The table in Section 7 of Appendix B details the findings, which yield an average CCF of 1.00 with a standard deviation of 0.005 and an average predicted distance from actual source of 4.92 m with a standard deviation of 0.2. Both figures provide visual representations of the accuracy of these results.

Finally, propylene released in Pixel 3 was measured on 20 November 2002 at 60-second intervals, and the results are shown in Section 7 of Appendix B. The table gives an average CCF of 1.00 with a standard deviation of 0.000 and an average distance from actual to predicted release of 4.61 m with a standard deviation of 0.7. Again, the readings were very stable, and their stability is evident in the provided figures.

The first set of data to be discussed from Pixel 2, measured on 20 November 2002, involved the monitoring at 10-second intervals of an acetylene gas release. As can be seen in Section 8 of Appendix B, when the results are analyzed with an average grouping of four, the average CCF is 0.75 with a standard deviation of 0.067, and the average distance from actual release to the predicted one is 7.31 meters (m) with a standard deviation of 0.525. The table also reveals that

the CCF never moved above 0.89, and that after group #6, the distance from predicted to actual remained steady at 7.40 m.

The next set of results from Pixel 2 was also measured on 20 November 2002, and depicts the release of acetylene monitored at 30-second intervals. The table in Section 8 of Appendix B details the findings, which yield an average CCF of 0.68 with a standard deviation of 0.091 and an average predicted distance from actual source of 8.13 m with a standard deviation of 1.0. Here the CCF is at its highest in the first two groupings, moving from 0.91 to 0.84, and then varying below 0.70 for the remainder of the groupings. The distance reads steady at 7.40, with the exception of a jump to 9.12 for group #5 and elevated levels in the last four groups.

Finally, acetylene released in Pixel 2 was measured on 21 November 2002 at 60-second intervals, and the results are shown in Section 8 of Appendix B. The table gives an average CCF of 0.78 with a standard deviation of 0.046 and an average distance from actual to predicted release of 6.73 m with a standard deviation of 1.3. The CCF value never rises above 0.84, and the distance values, while residing for the most part at 7.40, exhibit a wide range of readings, from 3.82 to 7.77 over the course of the nine groups.

The data measured from Pixel 1 was quite inconsistent, as can be seen in the data tables and figures in Section 9 of Appendix B. Possible explanations for this phenomenon will be explored later in Section 7.3.

7.3 Further Discussion

7.3.1 Issues with Radial Horizontal Scans

Table 7-2 below gives the summary of the source location and the percentage error when compared to the diagonal length of the area (170 m) for 60 sec/mirror scanning. When the measurement conditions are stable, the displacement of the artificial hot spot relative to the area diagonal distance is 10% or less. Although the selection of locations was arbitrary, the results are given in the order of pixel number in which release was made. Pixel number 1 is not included because of the high fluctuations in location. This is because all the beams are present in pixel 1 and when the release gradient is non-isotropic, which is true in our case, the NNLS algorithm puts the plume location at the center of a pixel, which corresponds to the beam that detects the released gas the most. The high error in pixel number 5 in Table 7-1 can be attributed to a very sharp wind direction shift after the 6^{th} cycle. The beams for pixel 5 and pixel 9 pass very close to each other and the one corresponding to pixel 9 begins detecting most of the released gas after the wind shift.

Table 7-2: Summary for 60 sec/mirror scanning

Pixel	D (m)	Error wrt diagonal distance (170 m)	Remarks
2	6.7	4.0%	
3	4.6	2.7%	
4	17.7	10.4%	
5	32.7	19.2%	very sharp wind shift
7	10.0	5.9%	
8	15.7	9.3%	
9	17.5	10.3%	

Table 7-3 below gives the summary of the source location and the percentage error when compared to the diagonal length of the area (170 m) for 30 sec/mirror scanning. Except when experimental conditions are unstable, the displacement of the artificial hot spot relative to the area diagonal distance is 10% or less. This is also true for the 10 sec/mirror scanning, which is shown in Table 7-4 below.

Table 7-3: Summary for 30 sec/mirror scanning

Pixel	D (m)	Error wrt diagonal distance (170 m)	Remarks
2	8.1	4.8%	
3	4.9	2.9%	
4	21.4	12.6%	sharp wind shift
5	5.4	3.2%	
6	8.6	5.1%	
7	4.1	2.4%	
8	6.9	4.0%	
9	21.1	12.4%	

Table 7-4: Summary for 10 sec/mirror scanning

Pixel	D (m)	Error wrt diagonal distance (170 m)	Remarks
2	7.3	4.3%	
3	17.5	10.3%	last 2 cycles large error
3	5.1	3.0%	
4	21.7	12.8%	low and variable wind
5	5.4	3.2%	
7	10.1	5.9%	
8	8.4	4.9%	one cycle has anomalous
9	17.1	10.0%	

All of the above results are obtained using the radial plume re-construction of a moving average of grouping of four cycles and then averaging the dislocation distance (D). In some cases of atmospheric instabilities (such as a sharp wind shift, etc.), it may be advisable to perform re-construction every cycle and from the data combined with wind direction it may be possible to conclude the actual hot spot. Analysis on this front will be continued when demonstrations in real time are performed at various defense installations.

One recommendation for future controlled release studies for hot spot location is to modify the geometry of the simulated trace gas release to more closely resemble an actual fugitive source in the environment. One way to do this is to construct, with soaker hoses, a hexagonal structure (smaller than one pixel area would be ideal), with diagonals connected at the center of the structure. The release should be made at the center of the structure, which would ensure that the gradient of emission is along the diagonals of the structure.

7.3.2 Issues with Radial Vertical scans for flux measurements

Our results also seem to state that a three-beam configuration is sufficient for obtaining reliable flux measurements. The advantage of using five-beam configuration is that the additional two beams allow one to obtain a mass-equivalent plume-shape in order to assess the extent of plume divergence when the source is close by, as in the case a fugitive emission of methane from an active landfill, for example.

It is advisable that two-beam configuration be used mainly for upwind background measurements where the vertical gradient information is close to constant and two-beam measurements will be accurate enough for background estimation.

It was also noted that no differences were found among 10 sec, 30 sec or 60 sec scan/mirror. Therefore, it is recommended that 30 sec/mirror, in any number of mirrors configuration, may be a better choice for stable conditions in order to have a reasonable detection (and low signal-to-noise ratio) limit and will be followed during the demonstration at the bases.

It is to be noted that the results shown here are from Ethylene and Propane release only. Nitrous oxide (N_2O) was found to be under-estimated in all cases, possibly due to adsorption and other reactions in the atmosphere. This phenomenon must be inspected further. The gases were released in large H-structures as well as a small H-structure and significant differences were not noticed. This may be because both the H-structures were within the total length of the measurement vertical plane and when winds are favorable, not much of the release are likely to be lost. This aspect will be looked into while performing future demonstrations.

8. References

1. Childers, J.W.; Thompson, E.L.; Harris, D.B.; Kirchgessner, D.A.; Clayton, M.; Natschke D.F.; and Phillips, W.J. *Multi-Pollutant Concentration Measurements Around a Concentrated Swine Production Facility Using Open-Path FTIR Spectrometry.* Atmos. Environ. 2001, In Press.
2. Harris, D.B.; Hashmonay, R.A.; Natschke, D.; Wagoner, K.; Thompson, E.L., Jr.; and Vogel, C.A. *Innovative Approach for Measuring Ammonia and Methane Fluxes from a Hog Farm Using Open-Path Fourier Transform Infrared Spectroscopy.* Proceedings of 94th Annual Conference & Exhibition, Orlando, Florida, June 24–28, 2001.
3. Hashmonay, R. A.; Natschke, D.F.; Wagoner, K.; Harris, D.B.; and Thompson, E.L. *Field Evaluation of a Method for Estimating Gaseous Fluxes from Area Sources Using Open-Path Fourier Transform Infrared.* ES&T Journal, 2001, *35*, 2309–2313.
4. Hashmonay, R. A. *Use Of Optical Remote Sensing Devices In Determining Fugitive Emissions*. Proceedings of A&WMA 94th Annual Conference & Exhibition, June 24–28, 2001, Orlando, Florida.
5. Hashmonay, R.A.; and Yost, M.G. *Innovative Approach for Estimating Gaseous Fugitive Fluxes Using Computed Tomography and Remote Optical Sensing Techniques*. J. Air Waste Manage. Assoc. 1999, 49, 966.
6. Hashmonay, R.A.; Yost, M.G.; Harris, D.B.; and Thompson, E.L., Jr. *Simulation Study for Gaseous Fluxes from an Area Source Using Computed Tomography and Optical Remote Sensing*. Proceedings of SPIE Environmental Monitoring and Remediation Technologies Conference, Boston, Mass., November 1998; p 405.
7. Hashmonay, R.A.; and Yost, M.G. *Localizing Gaseous Fugitive Emission Sources by Combining Real Time Optical Remote Sensing and Wind Data*. J. Air Waste Manage. Assoc. 1999, 49, 1374.
8. Hashmonay, R.A.; Mamane, Y.; Shelef, G.; Kimchie, S.; Benayahu, Y.; and Cohen, A. *Estimates of Emission Rates of Fugitive Air Pollution Sources Using Optical Remote Sensing - Open Path FTIR.* Proceedings of the sixth international conference of the Israeli Society for Ecology & Environmental Quality Sciences, Jerusalem, Israel, July 1996, 172–175.
9. Hashmonay, R.A.; Yost, M.G.; Mamane, Y.; and Benayahu, Y. *Emission Rate Apportionment from Fugitive Sources Using Open-Path FTIR and Mathematical Inversion*. Atmos. Environ. 1999, 33 (5), 735.
10. Hashmonay, R.A.; and Harris, D.B. *Innovative Approaches for Estimating Fugitive Air Emissions Using Open-Path FTIR and Computed Tomography.* Poster Presented in SERDP–ESTCP Symposium "Partners in Environmental Technology," Arlington, Va., Nov. 2000.
11. Hashmonay, R.A.; Yost, M.G.; and Wu, C.F. *Computed Tomography of Air Pollutants Using Radial Scanning Path-Integrated Optical Remote Sensing*. Atmos. Environ. 1999, 33 (2), 267.

References (Concluded)

12. Hashmonay, R.A. *Real Time Mapping of Indoors Gaseous Air Contaminants Using Radial Scanned Tunable Diode Laser Absorption Spectroscopy System*. Proceedings of a Symposium, Engineering Solutions to Indoor Air Quality Problems, Raleigh N.C., July 2000, 332–340.
13. Russwurm, G.M.; and Childers, J.W. *FT-IR Open-Path Monitoring Guidance Document.* 3rd Edition, TR-4423-99-03, Submitted by ManTech Environmental Technology, Inc., under contract 68-D5-0049 to the U.S. EPA, Human Exposure and Atmospheric Sciences Division, National Exposure Research Laboratory: RTP, NC, 1999.
14. Tsai, M.Y.; Yost, M.G.; Wu, C.F.; Hashmonay, R.A.; and Larson, T.V. *Line Profile Reconstruction: Validation and Comparison of Reconstruction Methods*. Atmospheric Environment*, October 2001, Volume 35, Issue 28, , Pages 4791-4799*
15. USEPA. *Compendium Method TO-16: Long-Path Open-Path Fourier Transform Infrared Monitoring of Atmospheric Gases.* Center for Environmental Research Information, Office of Research and Development, USEPA, Cincinnati, OH, Jan. 1999.
16. Wu, C.F.; Yost, M.G.; Hashmonay, R.A.; and Park D.Y. *Experimental Evaluation of a Radial Beam Geometry for Mapping Air Pollutants Using Optical Remote Sensing and Computed Tomography*. Atmospheric Environment, 1999, 33(28), 4709–4716.
17. Wu, Chang-fu; Yost, Michael G.; and Hashmonay, Ram A. *One-Dimensional Reconstruction of OP-FTIR Measurements Using Polynomial Curve Fitting Procedures.* Proceedings of A&WMA 94th Annual Conference & Exhibition, June 24–28, 2001, Orlando, Florida.

9. Points of Contact

Point of Contact	Organization	Phone/Fax/E-mail	Role in Project
Patrick D. Sullivan	Air Force Research Laboratory Air Expeditionary Forces Technologies Division (AFRL/MLQL) 139 Barnes Drive, Suite 2, Tyndall AFB, FL 32403-5323	850-283-0430 850-283-9707 patrick.sullivan@tyndall.af.mil	Project Manager
Ram Hashmonay	ARCADIS 4915 Prospectus Drive, Suite F Durham, NC 27713	919-544-4535 919-544-5690 rhashmonay@arcadis-us.com	Technical Manager
Robin R. Segall	Emission Measurement Center (MD-19) OAQPS, US EPA RTP, NC 27711	919-541-0893 919-541-xxxx segall.robin@epa.gov	Regulatory Liason

Appendix A: Data Tables and Figures from Radial Vertical Scans

Section 1: 5-Beam Scans

Details of Gas release:
First 5-beam experiment was performed in Somersworth, NH, on October 2, 2002, which is prior to the Duke Forest control experiments. This was part of measurements from an old landfill and Ethylene gas release was initiated to validate the flux measurements of other gases emitted from the landfill area. Winds were moderate and very consistently directed. A total of 10 lbs of Ethylene was released upwind of the 5-beam configuration over a period of 75 minutes. This amount yields an average flux of 1.01 g/s. The flow rate was high during the first few minutes, and then reduced to avoid freezing on the cylinder opening and attached fittings. The average wind direction was 2° from perpendicular to the 5-beam configuration. Average wind speed was 1.8 m/s The FTIR acquired data by scanning from mirror to mirror with each measurement/mirror averaged over 60 seconds. A total of 12 cycles was recorded for a period of 75 minutes. The Radial Plume Mapping (RPM) reconstruction for the average of the concentration and wind data gave average flux of 0.98 g/s. Figures below provide the RPM reconstruction from averaged data

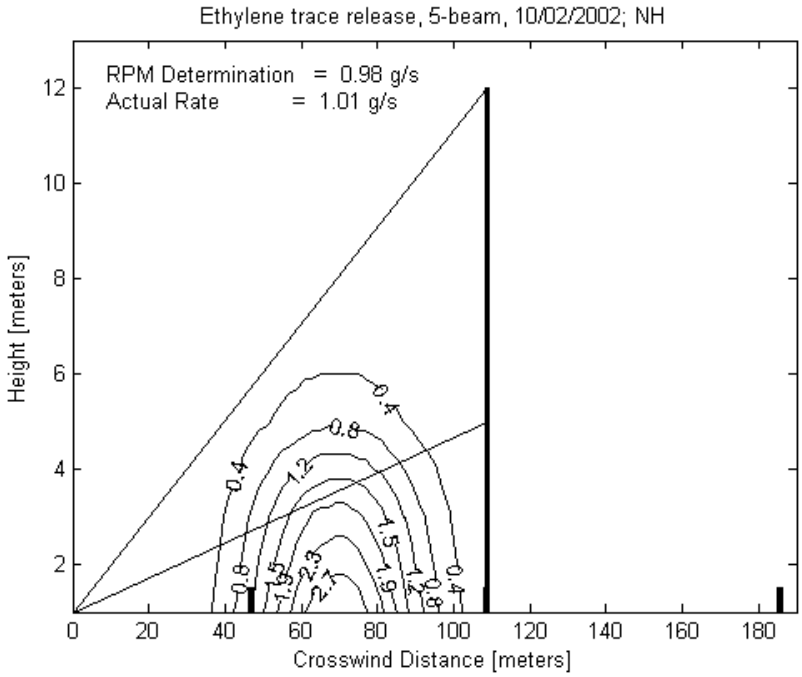

Details of Gas release: Ethylene 11/25/02. 12 cycles, 60 Sec

Run Average:

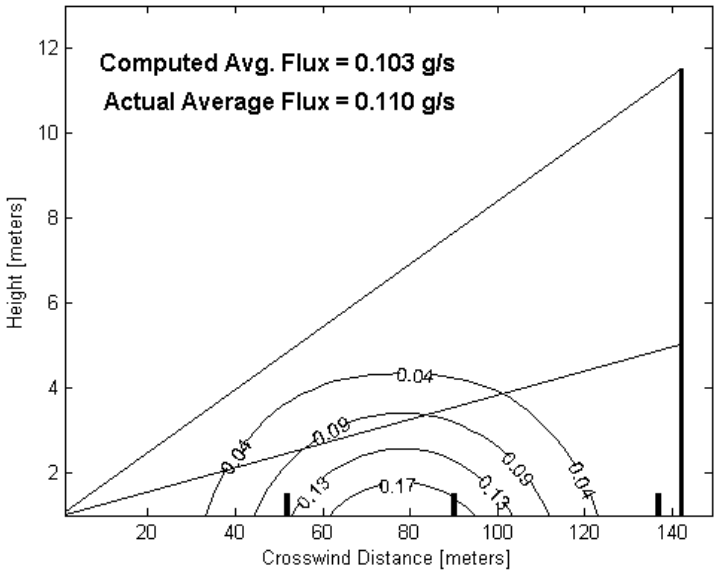

Grouping of 3:

Group	CCF	Flux(g/s)	WS(m/s)	WD(deg.)
1	0.95	0.08	2.2	1.7
2	0.96	0.1	2.1	2.7
3	0.96	0.09	2.2	7.5
4	0.96	0.11	2.4	8.1
5	0.96	0.11	2.7	2.2
6	0.97	0.13	2.5	2.6
7	0.98	0.16	2.2	1.6
8	0.96	0.12	1.8	2.4
9	0.98	0.11	1.7	-7.2
10	0.94	0.12	1.8	-3.0
average		0.11		
Actual Release:				
total time (min)	Weight released (lbs)	Flux (g/s)		
68	1	0.11		

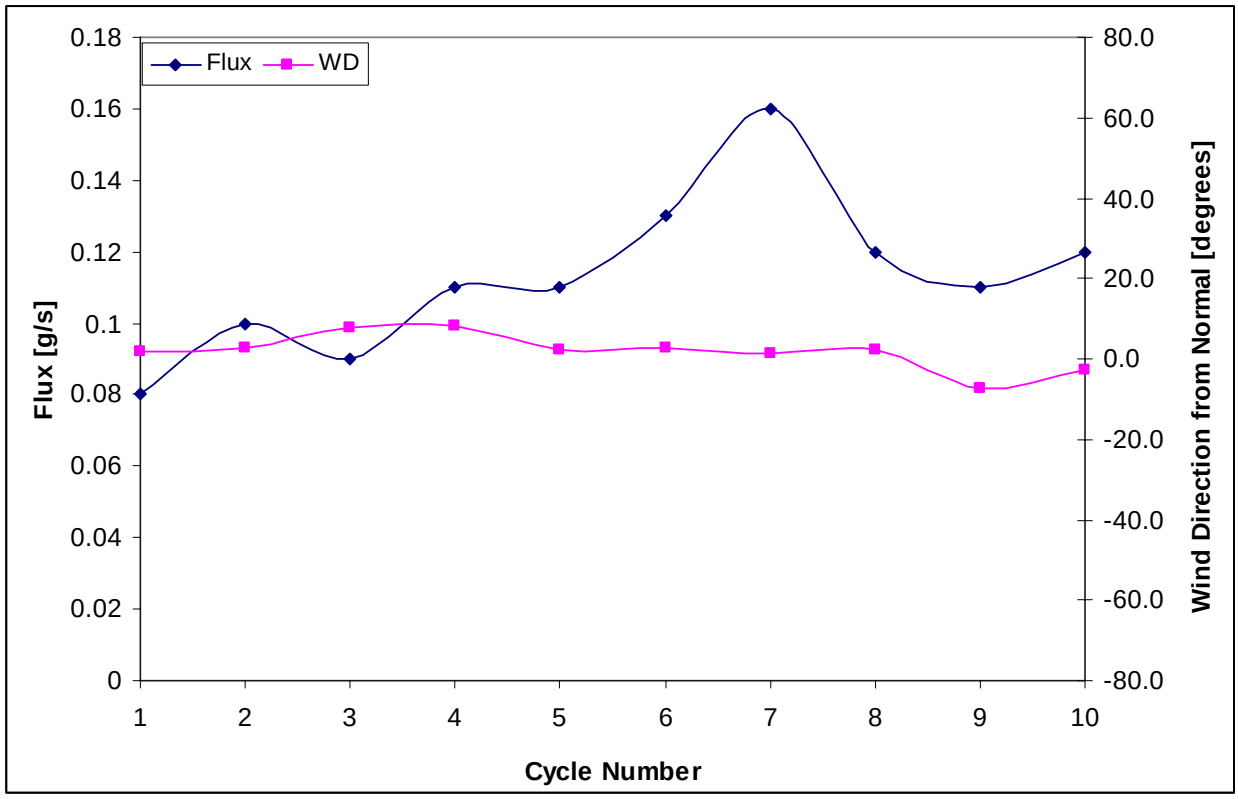
Flux
WD
0.18
0.16
0.14
0.12
0.1
0.08
0.06
0.04
0.02
0
80.0
60.0
40.0
20.0
0.0
-20.0
-40.0
-60.0
-80.0
1
2
3
4
5
6
7
8
9
10
Flux [g/s]
Wind Direction from Normal [degrees]
Cycle Number

Details of Gas release: Ethylene 11/25/02. 24 cycles, 30 Sec

Grouping of 3:

Group	CCF	Flux(g/s)	WS(m/s)	WD(deg.)
1	0.97	0.13	2.0	5
2	0.98	0.17	2.3	8
3	0.98	0.23	2.4	13
4	0.98	0.27	2.5	5
5	0.99	0.27	2.4	1
6	0.99	0.25	2.2	-6
7	0.99	0.22	1.8	-2
8	0.98	0.16	1.5	0
9	0.98	0.14	1.4	7
10	1.00	0.23	1.6	10
11	0.99	0.31	1.8	10
12	0.99	0.34	1.9	5
13	0.97	0.2	1.7	3
14	0.99	0.2	1.6	4
15	1.00	0.3	1.4	13
16	1.00	0.28	1.3	16
17	1.00	0.26	1.2	17
18	0.99	0.14	1.2	9
19	0.99	0.16	1.1	12
20	1.00	0.13	0.9	16
21	0.99	0.12	0.7	25
22	0.97	0.29	0.9	19
Average		0.22		
total time (min)	Weight released (lbs)	Flux (g/s)		
69	1.8	0.20		

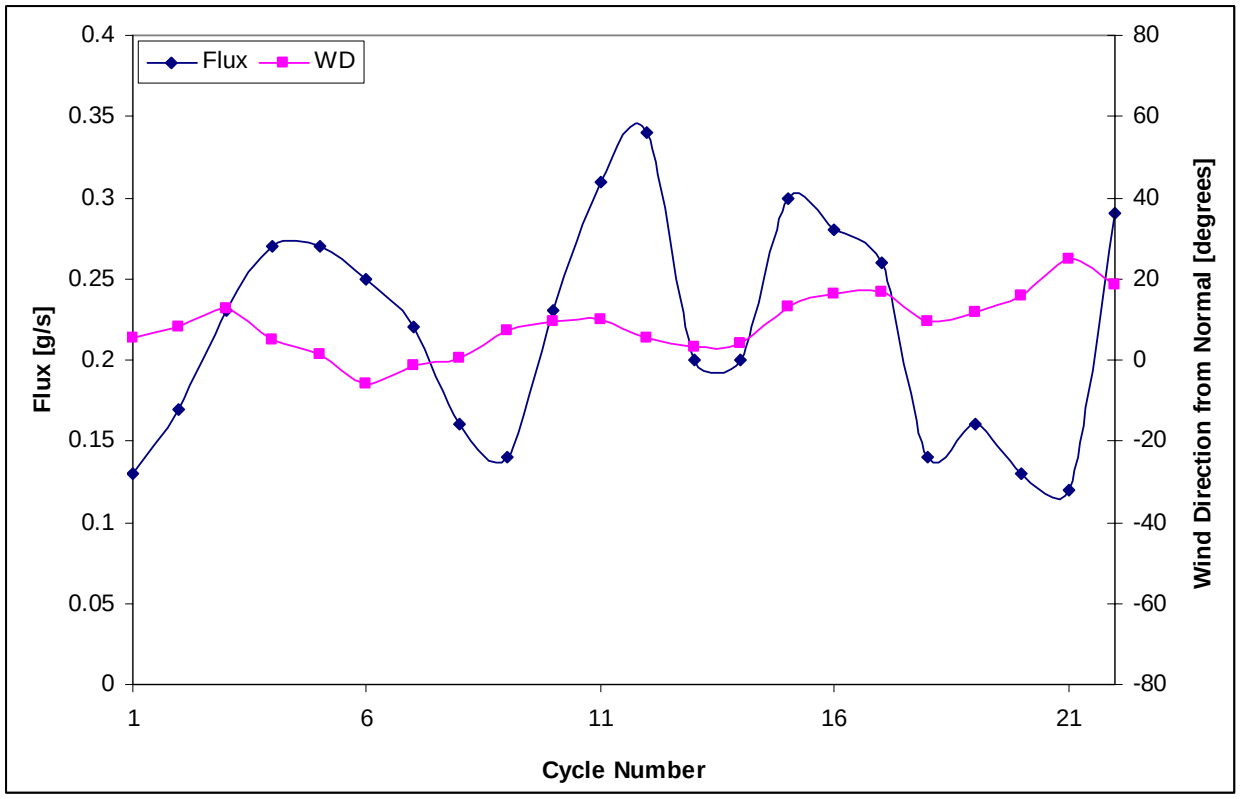
Flux
WD
0.4
0.35
0.3
0.25
0.2
0.15
0.1
0.05
0
80
60
40
20
0
-20
-40
-60
-80
1
6
11
16
21
Flux [g/s]
Wind Direction from Normal [degrees]
Cycle Number

Details of Gas release: Ethylene 12/23/02. 72 cycles, 10 Sec

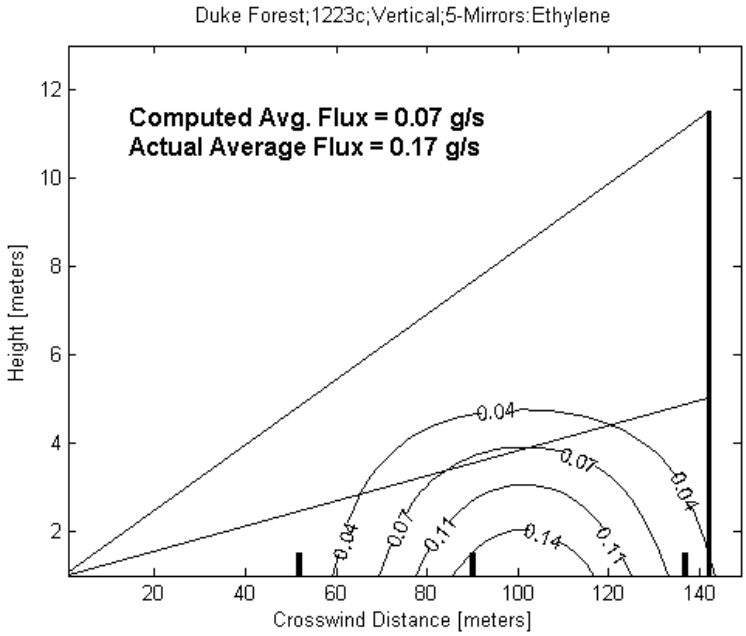

Grouping of 3:

Group	CCF	Flux(g/s)	WS(m/s)	WD(deg.)
1	0.97	0.04	1.4	51
2	0.94	0.07	1.6	43
3	0.91	0.11	1.8	36
4	0.97	0.17	2.0	33
5	0.95	0.24	1.9	35
6	0.95	0.23	1.9	36
7	1.00	0.2	2.0	34
8	1.00	0.18	2.1	38
9	0.99	0.18	2.1	37
10	0.98	0.18	2.1	37
11	1.00	0.16	2.2	34
12	0.99	0.17	2.2	32
13	0.92	0.17	2.2	33
14	0.95	0.11	2.0	38
15	0.95	0.08	1.8	47
16	0.92	0.05	1.7	54
17	0.92	0.05	1.5	55
18	0.95	0.07	1.6	60
19	0.90	0.05	1.6	61

Group	CCF	Flux(g/s)	WS(m/s)	WD(deg.)
20	0.91	0.08	1.9	57
21	0.96	0.09	1.9	51
22	0.93	0.1	1.9	50
23	0.89	0.09	1.8	53
24	0.95	0.06	1.8	58
25	0.97	0.05	1.8	60
26	0.95	0.05	1.7	56
27	0.91	0.06	2.0	56
28	0.93	0.07	2.3	55
29	0.98	0.13	2.5	57
30	0.98	0.17	2.5	56
31	0.97	0.14	2.4	60
32	0.91	0.08	2.5	65
33	0.98	0.02	2.5	69
34	0.91	0.03	2.5	70
35	0.94	0.03	2.5	71
36	0.97	0.05	2.6	68
37	1.00	0.02	2.5	63
38	0.95	0.04	2.4	63
39	0.92	0.07	2.2	64
40	0.98	0.1	2.2	63
41	0.97	0.1	2.1	62
42	0.96	0.08	2.1	61
43	0.97	0.09	1.9	62
44	0.96	0.08	1.9	63
45	0.95	0.09	2.0	61
46	0.99	0.1	2.1	58
47	0.97	0.12	2.2	54
48	0.97	0.14	2.0	47
49	0.97	0.14	1.8	44
50	0.97	0.15	1.8	32
51	0.97	0.16	1.7	35
52	0.97	0.17	1.7	41
53	0.97	0.13	1.6	47
54	0.98	0.1	1.6	39
55	0.93	0.09	1.8	28
56	0.96	0.09	1.8	31
57	0.95	0.09	1.9	36
58	0.94	0.08	1.9	41
59	0.97	0.09	1.8	44
60	0.91	0.1	1.8	47

Group	CCF	Flux(g/s)	WS(m/s)	WD(deg.)
61	0.92	0.06	1.7	60
62	0.96	0.03	1.7	73
63	0.94	0	1.8	86
64	0.92	0	1.8	88
65	0.93	0	1.6	86
66	0.97	0	1.6	86
67	0.99	0	1.6	86
68	0.97	0.01	1.6	80
69	0.97	0.02	1.5	68
70	0.97	0.04	1.5	54
Average		0.09		
total time (min)	Weight released (lbs)	Flux (g/s)		
78	2.2	0.21		

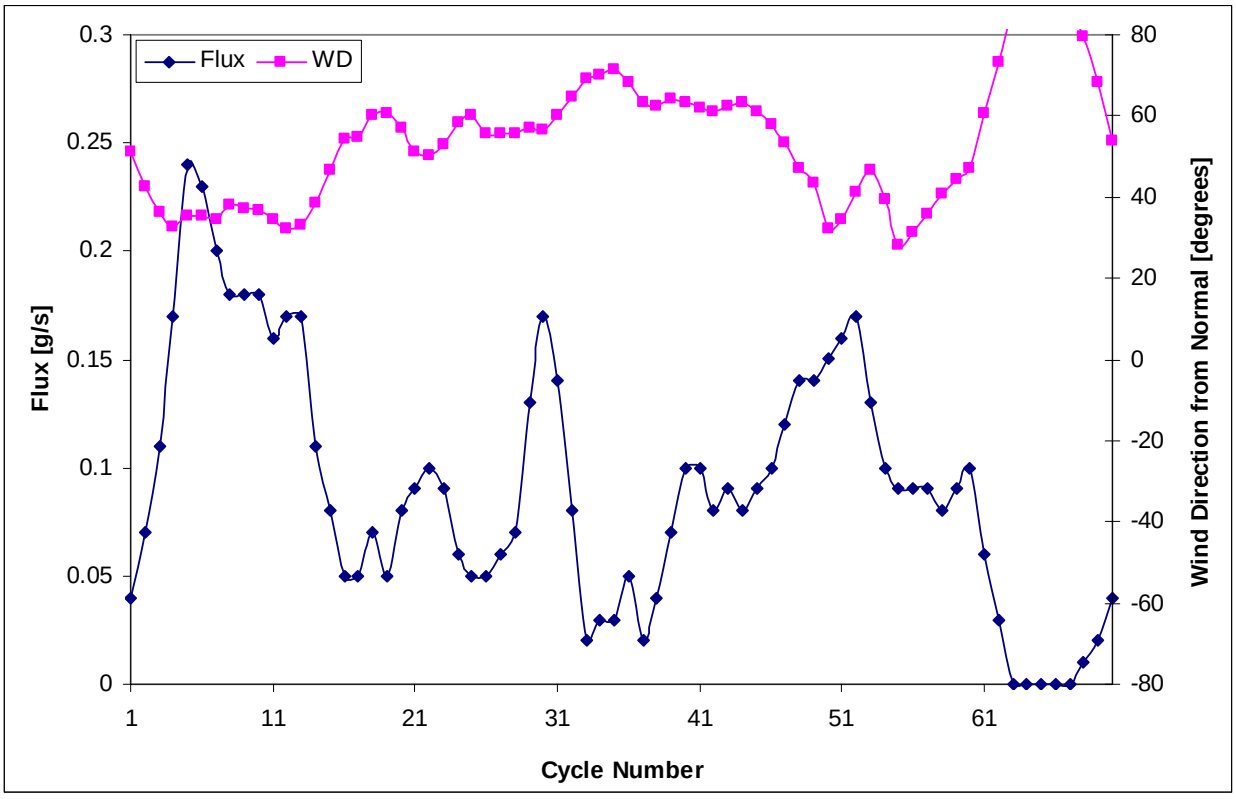

Section 2: 3-Beam Scans

Details of Gas release: Ethylene 01/29/03. 20 cycles, 60 Sec

Grouping of 3:

Group	CCF	Flux(g/s)	WS(m/s)	WD(deg.)
1	1.00	0.09	1.3	-16
2	1.00	0.09	1.2	-15
3	1.00	0.1	1.3	-10
4	0.99	0.1	1.4	-13
5	1.00	0.13	1.6	-12
6	1.00	0.14	1.8	-12
7	1.00	0.13	1.8	-10
8	1.00	0.18	2.2	-6
9	1.00	0.18	2.3	-4
10	1.00	0.24	2.6	-3
11	1.00	0.22	2.4	-6
12	1.00	0.22	2.6	-8
13	1.00	0.22	2.7	-8
14	1.00	0.22	2.9	-5
15	1.00	0.23	2.9	-8
16	1.00	0.2	3.0	-11
17	1.00	0.17	2.8	-17
18	1.00	0.17	3.1	-12
Average		0.17		
total time (min)	Weight released (lbs)	Flux (g/s)		
126	3.3	0.20		

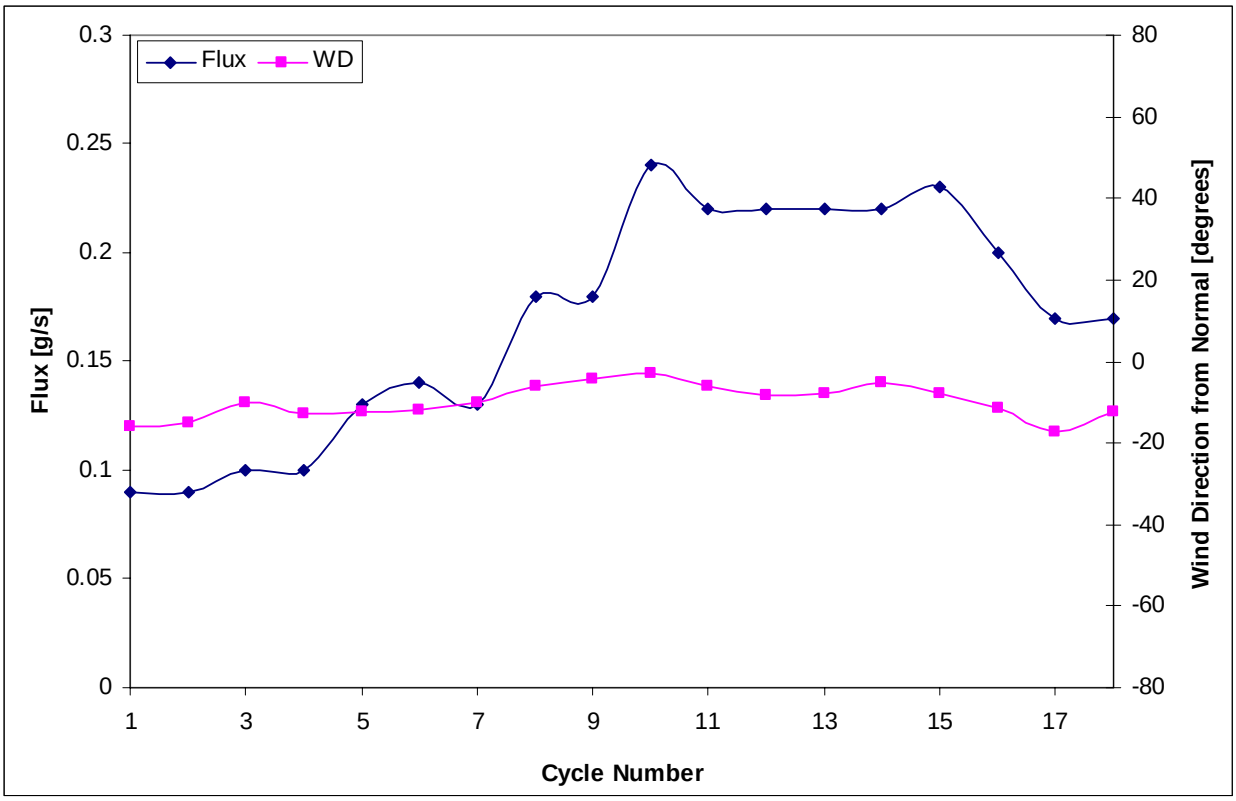
Flux
WD
0.3
0.25
0.2
0.15
0.1
0.05
0
80
60
40
20
0
-20
-40
-60
-80
1
3
5
7
9
11
13
15
17
Flux [g/s]
Wind Direction from Normal [degrees]
Cycle Number

Details of Gas release: Ethylene 01/29/03. 40 cycles, 30 Sec
Grouping of 3:

Group	CCF	Flux(g/s)	WS(m/s)	WD(deg.)
1	0.73	0.08	2.3	-7
2	0.90	0.06	2.1	-8
3	0.72	0.08	2.0	-12
4	0.70	0.08	2.1	-14
5	0.55	0.1	2.2	-18
6	0.56	0.11	2.5	-14
7	0.97	0.1	2.7	-9
8	0.99	0.11	2.9	-6
9	1.00	0.13	2.7	-2
10	1.00	0.13	2.8	-3
11	1.00	0.14	2.8	-3
12	1.00	0.16	2.7	-6
13	1.00	0.14	2.3	-7
14	1.00	0.12	2.0	-10
15	1.00	0.09	2.0	-11
16	1.00	0.1	2.1	-10
17	1.00	0.14	2.0	-9
18	1.00	0.19	1.9	-1
19	1.00	0.2	1.8	9
20	1.00	0.19	2.0	15
21	1.00	0.19	2.2	9
22	1.00	0.2	2.2	6
23	1.00	0.2	2.2	2
24	1.00	0.19	2.0	3
25	1.00	0.18	1.9	2
26	1.00	0.19	2.0	4
27	1.00	0.17	1.8	1
28	1.00	0.17	1.7	-2
29	1.00	0.15	1.7	-8
30	1.00	0.15	1.9	-5
31	1.00	0.14	1.9	-2
32	1.00	0.14	1.7	-2
33	1.00	0.14	1.6	-6
34	1.00	0.13	1.6	-15
35	1.00	0.12	1.6	-11
36	1.00	0.1	1.5	-9
37	1.00	0.09	1.4	-9
38	1.00	0.09	1.5	-15

Group	CCF	Flux(g/s)	WS(m/s)	WD(deg.)
Average		0.14		
total time (min)	Weight released (lbs)	Flux (g/s)		
73	1.4	0.15		

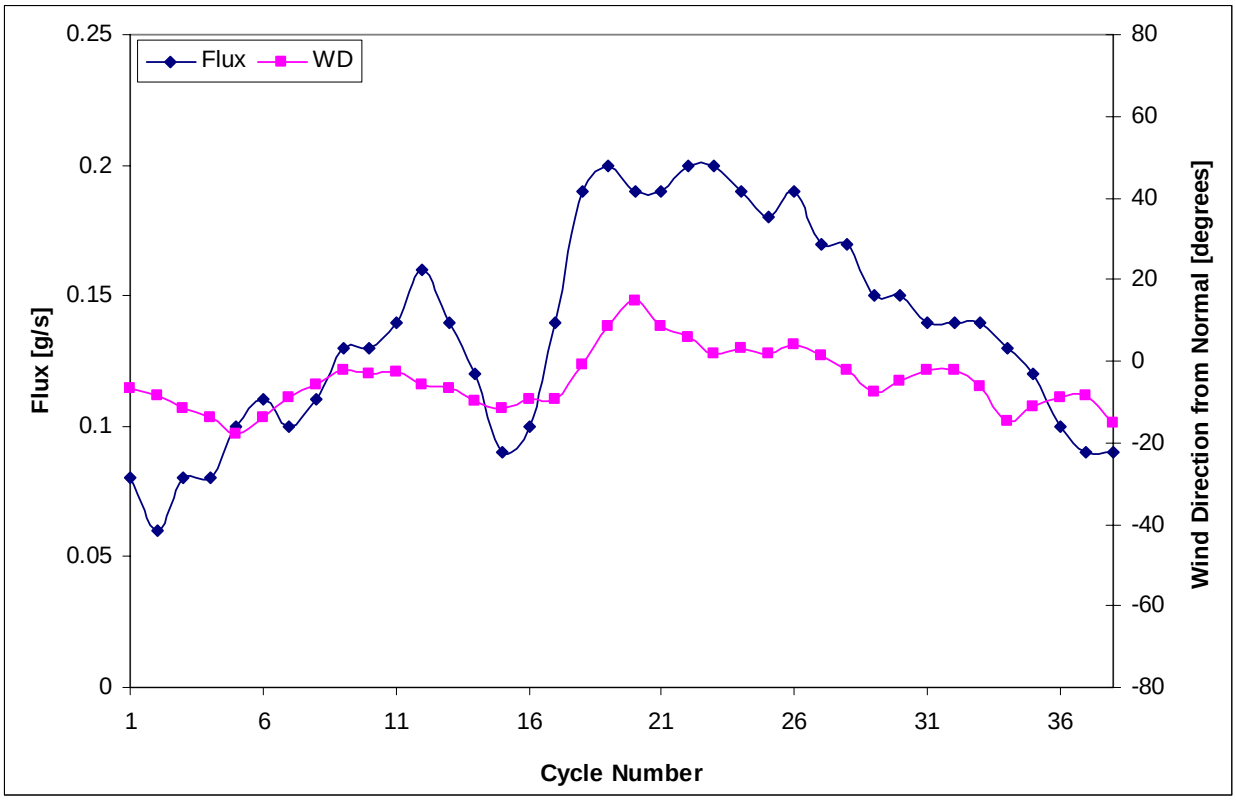

Details of Gas release: Ethylene 01/09/03. 79 cycles, 10 Sec
Grouping of 3:

Group	CCF	Flux(g/s)	WS(m/s)	WD(deg.)
1	0.91	0.11	2.7	10
2	0.94	0.15	2.8	12
3	1.00	0.23	3.2	15
4	0.99	0.26	3.7	13
5	0.93	0.17	3.5	14
6	0.92	0.14	3.3	14
7	0.93	0.12	3.0	13
8	0.91	0.12	3.0	12
9	0.98	0.11	2.9	16
10	0.98	0.13	3.6	20
11	0.97	0.15	4.4	23
12	0.96	0.17	4.8	18
13	0.93	0.15	4.3	13
14	0.96	0.14	3.7	7
15	0.97	0.14	3.7	11
16	0.98	0.17	4.1	6
17	0.96	0.16	4.5	3
18	0.97	0.17	4.5	-1
19	0.66	0.24	4.1	-1
20	0.66	0.23	3.7	-1
21	0.95	0.18	3.4	0
22	0.96	0.16	3.5	13
23	0.92	0.15	3.7	25
24	0.91	0.12	3.8	33
25	0.99	0.12	3.4	27
26	0.97	0.11	3.0	21
27	0.97	0.11	2.9	8
28	0.98	0.12	2.9	3
29	0.98	0.12	3.1	-2
30	0.98	0.11	2.8	4
31	0.92	0.14	2.6	8
32	0.95	0.11	2.3	30
33	0.95	0.1	2.5	38
34	0.93	0.07	2.9	48
35	0.77	0.09	2.8	44
36	0.77	0.09	2.6	45
37	0.97	0.1	2.7	49
38	0.92	0.08	3.1	51

Group	CCF	Flux(g/s)	WS(m/s)	WD(deg.)
39	0.87	0.09	3.5	46
40	0.94	0.1	3.3	40
41	0.96	0.12	3.0	33
42	0.90	0.09	2.5	36
43	0.95	0.09	2.4	34
44	0.94	0.09	2.4	32
45	0.97	0.11	2.6	27
46	0.98	0.1	2.7	24
47	0.94	0.09	2.7	29
48	0.92	0.09	2.7	33
49	0.89	0.09	2.4	39
50	0.98	0.07	2.0	37
51	0.98	0.07	1.5	34
52	0.98	0.07	1.7	28
53	0.95	0.1	2.0	22
54	0.89	0.12	2.2	22
55	1.00	0.14	2.5	22
56	0.97	0.1	2.9	22
57	0.97	0.1	3.0	13
58	0.95	0.09	2.4	12
59	0.95	0.08	1.9	10
60	0.96	0.09	2.1	22
61	0.97	0.13	2.3	23
62	1.00	0.15	2.5	25
63	0.95	0.1	2.4	24
64	0.98	0.1	2.4	13
65	0.98	0.11	2.6	3
66	0.97	0.13	2.7	-3
67	0.99	0.14	2.4	5
68	0.98	0.11	2.2	14
69	0.90	0.09	2.1	25
70	0.96	0.08	2.2	27
71	0.91	0.08	2.2	30
72	0.97	0.08	2.1	12
73	0.90	0.12	2.7	4
74	0.90	0.13	3.4	-2
75	0.91	0.16	3.5	8
76	0.96	0.14	3.0	12
78	0.96	0.12	2.6	17
Average.		0.12		

Group	CCF	Flux(g/s)	WS(m/s)	WD(deg.)
total time (min)	Weight released (lbs)	Flux (g/s)		
83	1.6	0.15		

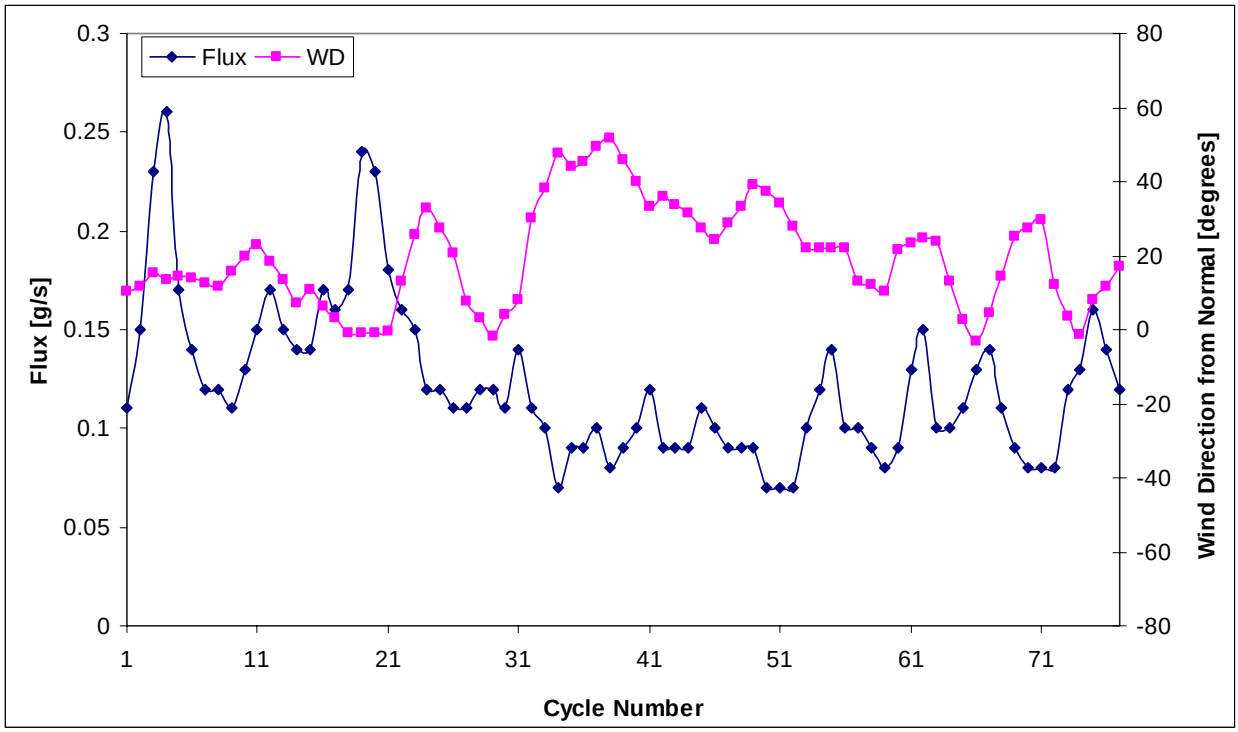

Details of Gas release: Ethylene 05/06/03. 48 cycles, 10 Sec

Grouping of 3:

Group	CCF	Flux(g/s)	WS(m/s)	WD(deg.)
1	0.98	0.19	3.7	9
2	0.99	0.2	3.6	9
3	0.99	0.17	3.4	11
4	0.94	0.35	3.7	16
5	1.00	0.23	3.3	16
6	1.00	0.24	3.2	18
7	0.98	0.27	3.3	15
8	1.00	0.24	3.2	13
9	1.00	0.24	3.2	22
10	1.00	0.21	3.3	27
11	1.00	0.18	3.7	29
12	0.99	0.16	3.9	31
13	0.99	0.2	3.9	32
14	0.97	0.18	3.1	32
15	0.99	0.23	2.4	22
16	0.96	0.15	2.0	19
17	1.00	0.13	2.2	27
18	1.00	0.12	2.3	27
19	0.99	0.13	2.2	28
20	0.99	0.14	2.4	27
21	0.99	0.14	2.6	34
22	0.98	0.12	2.6	31
23	0.99	0.14	2.3	32
24	0.99	0.17	2.3	19
25	1.00	0.19	2.6	26
26	1.00	0.19	2.9	24
27	1.00	0.17	3.0	28
28	1.00	0.18	2.8	25
29	1.00	0.14	2.6	24
30	1.00	0.14	2.4	30
31	1.00	0.17	3.0	31
32	1.00	0.22	3.6	31
33	1.00	0.2	3.8	25

Group	CCF	Flux(g/s)	WS(m/s)	WD(deg.)
34	1.00	0.21	3.5	18
35	1.00	0.21	3.3	11
36	1.00	0.27	3.7	15
37	1.00	0.27	3.4	18
38	0.99	0.29	3.8	23
39	1.00	0.31	3.7	22
40	1.00	0.32	4.2	20
41	1.00	0.26	4.0	22
42	0.99	0.2	4.0	19
43	1.00	0.25	4.0	19
44	1.00	0.25	3.6	18
45	1.00	0.28	3.6	22
46	1.00	0.24	3.4	21
47	0.99	0.27	3.3	18
48	1.00	0.26	3.4	11
Average		0.20		
total time (min)	Weight released (lbs)	Flux (g/s)		
47	1.5	0.24		

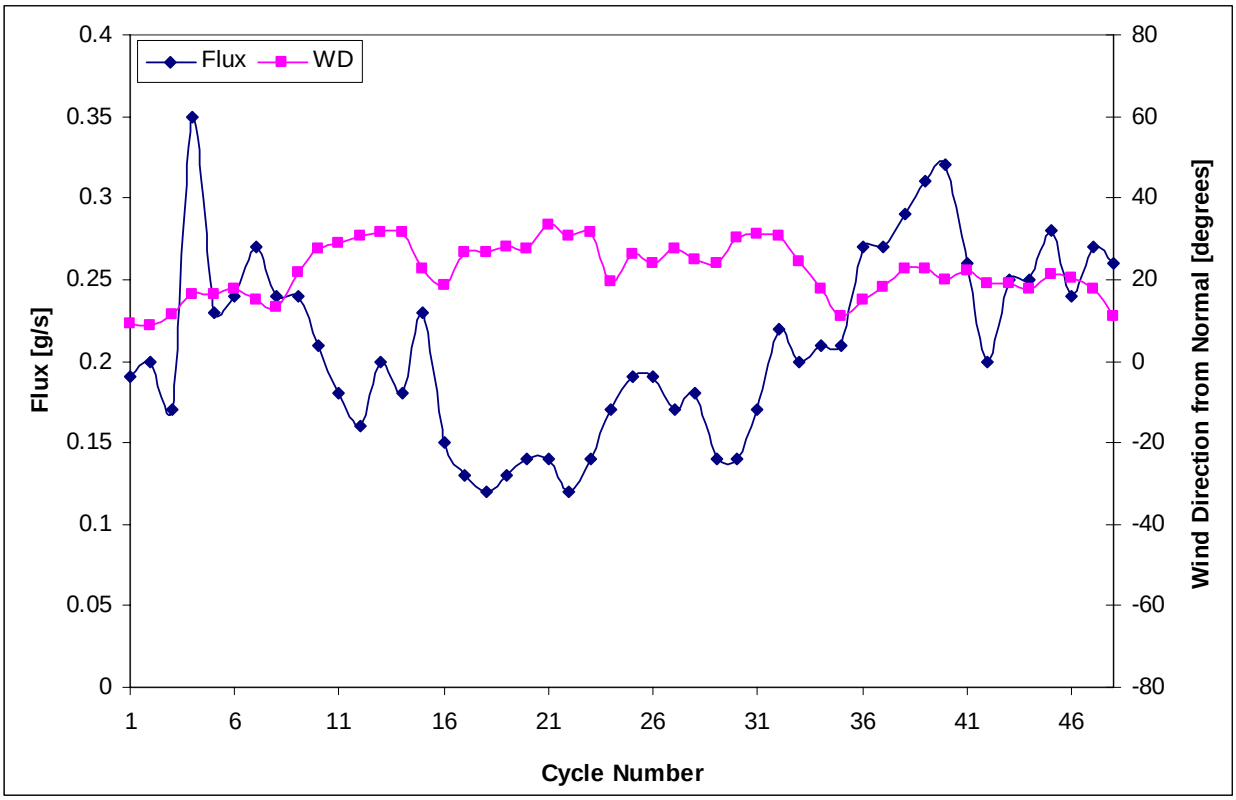

Details of Gas release: Propane 05/06/03. 48 cycles, 10 Sec

Grouping of 3:

Group	CCF	Flux(g/s)	WS(m/s)	WD(deg.)
1	0.97	0.3	3.7	9
2	0.71	0.34	3.6	9
3	0.90	0.4	3.4	11
4	0.98	0.29	3.7	16
5	0.99	0.22	3.3	16
6	0.99	0.21	3.2	18
7	1.00	0.27	3.3	15
8	0.97	0.24	3.2	13
9	0.98	0.2	3.2	22
10	0.99	0.22	3.3	27
11	0.99	0.23	3.7	29
12	0.99	0.26	3.9	31
13	0.94	0.27	3.9	32
14	0.97	0.2	3.1	32
15	0.93	0.2	2.4	22
16	0.98	0.16	2.0	19
17	0.98	0.15	2.2	27
18	1.00	0.2	2.3	27
19	0.96	0.22	2.2	28
20	0.99	0.26	2.4	27
21	0.97	0.15	2.6	34
22	0.99	0.15	2.6	31
23	1.00	0.15	2.3	32
24	0.98	0.18	2.3	19
25	1.00	0.22	2.6	26
26	0.99	0.23	2.9	24
27	1.00	0.21	3.0	28
28	1.00	0.19	2.8	25
29	0.99	0.16	2.6	24
30	1.00	0.17	2.4	30
31	1.00	0.21	3.0	31
32	1.00	0.25	3.6	31
33	0.96	0.22	3.8	25
34	0.99	0.23	3.5	18
35	1.00	0.26	3.3	11

Group	CCF	Flux(g/s)	WS(m/s)	WD(deg.)
36	1.00	0.28	3.7	15
37	0.99	0.25	3.4	18
38	1.00	0.3	3.8	23
39	1.00	0.33	3.7	22
40	1.00	0.37	4.2	20
41	0.99	0.29	4.0	22
42	0.98	0.27	4.0	19
43	0.99	0.28	4.0	19
44	1.00	0.3	3.6	18
45	1.00	0.32	3.6	22
46	0.99	0.32	3.4	21
47	1.00	0.25	3.3	18
48	0.99	0.28	3.4	11
Average		0.24		
total time (min)	Weight released (lbs)	Flux (g/s)		
47	1.5	0.24		

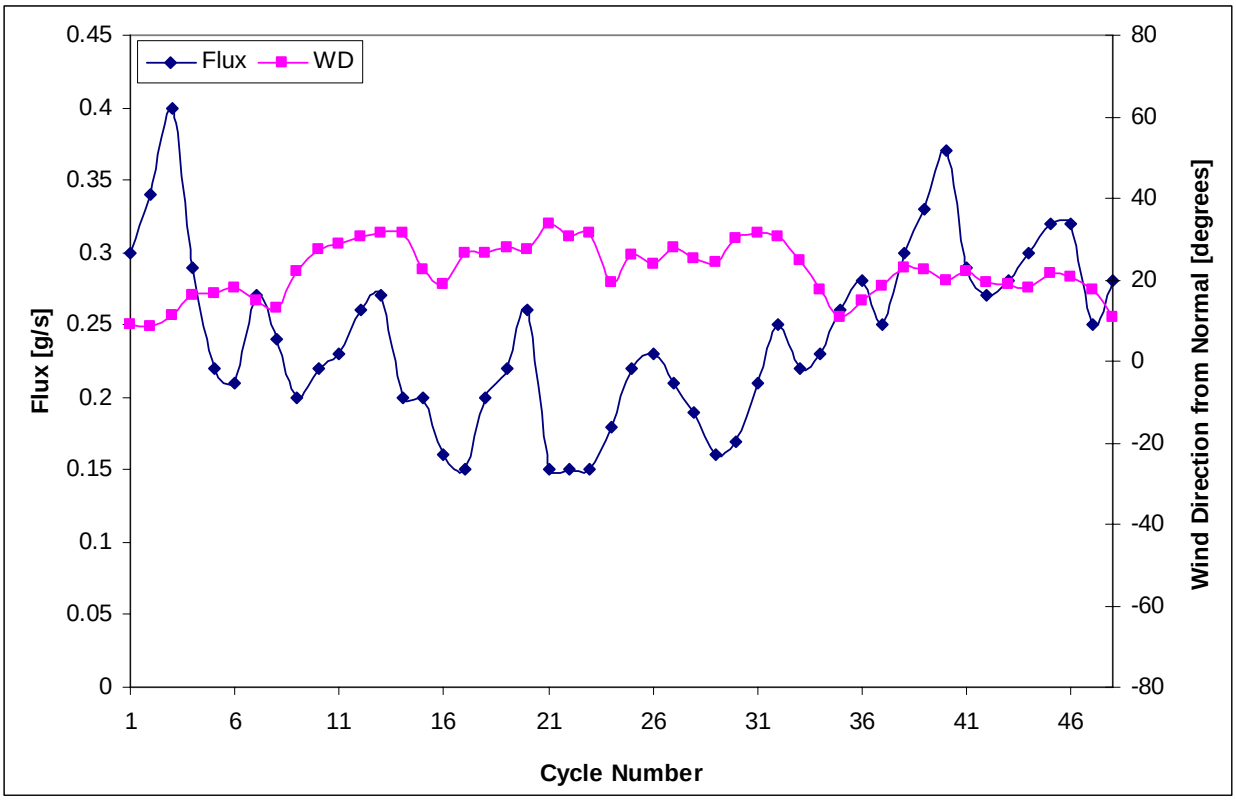

Appendix B: Data Tables and Figures from Radial Horizontal Scans

Section 1: Pixel 9

Details of Gas release: Gas: Acetylene; Pixel: 9; Scan time/mirror: 10 Sec; Date: 02/05/03

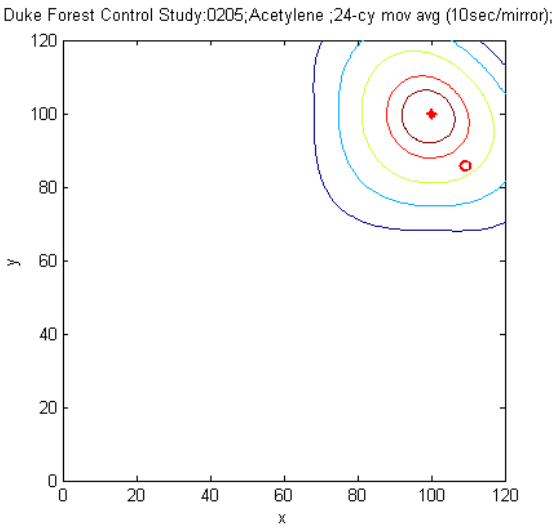

CCF	Distance(m)	group#
1.00	17.08	1
1.00	17.08	2
1.00	17.08	3
1.00	17.08	4
1.00	17.08	5
1.00	17.08	6
1.00	17.08	7
1.00	17.08	8
1.00	17.08	9
1.00	17.08	10
1.00	17.08	11
1.00	17.08	12
1.00	17.08	13
1.00	17.08	14
1.00	17.08	15
1.00	17.08	16
1.00	17.08	17
1.00	17.08	18
1.00	17.08	19
Average		
1.00	17.08	
Sdev		
0.00	0.00	

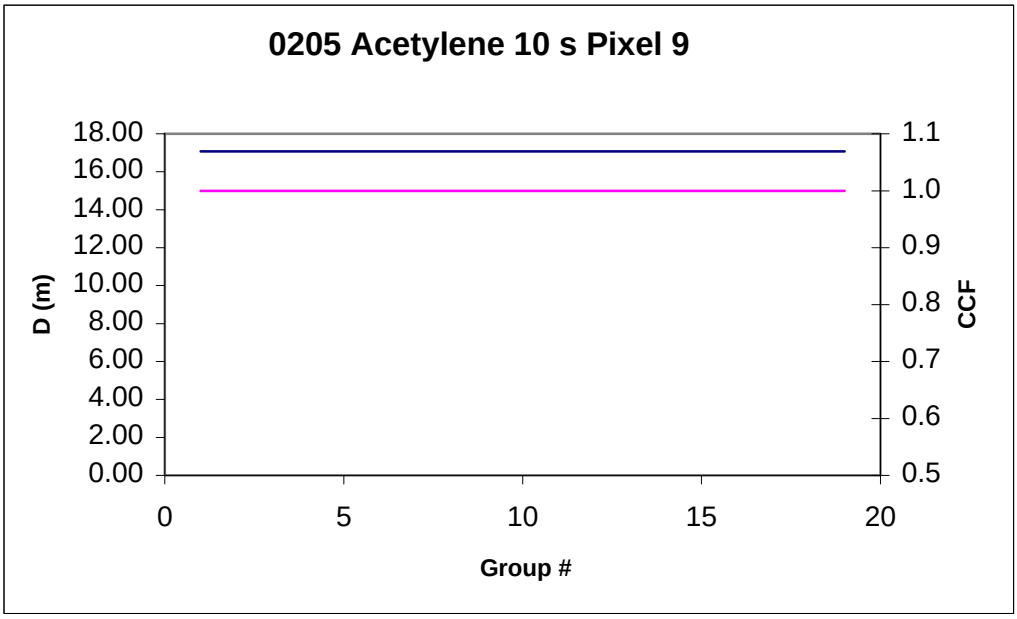

Details of Gas release: Gas: Ethylene; Pixel: 9; Scan time/mirror: 30 Sec; Date: 11/14/03

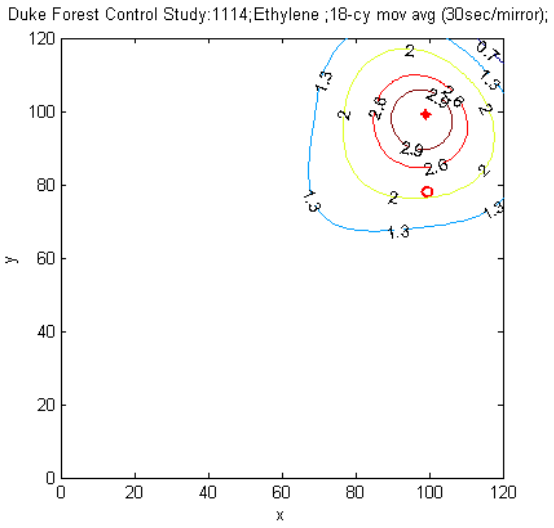

CCF	Distance(m)	group#
1.00	21.89	1
1.00	21.89	2
1.00	21.93	3
1.00	21.89	4
1.00	21.89	5
1.00	21.93	6
1.00	21.89	7
1.00	21.89	8
1.00	22.02	9
1.00	21.93	10
1.00	21.93	11
1.00	21.93	12
1.00	21.93	13
1.00	21.93	14
1.00	8.90	15
Average		
1.00	21.05	
Sdev		
0.00	3.36	

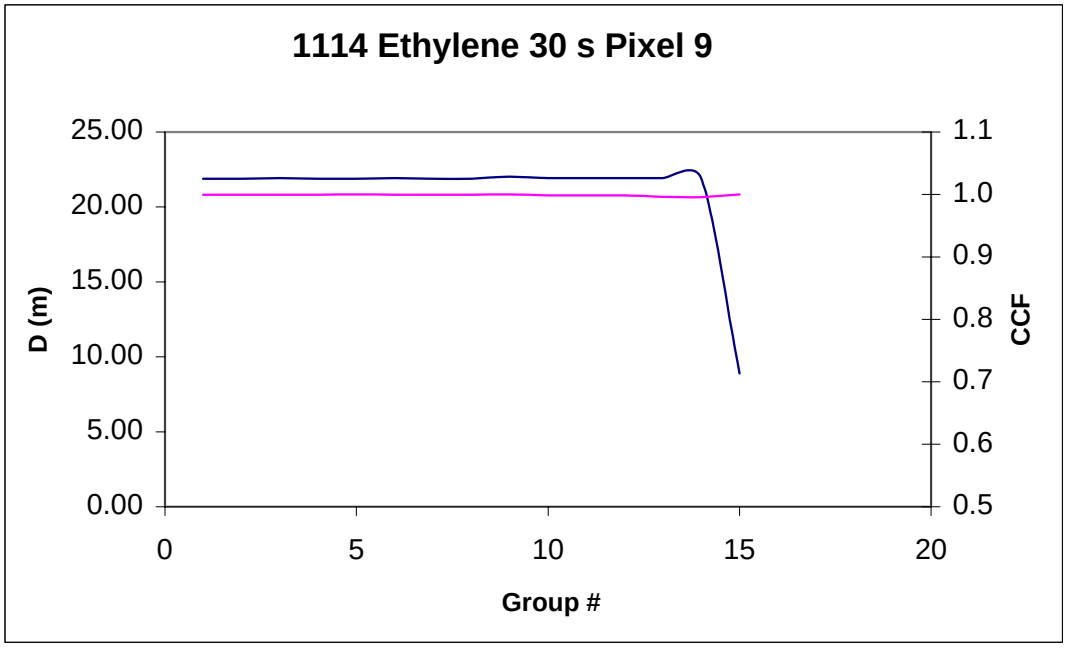

Details of Gas release: Gas: Acetylene; Pixel: 9; Scan time/mirror: 60 Sec; Date: 02/05/03

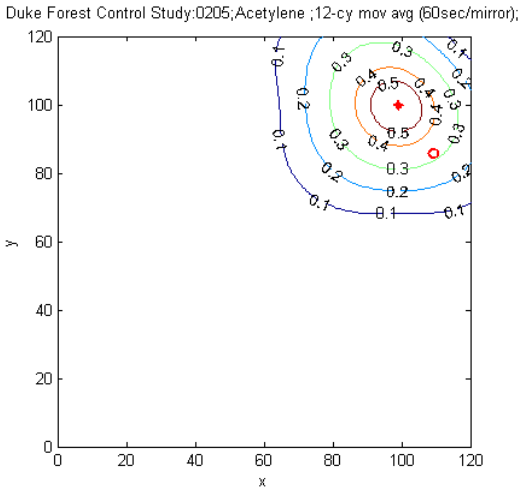

CCF	Distance(m)	group#
1.00	17.65	1
1.00	18.26	2
1.00	17.65	3
1.00	17.65	4
1.00	17.65	5
1.00	17.08	6
1.00	17.08	7
1.00	17.08	8
1.00	17.08	9
Average		
1.00	17.46	
Sdev		
0.00	0.41	

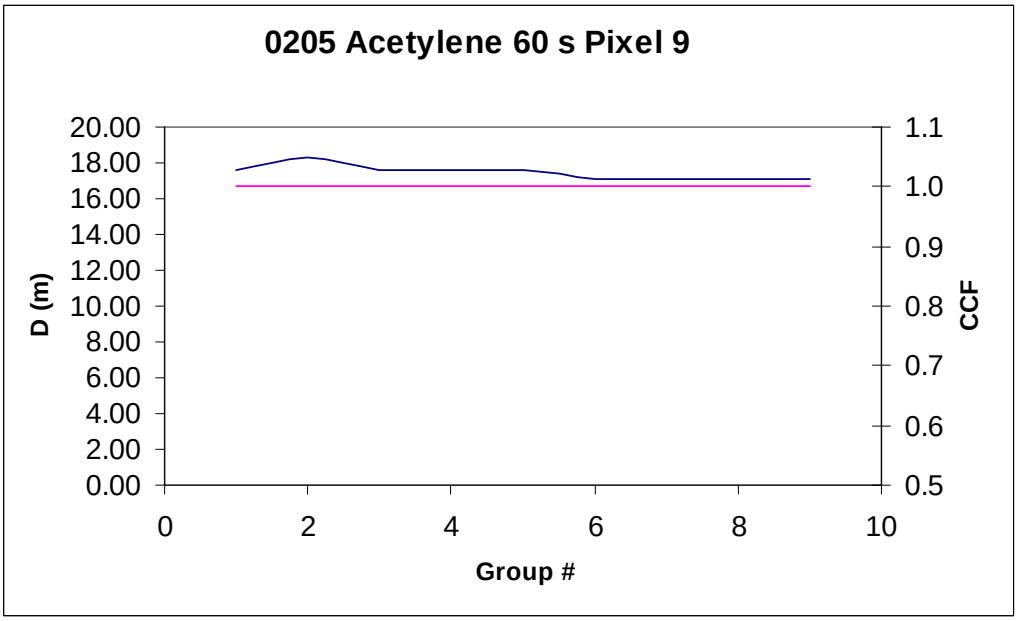

Section 2: Pixel 8

Details of Gas release: Gas: Acetylene; Pixel: 8; Scan time/mirror: 10 Sec; Date: 11/13/02

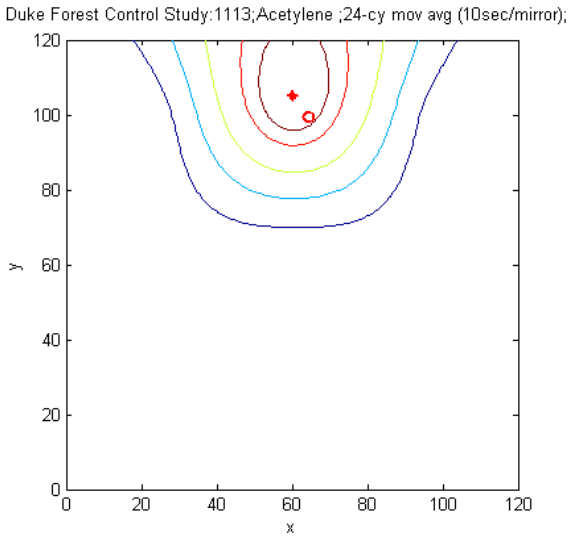

CCF	Distance(m)	group#
1.00	6.88	1
1.00	6.88	2
1.00	6.77	3
1.00	35.68	4
1.00	9.13	5
1.00	7.36	6
1.00	6.88	7
1.00	6.88	8
1.00	6.88	9
1.00	6.88	10
1.00	6.88	11
1.00	6.88	12
1.00	6.88	13
1.00	6.88	14
1.00	6.88	15
1.00	6.88	16
1.00	6.88	17
1.00	6.88	18
1.00	6.88	19
1.00	6.88	20
1.00	6.88	21
Average		
1.00	8.38	
Sdev		
0.00	6.28	

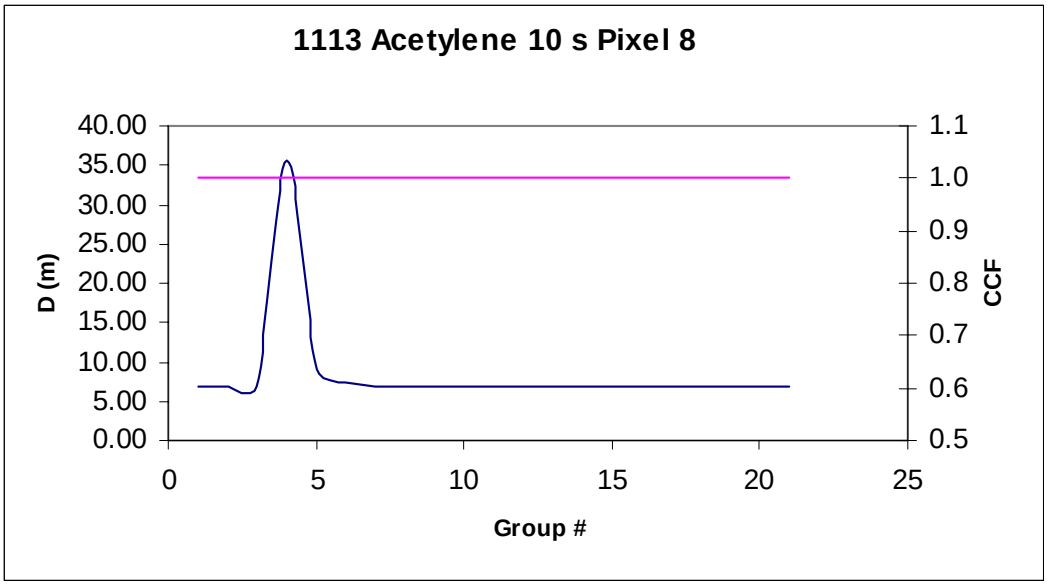

Details of Gas release: Gas: Acetylene; Pixel: 8; Scan time/mirror: 30 Sec; Date: 11/13/02

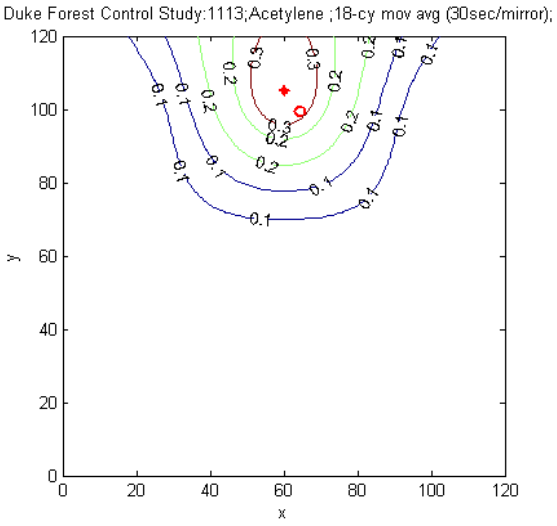

CCF	Distance(m)	group#
1.00	6.88	1
1.00	6.88	2
1.00	6.88	3
1.00	6.88	4
1.00	6.88	5
1.00	6.88	6
1.00	6.88	7
1.00	6.88	8
1.00	6.88	9
1.00	6.88	10
1.00	6.88	11
1.00	6.88	12
1.00	6.88	13
1.00	6.88	14
1.00	6.88	15
Average		
1.00	6.88	
Sdev		
0.00	0.00	

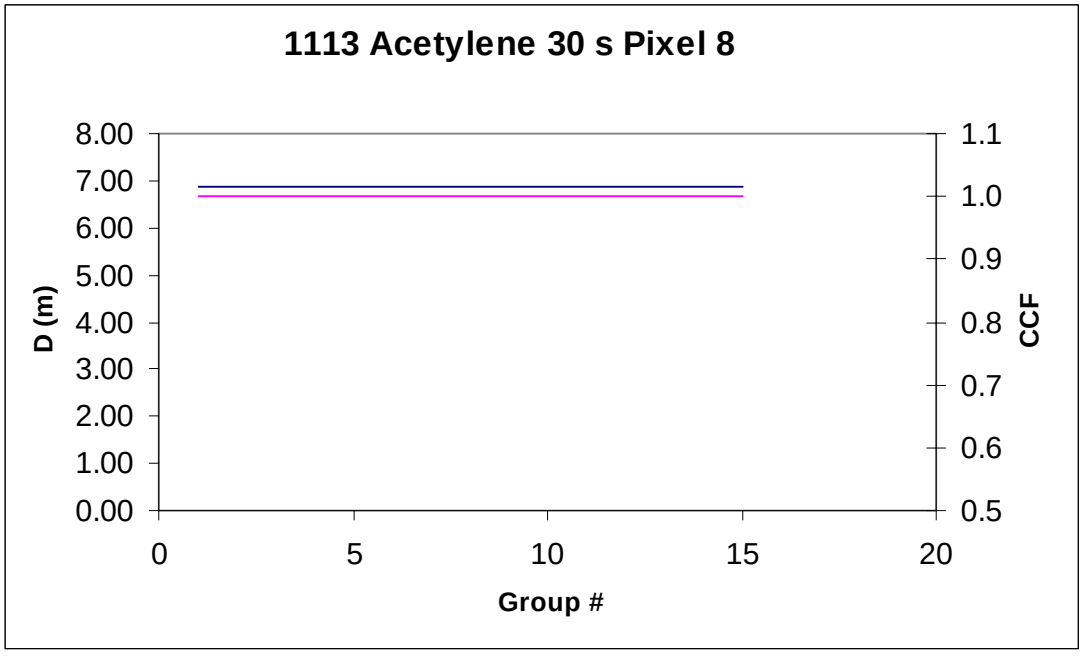

Details of Gas release: Gas: Ethylene; Pixel: 8; Scan time/mirror: 60 Sec; Date: 02/05/03

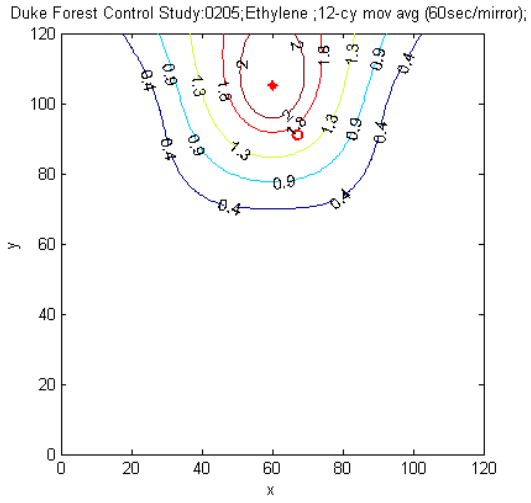

CCF	Distance(m)	group#
1.00	15.73	1
1.00	15.73	2
1.00	15.73	3
1.00	15.73	4
1.00	15.73	5
1.00	15.73	6
1.00	15.73	7
1.00	15.73	8
1.00	15.73	9
Average		
1.00	15.73	
Sdev		
0.00	0.00	

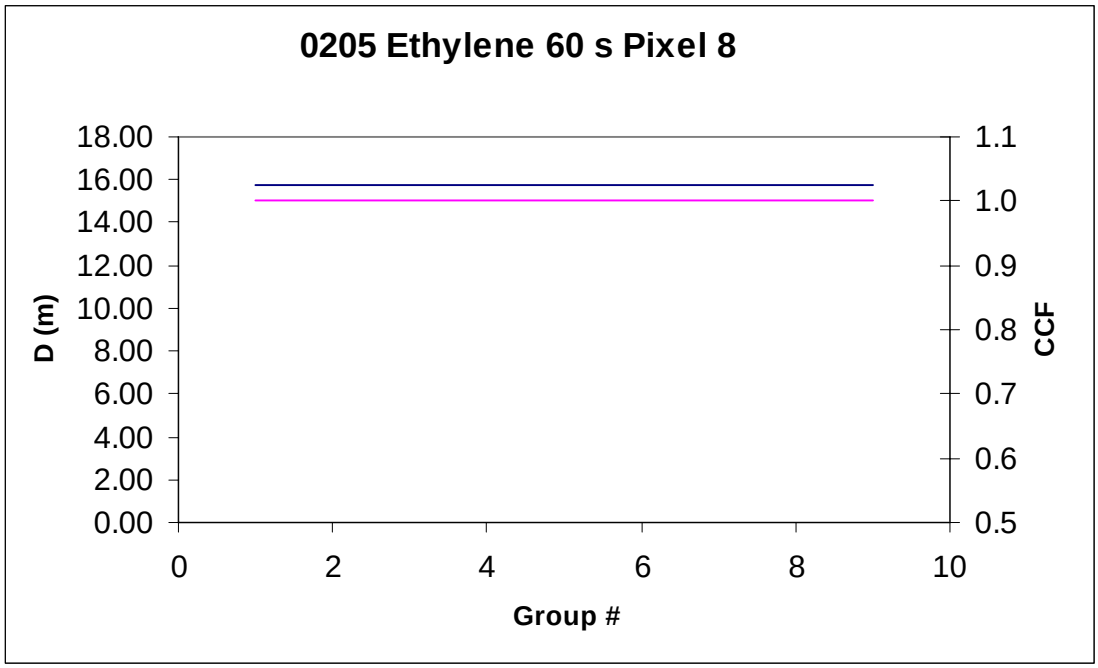

Section 3: Pixel 7

Details of Gas release: Gas: Propylene; Pixel: 7; Scan time/mirror: 60 Sec; Date: 02/05/03

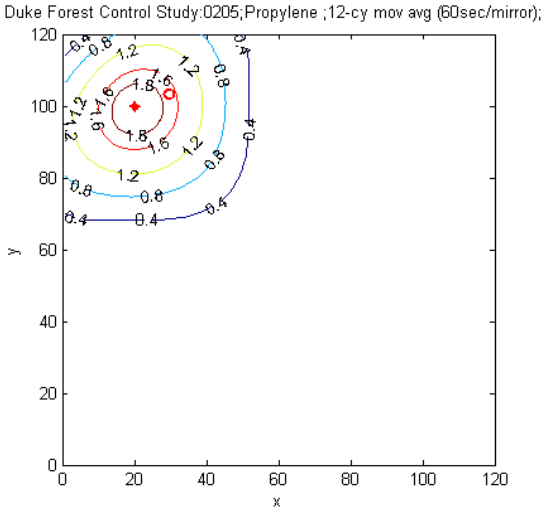

CCF	Distance(m)	group#
1.00	10.06	1
1.00	10.06	2
1.00	10.06	3
1.00	10.06	4
1.00	10.06	5
1.00	10.06	6
1.00	10.06	7
1.00	10.06	8
1.00	10.06	9
Average		
1.00	10.06	
Sdev		
0.000	0.00	

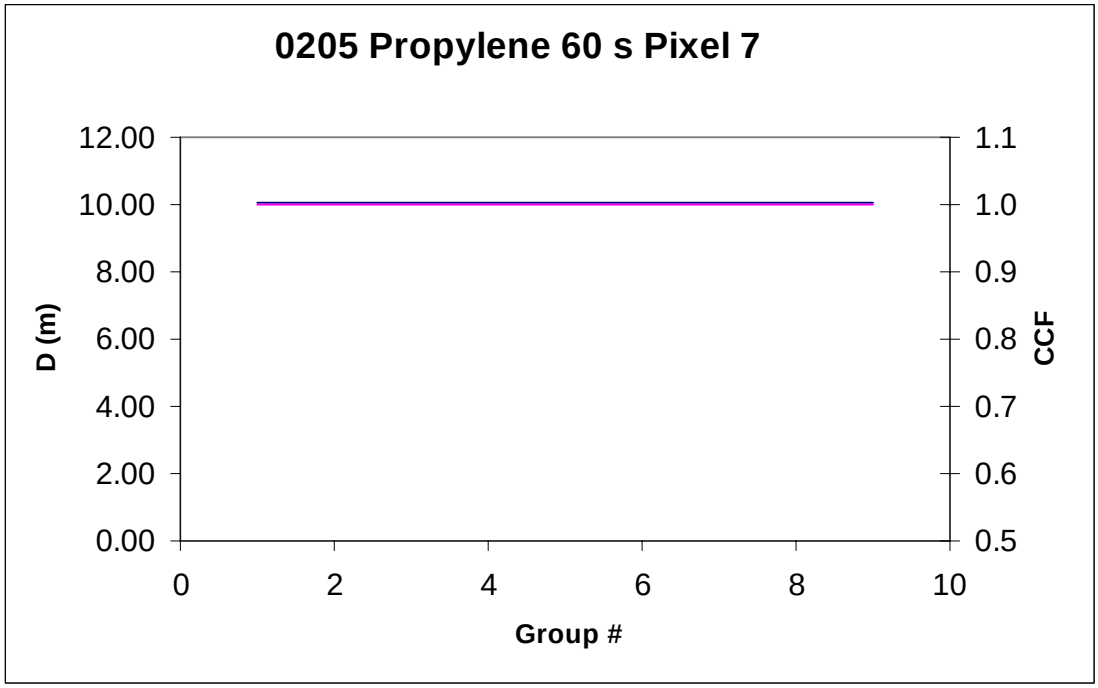

Details of Gas release: Gas: Propane; Pixel: 7; Scan time/mirror: 30 Sec; Date: 11/13/02

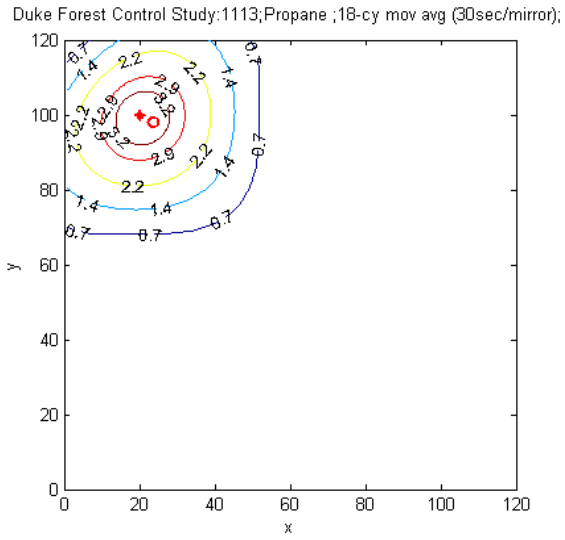

CCF	Distance(m)	group#
1.00	4.12	1.00
1.00	4.12	2.00
1.00	4.12	3.00
1.00	4.12	4.00
1.00	4.12	5.00
1.00	4.12	6.00
1.00	4.12	7.00
1.00	4.12	8.00
1.00	4.12	9.00
1.00	4.12	10.00
1.00	4.12	11.00
1.00	4.12	12.00
1.00	4.12	13.00
1.00	4.12	14.00
Average		
1.00	4.12	
Sdev		
0.00	0.00	

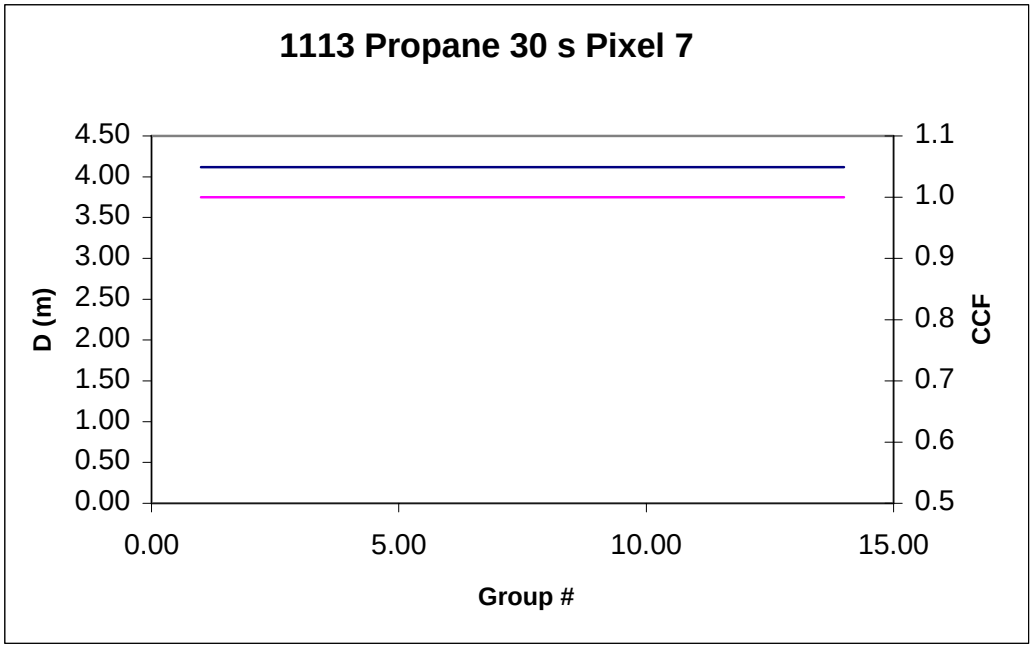

Details of Gas release: Gas: Propylene; Pixel: 7; Scan time/mirror: 10 Sec; Date: 02/05/03

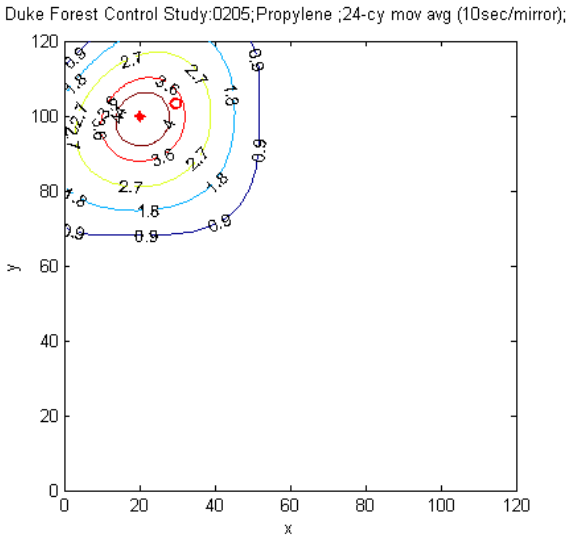

CCF	Distance(m)	group#
1.00	10.06	1
1.00	10.06	2
1.00	10.06	3
1.00	10.06	4
1.00	10.06	5
1.00	10.06	6
1.00	10.06	7
1.00	10.06	8
1.00	10.06	9
1.00	10.06	10
1.00	10.06	11
1.00	10.06	12
1.00	10.06	13
1.00	10.06	14
1.00	10.06	15
1.00	10.06	16
1.00	10.06	17
1.00	10.06	18
1.00	10.06	19
Average		
1.00	10.06	
Sdev		
0.00	0.00	

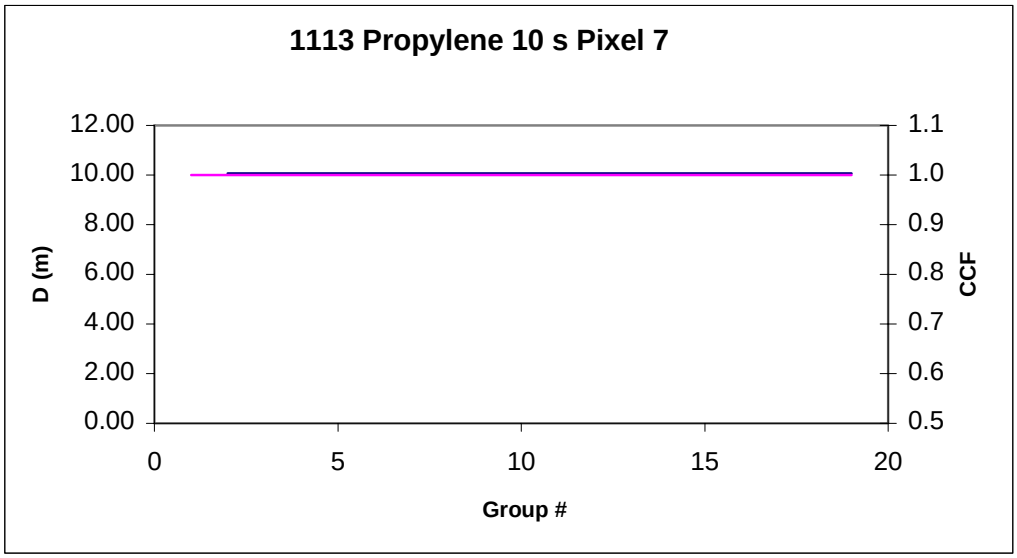

Section 4: Pixel 6

Details of Gas release: Gas: Propylene; Pixel: 6; Scan time/mirror: 30 Sec; Date: 11/14/02

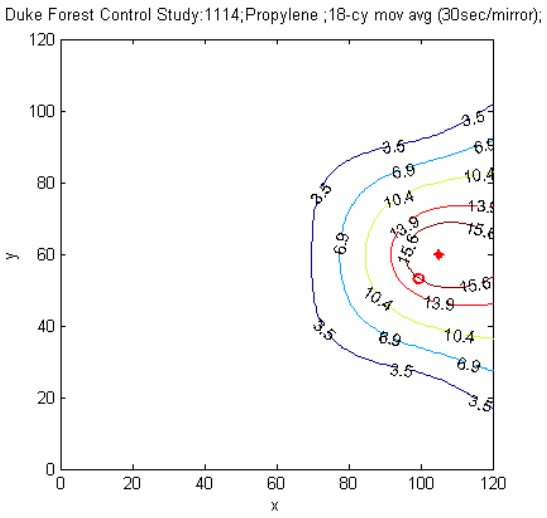

CCF	Distance(m)	group#
0.99	8.69	1
0.99	8.69	2
0.99	8.69	3
0.99	8.69	4
0.99	8.69	5
0.99	8.69	6
0.99	8.69	7
1.00	8.69	8
1.00	8.69	9
1.00	8.69	10
1.00	8.69	11
1.00	8.11	12
1.00	8.69	13
1.00	8.69	14
1.00	7.94	15
Average		
0.99	8.60	
Sdev		
0.004	0.24	

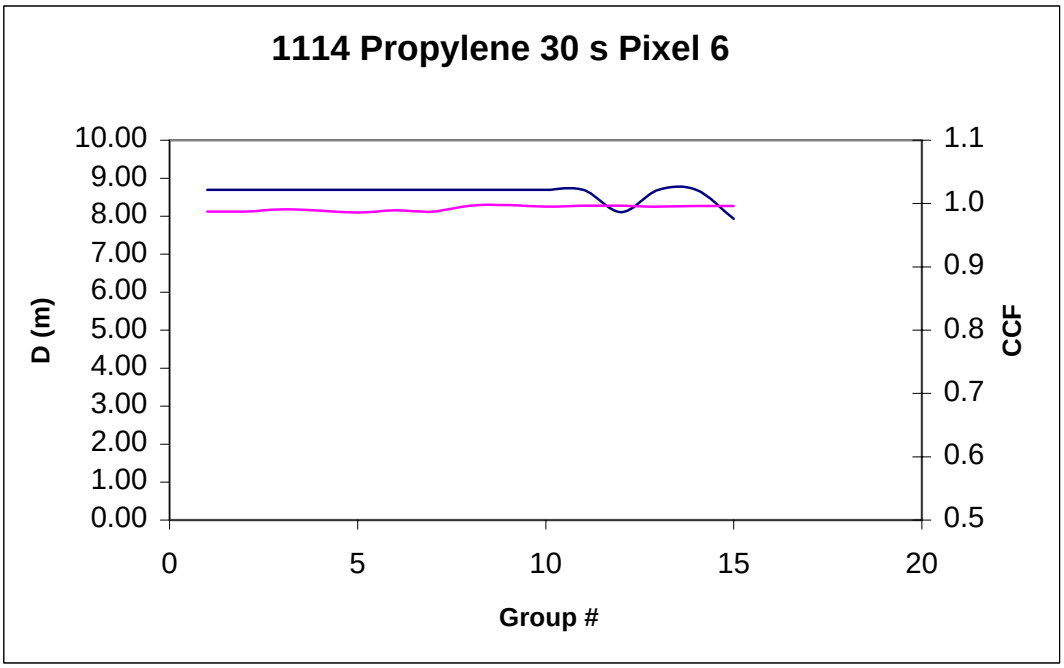

Section 5: Pixel 5

Details of Gas release: Gas: Ethylene; Pixel: 5; Scan time/mirror: 10 Sec; Date: 11/05/02

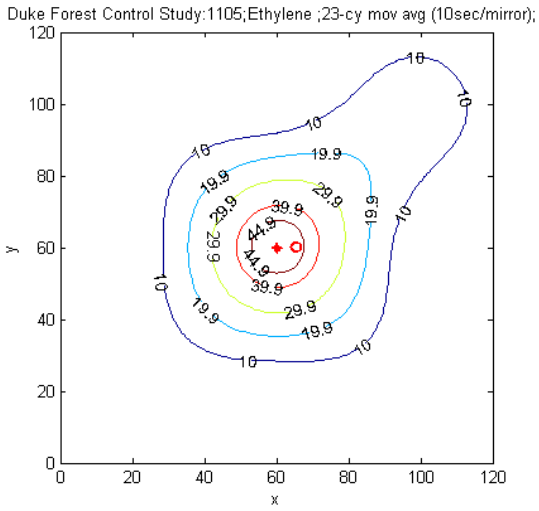

CCF	Distance(m)	group#
0.97	5.43	1
0.98	5.43	2
0.98	5.43	3
0.98	5.43	4
0.98	5.43	5
0.98	5.43	6
0.97	5.43	7
0.98	5.43	8
0.98	5.43	9
0.98	5.43	10
0.98	5.43	11
0.98	5.43	12
0.98	5.43	13
0.98	5.43	14
0.97	5.43	15
0.97	5.43	16
0.98	5.43	17
0.98	5.43	18
0.98	5.43	19
0.98	5.43	20
Average		
0.98	5.43	
Sdev		
0.004	0.000	

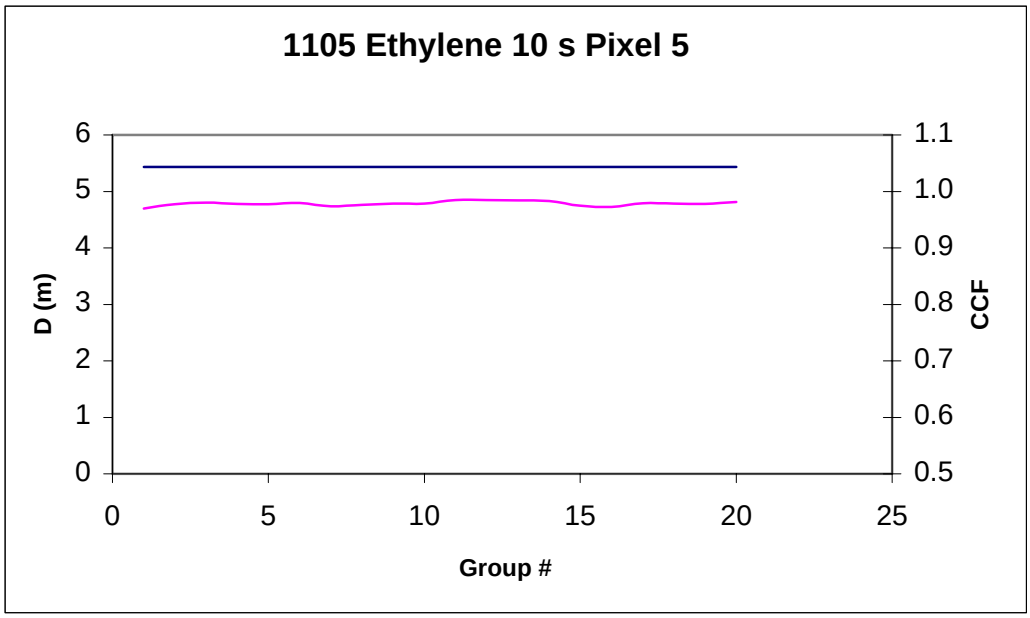

Details of Gas release: Gas: Propylene; Pixel: 5; Scan time/mirror: 30 Sec; Date: 11/05/02

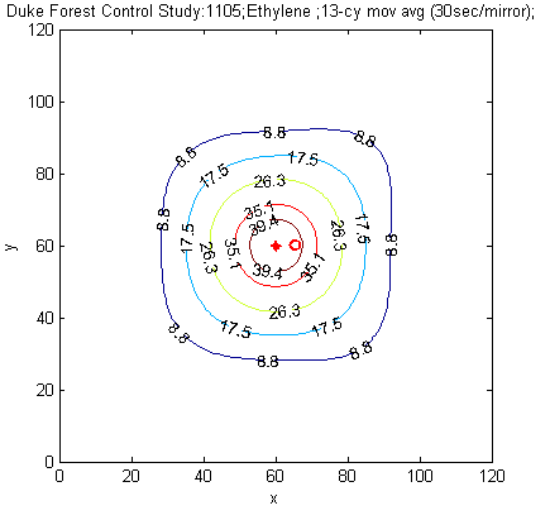

CCF	Distance(m)	group#
0.97	5.43	1
0.97	5.43	2
0.97	5.43	3
0.97	5.43	4
0.98	5.43	5
0.98	5.43	6
0.97	5.43	7
0.97	5.43	8
0.97	5.43	9
0.96	5.43	10
Average		
0.97	5.43	
Sdev		
0.006	0.000	

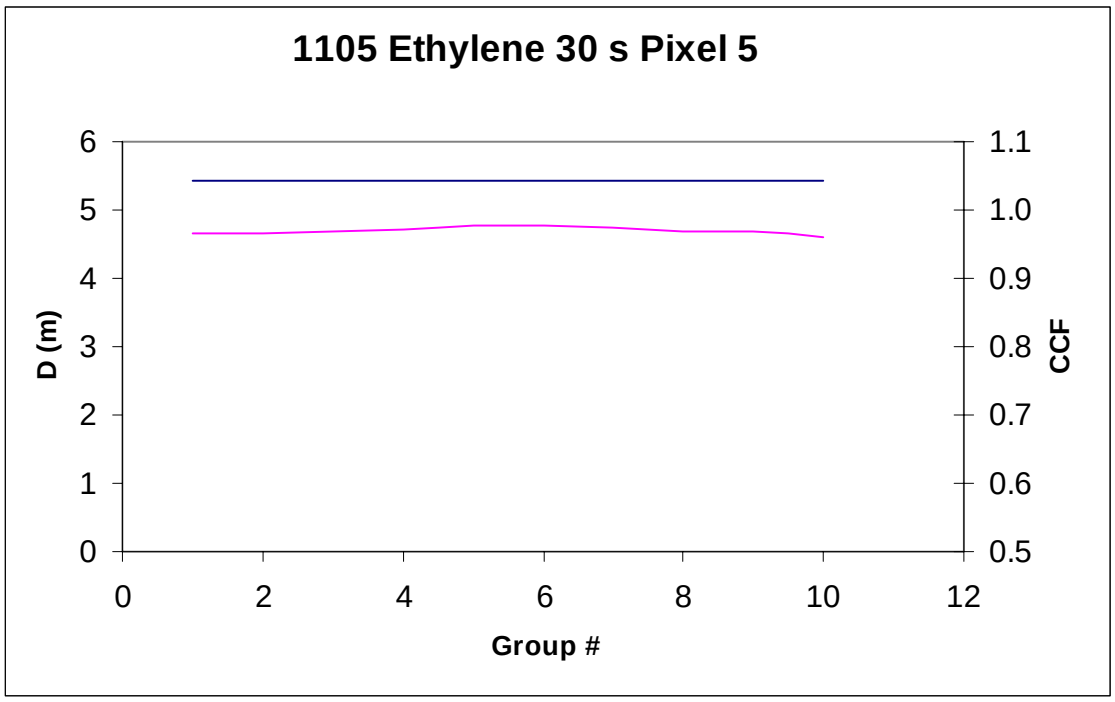

Details of Gas release: Gas: Propylene; Pixel: 5; Scan time/mirror: 60 Sec; Date: 12/12/02

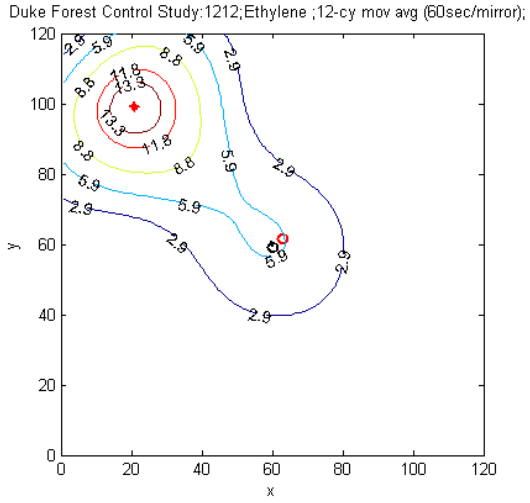

CCF	Distance(m)	group#
0.55	3.40	1
0.54	3.40	2
0.55	3.40	3
0.55	3.40	4
0.65	56.28	5
0.63	56.28	6
0.68	56.28	7
0.59	56.28	8
0.83	56.28	9
Average		
0.62	32.78	
Sdev		
0.094	27.87	

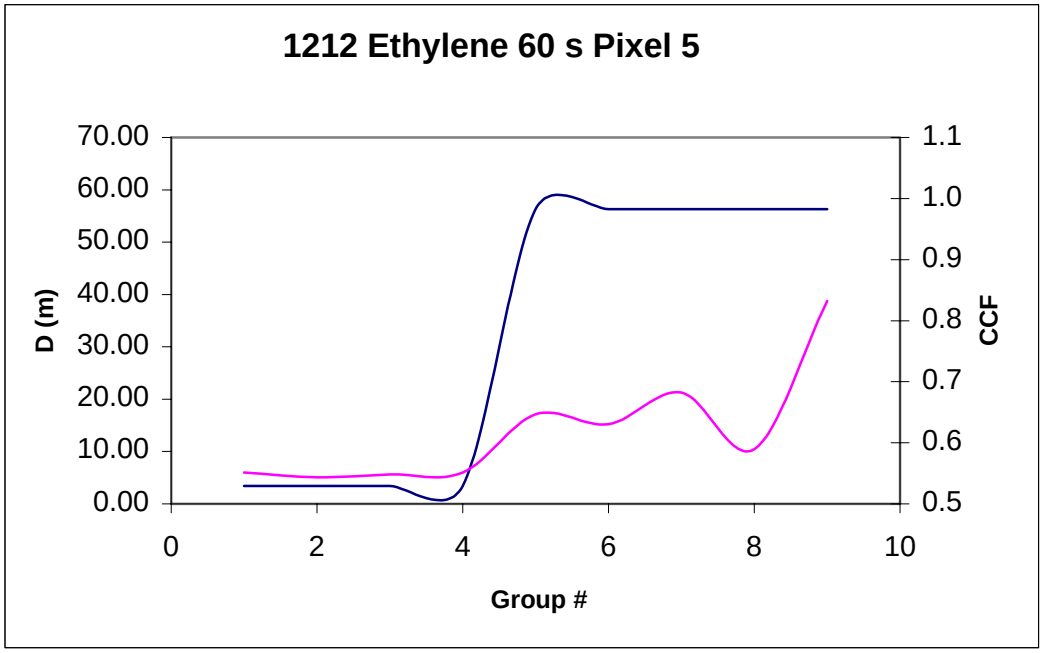

Section 6: Pixel 4

Details of Gas release: Gas: Propane; Pixel: 4; Scan time/mirror: 10 Sec; Date: 11/20/02

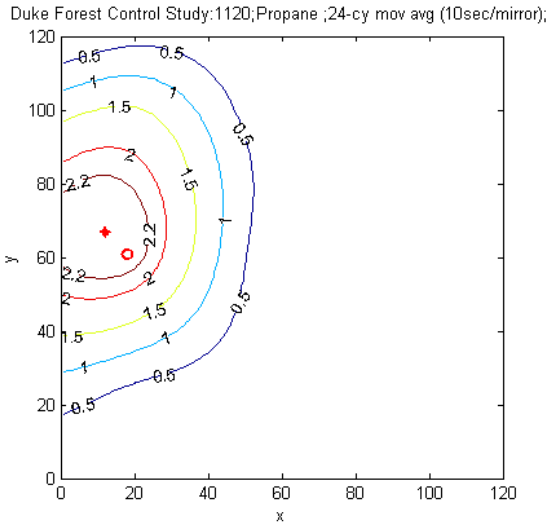

CCF	Distance(m)	group#
0.86	22.54	1
0.99	38.25	2
1.00	39.25	3
0.99	38.25	4
0.96	37.25	5
0.94	36.25	6
0.74	3.05	7
0.84	3.46	8
0.82	4.84	9
0.62	4.34	10
0.82	3.46	11
0.86	19.59	12
0.80	4.12	13
0.95	37.25	14
0.96	36.25	15
0.96	35.21	16
1.00	38.25	17
0.99	34.21	18
0.98	12.67	19
0.92	3.05	20
0.80	4.34	21
Average		
0.89	21.7	
Sdev		
0.103	15.8	

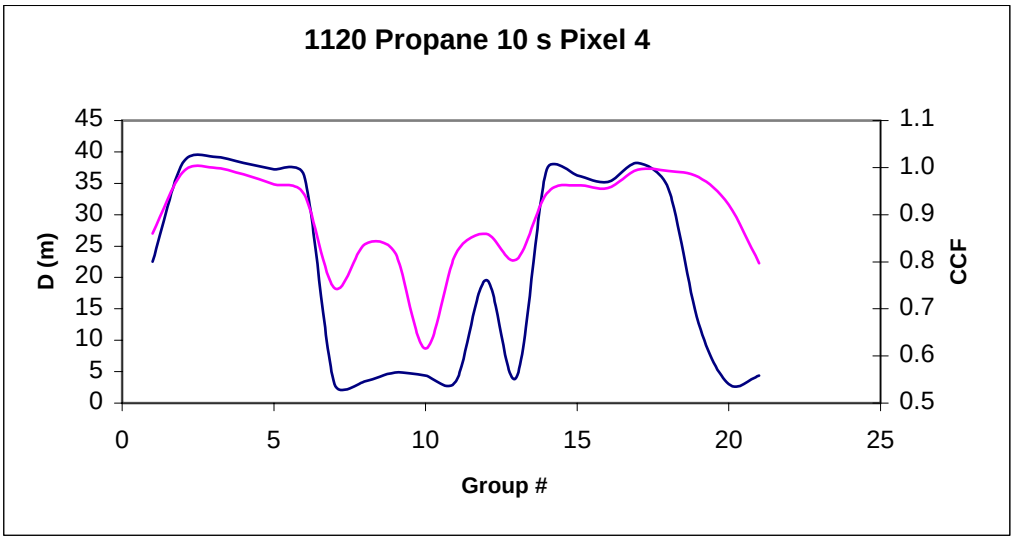

Details of Gas release: Gas: Propane; Pixel: 4; Scan time/mirror: 30 Sec; Date: 11/18/02

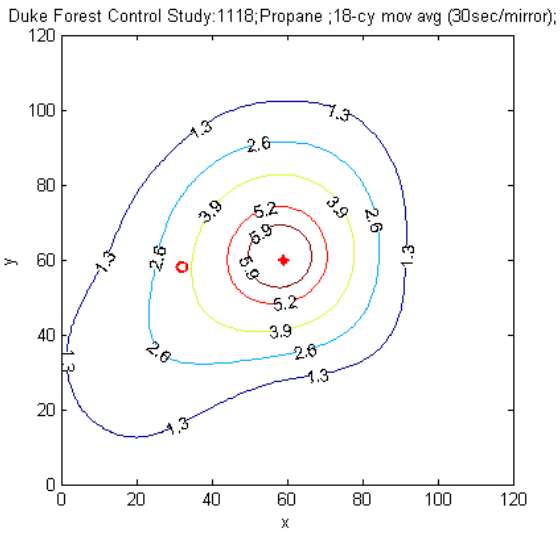

CCF	Distance(m)	group#
0.78	18.32	1
0.79	18.32	2
0.76	17.20	3
0.75	17.20	4
0.69	17.20	5
0.73	17.20	6
0.72	17.20	7
0.81	18.32	8
0.85	19.98	9
0.90	17.20	10
0.58	20.41	11
0.82	38.75	12
0.98	28.17	13
0.99	28.17	14
0.99	28.05	15
Average		
0.81	21.4	
Sdev		
0.119	6.4	

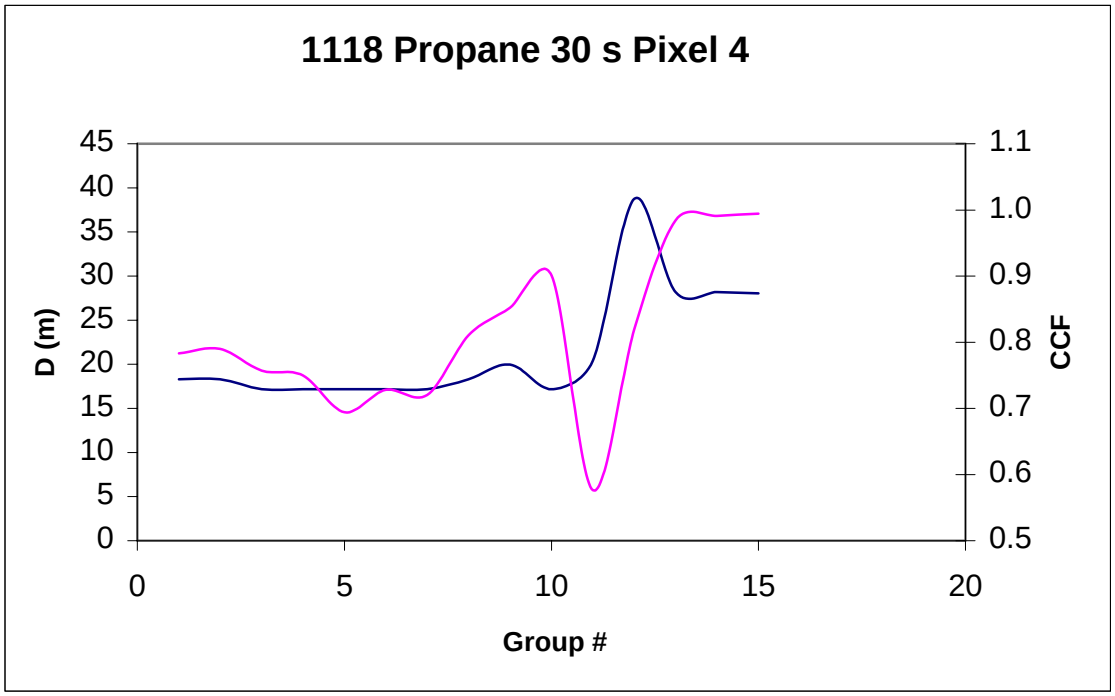

Details of Gas release: Gas: Propane; Pixel: 4; Scan time/mirror: 60 Sec; Date: 11/18/02

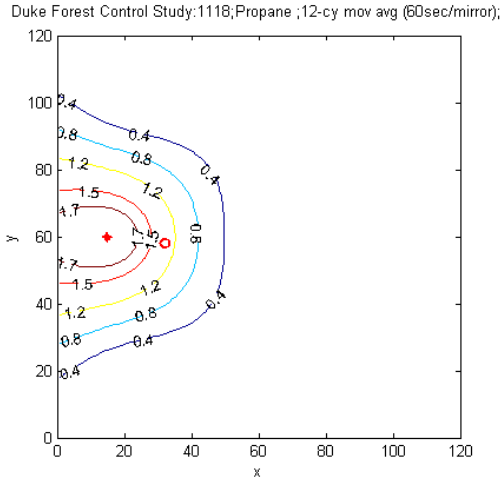

CCF	Distance(m)	group#
0.83	17.20	1
0.85	17.20	2
0.94	17.20	3
0.88	17.20	4
0.91	19.70	5
0.89	19.48	6
0.75	17.20	7
0.76	17.20	8
0.70	17.20	9
Average		
0.83	17.73	
Sdev		
0.080	1.059	

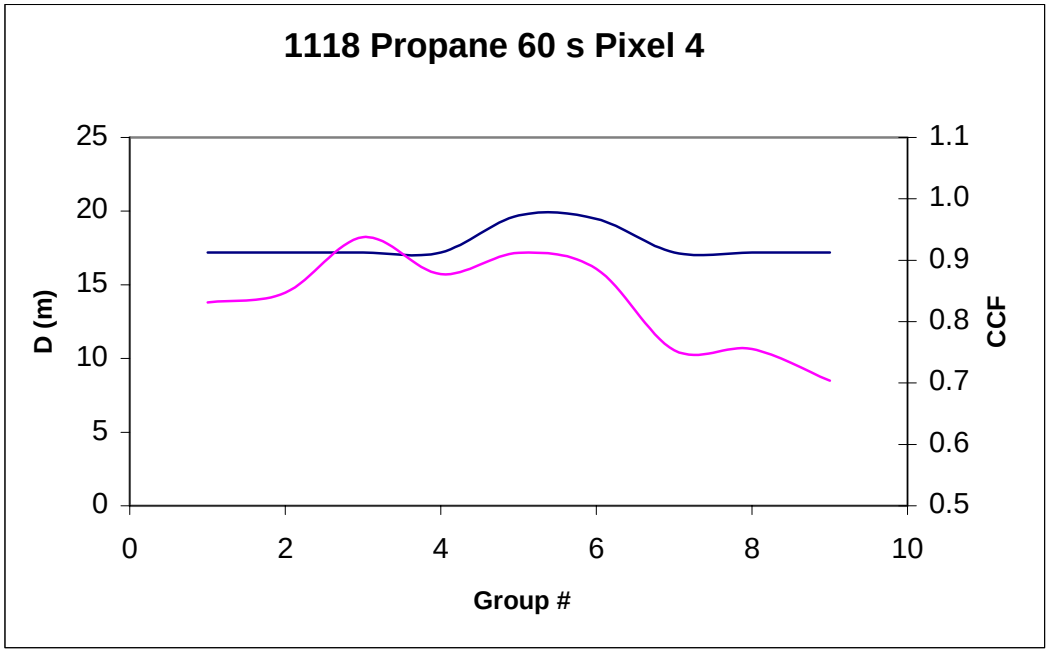

Section 7: Pixel 3

Details of Gas release: Gas: Propylene; Pixel: 3; Scan time/mirror: 10 Sec; Date: 11/19/02

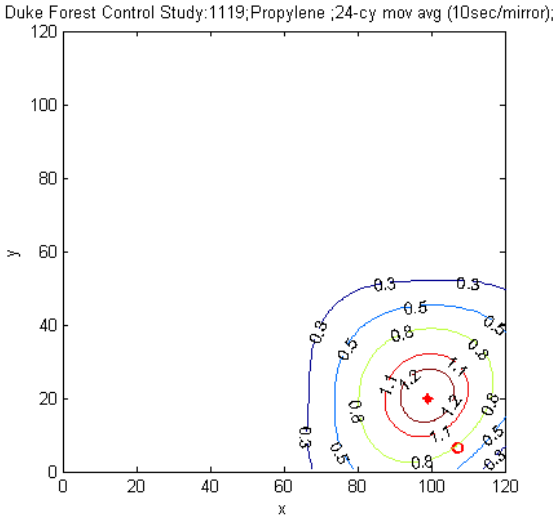

CCF	Distance(m)	group#
1.00	15.92	1
1.00	15.92	2
1.00	16.78	3
1.00	16.30	4
1.00	16.30	5
1.00	16.30	6
1.00	15.42	7
1.00	15.42	8
1.00	15.92	9
1.00	15.92	10
1.00	15.92	11
1.00	15.92	12
1.00	15.42	13
1.00	16.30	14
1.00	16.78	15
1.00	16.78	16
1.00	16.78	18
1.00	15.92	18
0.99	15.92	19
0.89	30.04	20
0.89	30.04	21
Average		
0.99	17.50	
Sdev		
0.034	4.3	

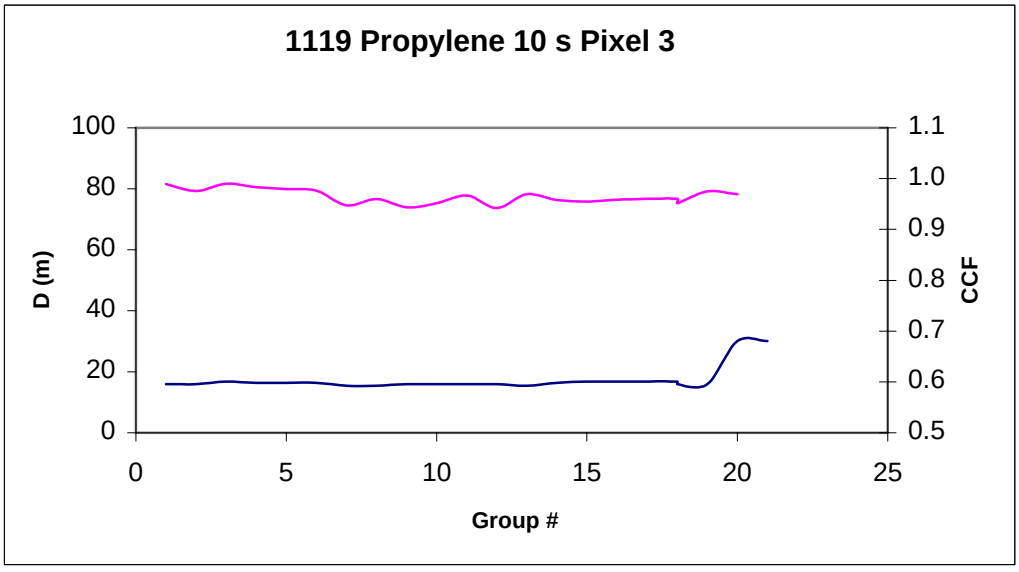

Details of Gas release: Gas: Propylene; Pixel: 3; Scan time/mirror: 30 Sec; Date: 11/20/02

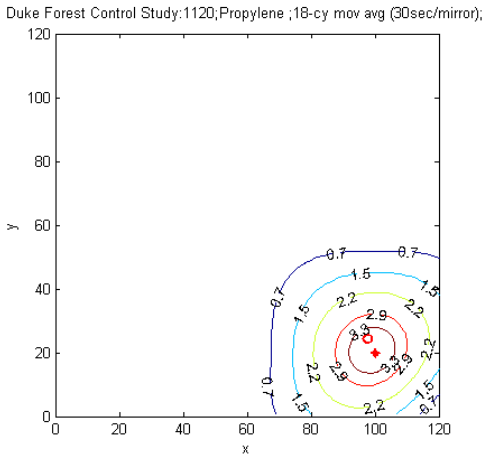

CCF	Distance(m)	group#
0.98	4.76	1
0.99	4.76	2
0.99	4.76	3
1.00	4.76	4
1.00	5.15	5
1.00	4.76	6
1.00	5.15	7
1.00	4.76	8
1.00	4.76	9
1.00	4.76	10
1.00	4.76	11
1.00	5.15	12
1.00	5.15	13
1.00	5.15	14
1.00	5.15	15
Average		
1.00	4.92	
Sdev		
0.005	0.2	

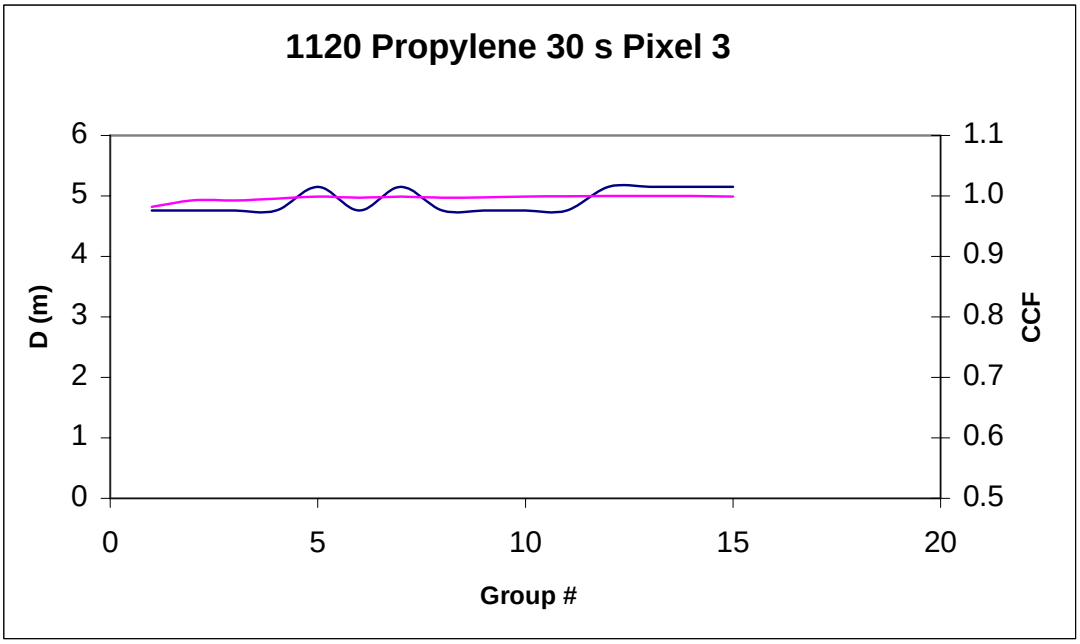

Details of Gas release: Gas: Propylene; Pixel: 3; Scan time/mirror: 10 Sec; Date: 11/20/02

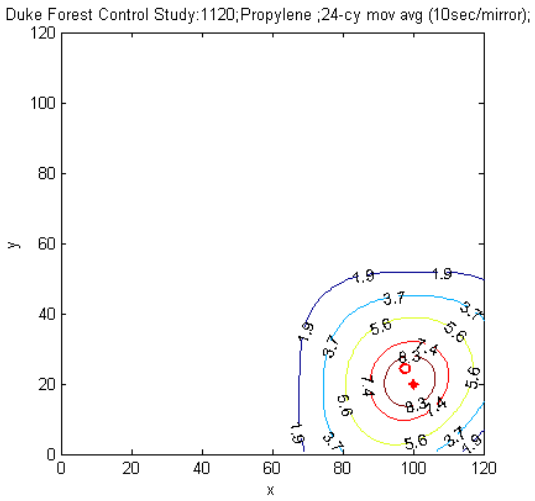

CCF	Distance(m)	group#
1.00	5.15	1
1.00	5.15	2
1.00	4.76	3
0.99	4.76	4
1.00	4.76	5
1.00	4.76	6
1.00	4.76	7
1.00	5.15	8
1.00	5.15	9
1.00	5.15	10
1.00	5.15	11
1.00	5.15	12
1.00	5.15	13
1.00	5.15	14
1.00	5.15	15
1.00	5.15	16
1.00	5.15	17
1.00	5.15	18
1.00	5.15	19
1.00	5.15	20
1.00	5.15	21
Average		
1.00	5.1	
Sdev		
0.002	0.2	

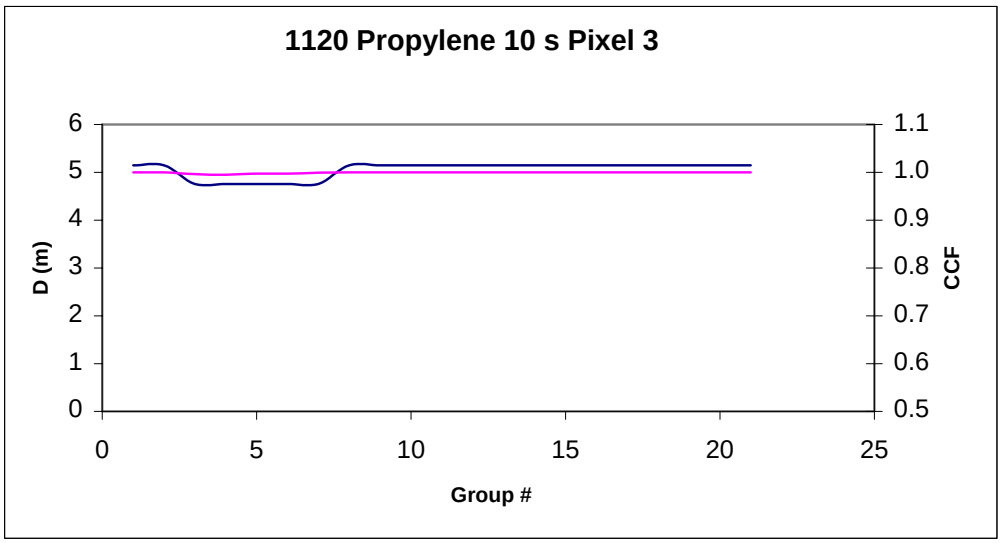

Details of Gas release: Gas: Propylene; Pixel: 3; Scan time/mirror: 60 Sec; Date: 11/21/02

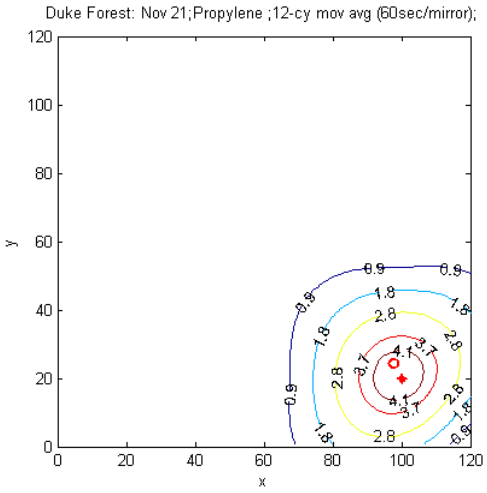

CCF	Distance(m)	group#
1.00	5.15	1
1.00	5.15	2
1.00	5.15	3
1.00	5.15	4
1.00	5.15	5
1.00	3.82	6
1.00	3.82	7
1.00	3.82	8
1.00	4.30	9
Average		
1.00	4.61	
Sdev		
0.000	0.7	

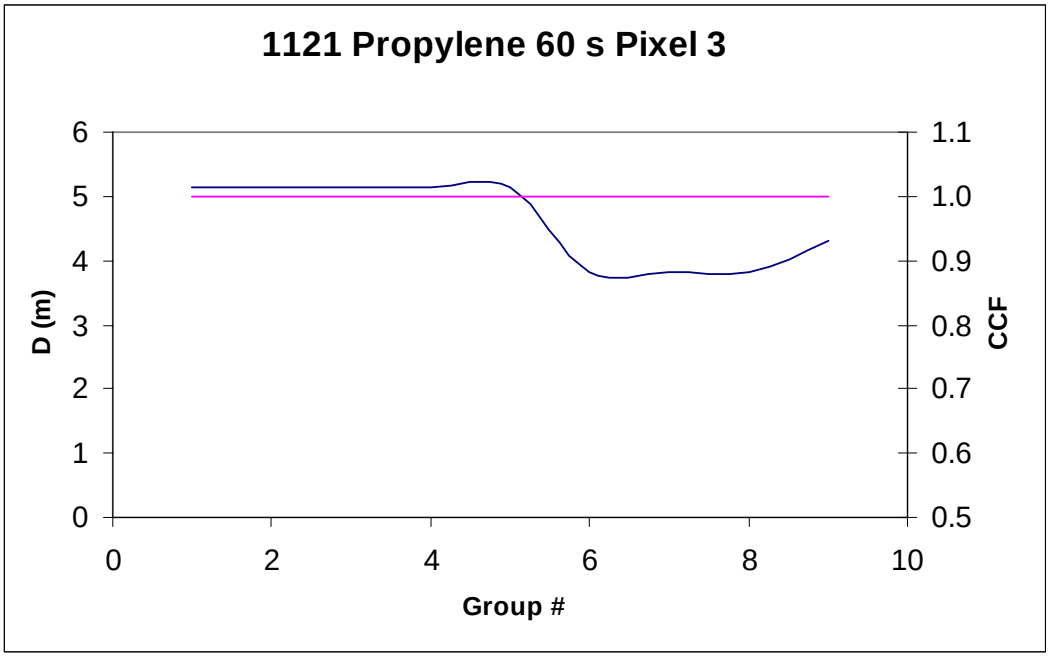

Section 8: Pixel 2

Details of Gas release: Gas: Acetylene; Pixel: 2; Scan time/mirror: 10 Sec; Date: 11/20/02

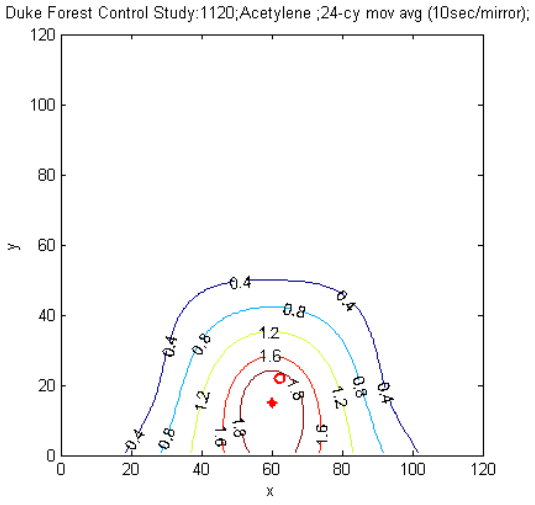

CCF	Distance(m)	group#
0.77	7.40	1
0.75	7.40	2
0.81	8.69	3
0.71	6.03	4
0.67	6.88	5
0.82	6.03	6
0.76	7.40	7
0.72	7.40	8
0.77	7.40	9
0.76	7.40	10
0.72	7.40	11
0.70	7.40	12
0.71	7.40	13
0.73	7.40	14
0.89	7.40	15
0.88	7.40	16
0.83	7.40	17
0.80	7.40	18
0.66	7.40	19
0.68	7.40	20
0.65	7.40	21
Average		
0.75	7.31	
Sdev		
0.067	0.525	

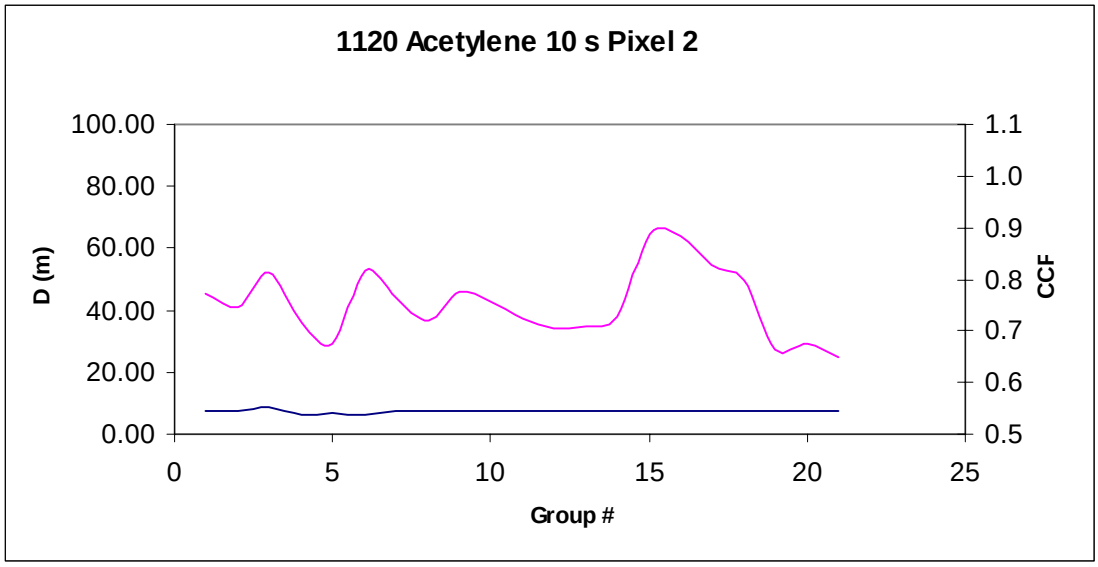

Details of Gas release: Gas: Acetylene; Pixel: 2; Scan time/mirror: 30 Sec; Date: 11/20/02

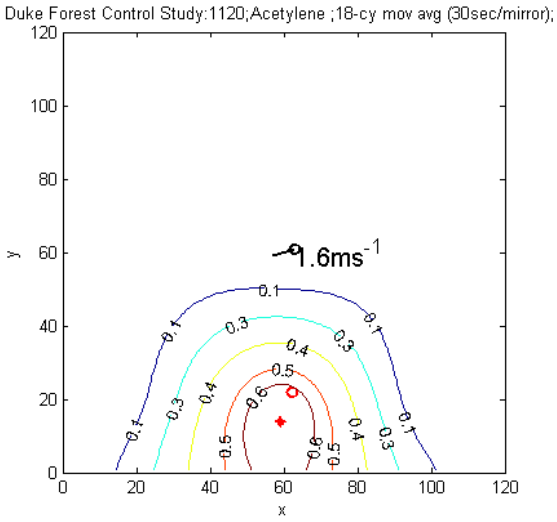

CCF	Distance(m)	group#
0.91	7.40	1
0.84	7.40	2
0.66	7.40	3
0.67	7.77	4
0.59	9.12	5
0.58	8.69	6
0.58	7.40	7
0.64	7.40	8
0.67	7.40	9
0.64	7.40	10
0.69	7.40	11
0.70	8.69	12
0.66	8.69	13
0.70	8.69	14
0.62	11.02	15
Average		
0.68	8.13	
Sdev		
0.091	1.0	

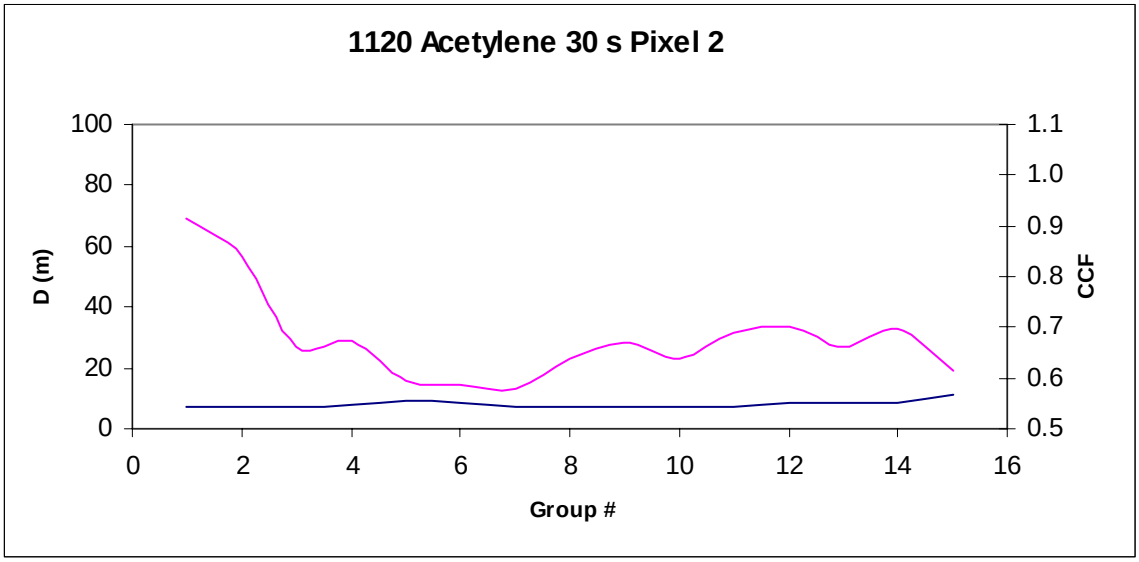

Details of Gas release: Gas: Acetylene; Pixel: 2; Scan time/mirror: 60 Sec; Date: 11/21/02

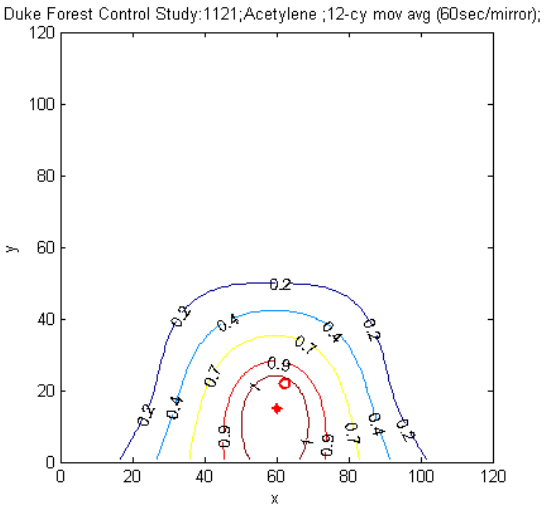

CCF	Distance(m)	group#
0.70	7.40	1
0.84	7.77	2
0.80	7.40	3
0.73	7.40	4
0.83	7.40	5
0.83	3.82	6
0.77	5.54	7
0.78	6.46	8
0.77	7.40	9
Average		
0.78	6.73	
Sdev		
0.046	1.3	

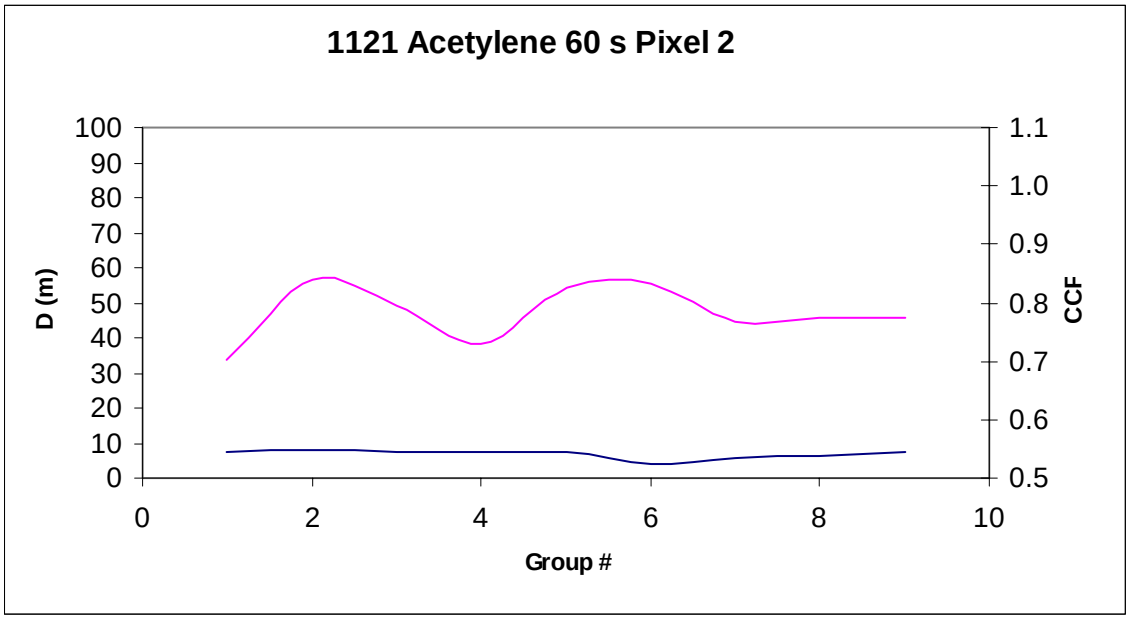

Section 9: Pixel 1

Details of Gas release: Gas: Ethylene; Pixel: 1; Scan time/mirror: 10 Sec; Date: 11/19/02

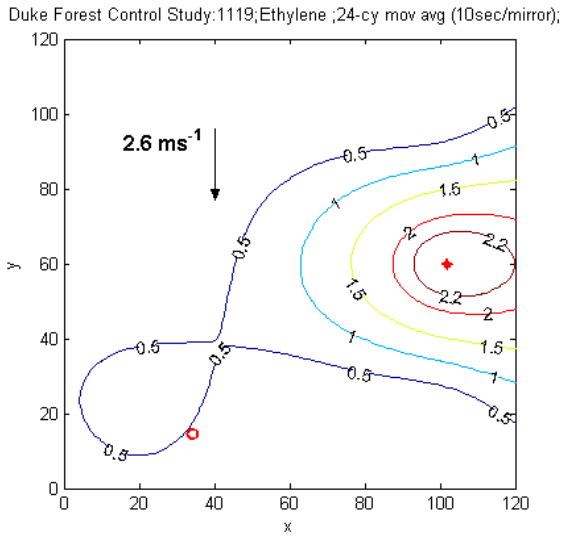

CCF	Distance(m)	group#
0.92	83.23	1
0.88	83.23	2
0.79	83.23	3
0.67	81.56	4
0.77	80.73	5
0.65	77.45	6
0.82	79.90	7
0.79	55.93	8
0.74	54.23	9
0.74	78.26	10
0.64	14.59	11
0.58	82.39	12
0.87	84.61	13
0.88	83.78	14
0.84	83.78	15
0.95	83.78	16
0.90	82.95	17
0.95	82.95	18
0.95	83.51	19
0.86	81.30	20
0.89	80.73	21
Average		
0.81	76.29	
Sdev		
0.11	16.40	

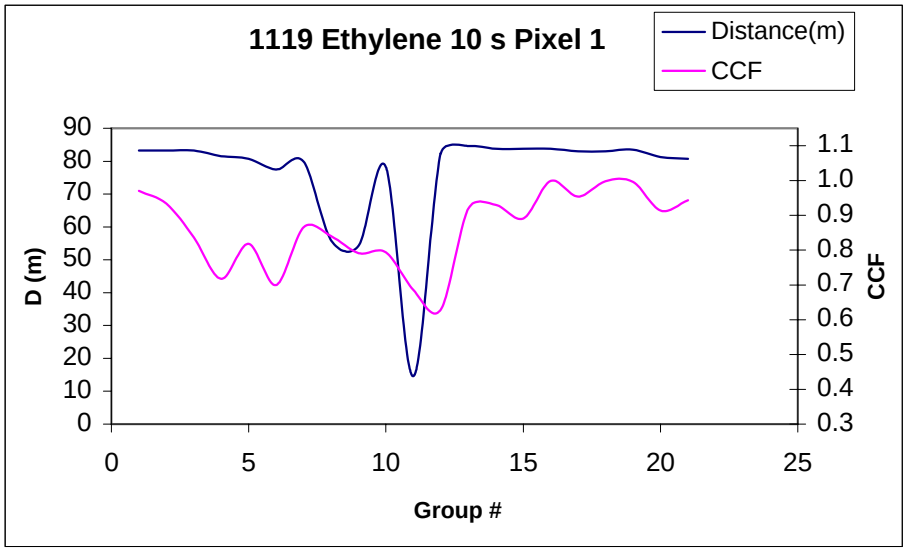

Details of Gas release: Gas: Ethylene; Pixel: 1; Scan time/mirror: 30 Sec; Date: 11/20/02

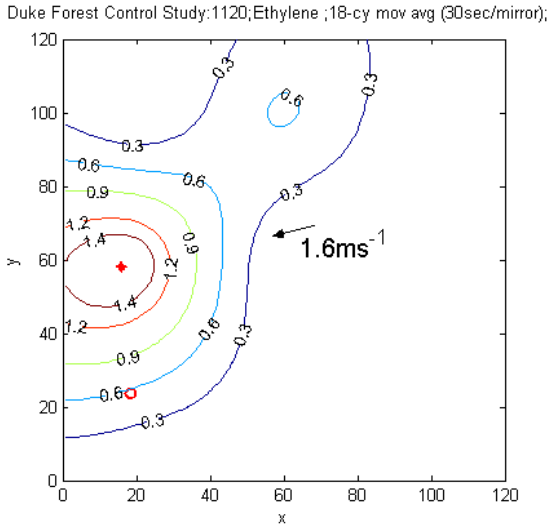

CCF	Distance(m)	group#
0.98	88.56	1
0.97	89.44	2
0.93	35.21	3
0.96	89.44	4
1.00	76.69	5
0.79	80.65	6
0.89	75.23	7
0.82	75.39	8
0.32	1.79	9
0.57	26.73	10
0.73	34.35	11
0.80	34.46	12
0.95	36.34	13
0.85	35.59	14
0.85	35.59	15
Average		
0.83	54.37	
Sdev		
0.18	28.56	

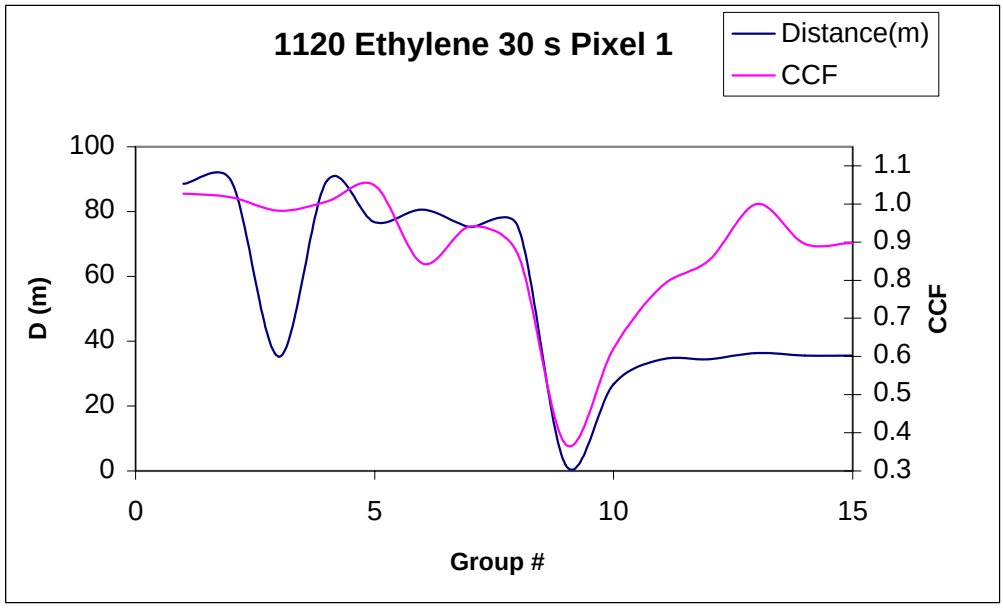

Details of Gas release: Gas: Ethylene; Pixel: 1; Scan time/mirror: 60 Sec; Date: 11/19/02

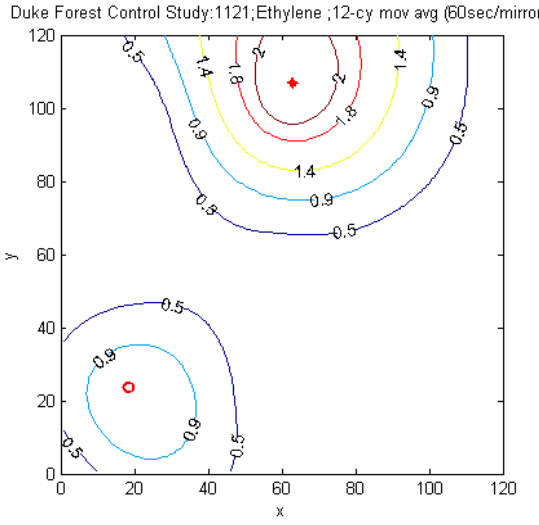

CCF	Distance(m)	group#
0.89	94.62	1
0.91	90.39	2
0.73	87.41	3
0.76	55.79	4
0.61	3.83	5
0.79	28.39	6
0.89	86.80	7
0.92	90.79	8
0.94	92.57	9
Average		
0.83	70.07	
Sdev		
0.11	33.28